Structural and metamorphic architecture of the Zanskar Himalaya, Suru Valley region, NW India: Implications for the evolution of the Himalayan metamorphic core

I.P. Cawood[1], M.R. St-Onge[1,2], O.M. Weller[3], M.P. Searle[1,4,5], D.J. Waters[1,4], T. Ahmad[6]

1. Department of Earth Sciences, University of Oxford, 3 South Parks Road, Oxford, OX1 3AN, UK.

2. Geological Survey of Canada, 601 Booth Street, Ottawa, Ontario, K1A 0E8, Canada.

3. Department of Earth Sciences, University of Cambridge, Downing Street, Cambridge, CB2 3EQ, UK.

4. Museum of Natural History, University of Oxford, Parks Road, Oxford, OX1 3PW, UK.

5. Camborne School of Mines, University of Exeter (Cornwall campus), Penryn, Cornwall, TR10 9EZ, UK.

6. Wadia Institute of Himalayan Geology, Dehradun 248 001, India.

ABSTRACT

New 1:50,000-scale geological mapping in the Zanskar Himalaya of NW India, covering 2,400 kilometer^2, is integrated with structural and petrographic analysis to document the evolution and key tectonometamorphic relationships within the Himalayan metamorphic core. The integrated dataset constrains the regional three-dimensional geology and relationships between lithostratigraphy, folds, faults, deformation fabrics, metamorphic isograds and growth of porphyroblasts within the context of five main deformation phases.

Following the initial collision of India and Asia, NW–SE-oriented deformation is recorded by D_1 (greenschist-facies) fabrics and D_2 (greenschist- to amphibolite-facies) fabrics. D_2 represents the main tectonometamorphic deformation phase associated with crustal thickening and produced the dominant regional penetrative fabric through crenulation and transposition of D_1 fabrics. Thrust-sense D_2 fabrics were reactivated during D_3 as the Greater Himalayan Sequence was exhumed along the normal-sense Zanskar Shear Zone, which is part of the South Tibetan Detachment System. D_3 fabrics, associated with movement on the Zanskar Shear Zone, were temporally continuous with crenulation and mesoscale folding, recording progressive kilometer-scale backfolding and backthrusting towards the NE between the Greater Himalayan Sequence-Tethyan Himalayan Sequence and the adjacent Indus Suture Zone. Finally, D_4 and D_5 are recorded as kilometer-scale open folding of older planar and linear structures.

The orientation of mineral isograd surfaces ranges from subparallel to oblique with respect to D_2 planar structural elements. The growth of pelitic and metabasic peak metamorphic phases from greenschist to upper-amphibolite facies is synchronous with or postdates D_2 fabrics. D_3 fabrics wrap thermal peak porphyroblasts and realign linear mineral phases. Tectonic thinning adjacent to D_3 normal faults is documented by reduced structural spacing of isograds and alignment of isograd surfaces parallel to the faults. D_4 and D_5 structures modify the trace of all regional metamorphic isograds. Collectively, these observations imply that the thermal peak of metamorphism was reached after the main phase of deformation (D_2), and predated movement on the Zanskar Shear Zone (D_3). The results document numerous classical elements of collisional orogenesis, including implied clockwise P-T paths, polyphase deformation, and a complete Barrovian metamorphic isograd sequence supplemented by complementary metabasic isograds. The Zanskar Himalaya, unlike other areas of the Himalayan metamorphic core, records metamorphic conditions primarily attained following substantial crustal thickening rather than during sub-

sequent decompression and exhumation. The reduced expression and/or discontinuous nature of exhuming fault systems, which produces variable levels of crustal exposure, may account for this lateral heterogeneity across the mountain belt. Deciphering the complex kinematics of continental tectonics requires the integration of observations and data over large length scales and a range of structural levels.

INTRODUCTION

Mountain building (orogenesis) leads to a complex evolution in the pressure-temperature (P-T) structure of the lithosphere with time (t). Given the broad length scales (up to thousands of kilometers) and time scales (up to hundreds of millions of years) that can characterize orogens, decoding their history is challenging and typically requires the integration of observations over large length scales and a range of structural levels (England & Jackson, 1989; Weller *et al.*, 2021). A critical step in this process is the identification of lithostratigraphic units and tectonothermal events, which can be achieved by integrating a range of datasets, including macroscale geological field mapping and microscale petrographic analysis to provide a reference frame for understanding the tectonic evolution of a region.

The Himalayan-Karakoram-Tibetan orogen is the largest orogen on Earth and is particularly well exposed along the frontal Himalayan ranges. Therefore, it provides a window into how continental crust accommodates deformation during continental collision. The orogen formed following the collision of the Indian and Asian plates in the early Cenozoic, with the suggested timing of collision varying depending on the criterion applied. Ages include: *ca.* 61 Ma, based on the stratigraphically defined provenance reversal of sediments on the Indian passive margin (An *et al.*, 2021); *ca.* 59 Ma, from the oldest Tethyan strata containing zircons of Asian affinity (DeCelles *et al.*, 2014; Hu *et al.*, 2015; Metcalf & Kapp, 2017); before *ca.* 51 Ma, reflecting a pulse of upper plate magmatic activity correlated to a decrease in the rate of convergence (Zhu *et al.*, 2015, 2019); *ca.* 51 Ma, determined from the youngest marine sedimentary strata in the suture zone (Green *et al.*, 2008); and before *ca.* 47 Ma, defined by the oldest post-collisional molasse sedimentation in the suture zone (St-Onge *et al.*, 2010). Following collision, significant crustal shortening, thickening, and Barrovian metamorphism occurred within and on the margin of the Indian continental crust. The highest-grade metamorphic rocks of the Himalaya are found within the Himalayan metamorphic core, which refers to a package of pervasively deformed mid-crustal

rocks that record Cenozoic metamorphism, deformation, and cooling (Cottle *et al.*, 2015). Numerous studies have documented that the metamorphic evolution of the Himalayan metamorphic core is characterized by two main events: an earlier (Eocene–Oligocene), higher-pressure phase dominated by kyanite-bearing assemblages; and a later (Oligocene–Miocene), lower-pressure phase associated with sillimanite-bearing assemblages (e.g., Kundig, 1989; Stäubli, 1989; Searle *et al.*, 1992, 1999a; Stephenson *et al.*, 2000, 2001; Walker *et al.*, 2001). Most regions of the Himalayan metamorphic core equilibrated under the latter sillimanite-grade conditions and thus are dominated by Oligocene to Miocene metamorphic ages (*ca.* 30–15 Ma; Kohn, 2014; Wang *et al.*, 2016; Goscombe *et al.*, 2018; Waters, 2019). The earlier Eocene–Oligocene metamorphic record is typically best preserved in the cores of larger grains of dateable phases (e.g., monazite) in assemblages that are otherwise relatively overprinted during latter stages of the metamorphic cycle (e.g., monazite; Cottle *et al.*, 2009; Larson *et al.*, 2010; Kellett *et al.*, 2014; Ambrose *et al.*, 2015; Iaccarino *et al.*, 2015; Khanal *et al.*, 2021). Therefore, the early tectonometamorphic architecture prior to sillimanite-grade metamorphism remains poorly preserved and constrained. In the Zanskar Himalaya of NW India, extensive kyanite-grade mineral assemblages prevail (Figs. 1 & 2; Honegger *et al.*, 1982; Searle & Fryer, 1986; Searle *et al.*, 1999a; Walker *et al.*, 2001). In particular, the Suru Valley region of NW India, the focus of this study, documents—on average—higher pressures (~+2 kbar) than those recorded in the rest of the Zanskar Himalaya (Fig. S1, located in the Supplemental Material[1]) and significant SW-vergent folding and thrusting along NE-dipping shear zones (e.g., Searle *et al.*, 1992). The abundance of higher-pressure assemblages and SW-vergent structures recorded in the Zanskar Himalaya is interpreted to result from substantial crustal thickening and burial following the onset of collision, thereby making it a choice location for studying the early tectonometamorphic architecture of the Himalayan metamorphic core (e.g., Searle *et al.*, 1992; Walker *et al.*, 2001). The Suru Valley region also features aspects that are relatively unique to the Himalaya, including the map-scale closure of mineral isograds (Searle & Rex, 1989), greenschist-facies metamorphosed assemblages of the Indus Suture Zone (Honegger, 1983), amphibolite-facies strata of the Neotethyan shelf within the Himalayan metamorphic core (Honegger *et al.*, 1982; Searle *et al.*, 2007), low modal abundance of migmatite (Honegger, 1983), and variation in localization of deformation and offset along the South Tibetan Detachment System (Inger, 1998). Therefore, detailed study of the relationship between deformation and metamorphism in the region is required to discern whether the region is truly heterogeneous, with implications for the along-strike applicability of tectonic models and

our understanding of orogenic processes.

Herein, we present the results of detailed field mapping and a three-dimensional (3-D) structural study of the Himalayan metamorphic core as exposed within the Suru Valley region of the Zanskar Himalaya. Notably, this region preserves a complete chlorite- to sillimanite+K-feldspar-zone Barrovian sequence completed by metabasic assemblages (e.g., Honegger *et al.*, 1982; Honegger, 1983; Walker *et al.*, 2001), although sillimanite-grade conditions and above comprise a smaller domain than in other areas of the Himalayan metamorphic core. The aim of this study is to understand the structural and metamorphic architecture of the Suru Valley area, and in particular: (1) how crustal-thickening is accommodated following initial continent-continent collision, (2) how peak metamorphic assemblages relate to deformation from the macroscale to microscale, (3) how the tectonometamorphic architecture of the Himalayan metamorphic core documented in the Suru Valley region compares along strike across the orogen, and (4) to discuss the wider implications for our understanding of orogenic processes. We start by presenting an outline of the geology of the Zanskar Himalaya, then document the relationships between lithostratigraphy, folds, thrusts, deformation fabrics, metamorphic isograds, and porphyroblast growth in the Suru Valley area to determine the sequence of deformation events and the spatial and relative temporal evolution of thickened Himalayan crust.

GEOLOGICAL OVERVIEW AND PREVIOUS WORK

Geological subdivision of the Himalaya

The separation of the Himalaya into a series of geological and/or geographic units may be traced back to the preliminary work of Heim & Gansser (1939). Since then, geographically, structurally, and stratigraphically defined zones have been used interchangeably (see discussion in Yin, 2006). Attempts to standardize the use of this terminology (e.g., Yin, 2006; Martin, 2017) are inconsistently applied in the literature, and the terms Tethyan Himalayan Sequence, Greater Himalayan Sequence, and Lesser Himalayan Sequence are most commonly used to describe fault-bounded lithotectonic assemblages (e.g., Kohn, 2014; Cottle *et al.*, 2015; Carosi *et al.*, 2018). The use of lithotectonic units has proved key to emphasizing the apparent along strike consistency of the geological record along the orogen, and they are best used when applied at broad length scales. Nevertheless, several issues impede the consistent application of lithotectonic units in all regions and at all scales: the debated location of bounding faults (Goscombe *et al.*, 2006;

Searle *et al.*, 2008; Larson & Godin, 2009; Webb *et al.*, 2011; Stübner *et al.*, 2014; Martin, 2016; Hughes *et al.*, 2019); undefined and/or depositional continuity between the domains (e.g., Honegger, 1983; Vannay & Steck, 1995; Long & Mcquarrie, 2010); and/or, most problematically, the discontinuous or segmented nature of the fault systems (e.g., Vannay & Steck, 1995; Epard & Steck, 2004; Kellett & Grujic, 2012; Stübner *et al.*, 2014; Kellett *et al.*, 2019). These problems have resulted in rock packages variably ascribed to different lithotectonic units, which has led to contrasting tectonic models. As such, recent studies have favoured terms that refer to broad metamorphic domains (e.g., Himalayan Metamorphic Front or Himalayan metamorphic core; Goscombe *et al.*, 2006; Cottle *et al.*, 2015).

Locally, in the Lahaul and Spiti regions of NW India, the boundary between the Tethyan Himalayan Sequence and the underlying Greater Himalayan Sequence remains poorly defined (Fig. 2). Evidence for a significant tectonic/structural contact is lacking (Vannay & Steck, 1995; Stübner *et al.*, 2014), and there is ongoing debate over the location of the boundary (Searle *et al.*, 1988; Thakur, 1998; Jain *et al.*, 1999; Webb *et al.*, 2011). Without a continuous bounding structure between lithotectonic domains, the terminology may not be uniformly applied. Therefore, where possible, this study favours the term Himalayan metamorphic core, following Cottle *et al.* (2015). Consistent with the scale, the Himalayan map shown in Figure 1 shows the classic lithotectonic subdivisions of the Himalaya, with all other maps (Figs. 2 & 3) grouping the Tethyan Himalayan Sequence and Greater Himalayan Sequence together with map units separated by lithostratigraphic and/or chronostratigraphic criteria.

Geological setting of the Zanskar Himalaya

The Zanskar Himalaya exposes rocks of the India-Asia suture zone and the north Indian passive continental margin (Fig 1; Searle *et al.*, 1988; Steck, 2003; Searle *et al.*, 2007). Noting the caveats above, lithostratigraphic units can broadly be grouped into the following three lithotectonic divisions from NE to SW: the Indus Suture Zone, the Tethyan Himalayan Sequence, and the Greater Himalayan Sequence. Within the Zanskar Himalaya, the Himalayan metamorphic core is dominated by the Greater Himalayan Sequence, but Cenozoic metamorphism and deformation has locally effected the lower portion of the Tethyan Himalayan Sequence and Indus Suture Zone.

Indus Suture Zone

The Indus Suture Zone in the Zanskar and Ladakh ranges is bounded to the north by the Ladakh batholith and to the south by a series of backthrusts that place folded Tethyan Himalayan Sequence rocks over the Indus Suture Zone (Fig. 1 & 2). The following units are included in the Indus Suture Zone:

1. Permian–Mesozoic slope-facies and proximal-basin deep-water marine sedimentary rocks (Lamayuru Complex), and Mesozoic deep-water sedimentary and basic volcanogenic rocks (Karamba Complex) that are distal equivalents of the Indian rift–passive shelf–slope succession (Thakur, 1981; Searle *et al.*, 1988; Gaetani & Garzanti, 1991; Robertson & Degnan, 1993; Robertson & Sharp, 1998).

2. Permian and Triassic exotic carbonate platform blocks (e.g., 'Mulbeck exotics'), which may represent platform edge extensional fault blocks or olistoliths of oceanic island carbonate associated with alkaline within-plate volcanic rock (Searle, 1983; Searle *et al.*, 1988; Robertson & Degnan, 1993; Sinha & Upadhyay, 1993; Robertson, 1998; Bhat *et al.*, 2023).

3. Upper Jurassic–Cretaceous intraoceanic island-arc sequence (Dras Arc Complex or Dras-Nindam terrane) dominated by andesite, basaltic andesite, dacite, and rhyolite (Dras Volcanics) as well as forearc volcaniclastic sedimentary rocks (Nindam Formation; Raz & Honegger, 1989; Reuber *et al.*, 1989; Robertson & Degnan, 1994; Clift *et al.*, 2000; Bhat *et al.*, 2019a). The Dras Arc Complex is a continuation of the lower crustal Chilas Complex of the Kohistan Arc to the west in Pakistan (e.g., Khan *et al.*, 1989).

4. Mélanges (locally ophiolitic) characterized by thrust imbricates, or broken formations, which include distal passive margin volcanic-sedimentary rocks (Lamayuru Complex and Karamba Complex), arc-type volcanic and volcaniclastic sedimentary rocks (Dras Arc Complex), sheared serpentinite, and rare glaucophane-bearing blueschist with a dominantly sedimentary mudstone matrix (Honegger *et al.*, 1989; Robertson, 2000; Bhat *et al.*, 2019b).

5. Post-collisional fluvio-alluvial conglomerate, shale, siltstone, and sandstone (Indus Group molasse) deposited in an intermontane basin along the Indus Suture Zone, with debris derived mainly derived from the Ladakh batholith to the north, units within the Indus Suture Zone, and less commonly from the Tethyan Himalayan Sequence to the south

(Garzanti & Van Haver, 1988; Searle *et al.*, 1988, 1990; Sinclair & Jaffey, 2001; Clift *et al.*, 2002; Wu *et al.*, 2007; St-Onge *et al.*, 2010).

Tethyan Himalayan Sequence

The Tethyan Himalayan Sequence is a Neoproterozoic to early Eocene sequence of siliciclastic and carbonate sedimentary rocks interstratified with the volcanic rocks of the Permian Panjal Traps (Fuchs, 1982; Searle, 1983; Gaetani *et al.*, 1986; Searle *et al.*, 1988). The Panjal Traps mark the opening of the Neotethys ocean and deposition of the early Permian–early Eocene Neotethyan sedimentary sequence on the Indian margin (Fig 2; Gaetani *et al.*, 1986; Shellnutt, 2018). The Tethyan Himalayan Sequence ranges from unmetamorphosed to lower-amphibolite facies. Balanced and restored cross sections show that following the intitial collision of India and Asia, the Tethyan Himalayan Sequence is estimated to have experienced at least 85 km of NE–SW shortening (Corfield & Searle, 2000). In the Zanskar Himalaya, the base of the Tethyan Himalayan Sequence (immediate hanging wall of the Zanskar Shear Zone) comprises the Haimanta Group, a thick succession of sedimentary and metasedimentary rocks that extends from the Chamba Formation at the base, through the Manjir, Phe, Parahio, Karsha, and Kurgiakh formations (Hughes *et al.*, 2018). Only the Cambrian rocks of the latter four formations are well exposed, with the Kurgiakh Formation ending at the regional Cambrian–Ordovician unconformity (Nanda & Singh, 1976; Gaetani *et al.*, 1986; Myrow *et al.*, 2006). The Haimanta Group is unconformably overlain by a sequence of Ordovician–early Eocene sedimentary rocks (Thaple–Chulung La formations; Fuchs, 1982; Baud *et al.*, 1984; Gaetani *et al.*, 1986; Garzanti *et al.*, 1987; Gaetani & Garzanti, 1991; Searle *et al.*, 2007). The Tethyan Himalayan Sequence is bounded to the north by the Indus Suture Zone and to the south, where present, by the Zanskar Shear Zone, a N- to NE-dipping, normal-sense shear zone (Figs. 1 & 2). The Zanskar Shear Zone is interpreted as the western strand of the South Tibetan Detachment System (e.g., Dèzes *et al.*, 1999), which is defined by a series of extensional shear structures that can be near continuously traced for ~2000 km along the Himalayan orogen (Fig. 1; Burchfiel *et al.*, 1992; Yin, 2006; Kellett *et al.*, 2019).

Greater Himalayan Sequence

The Greater Himalayan Sequence in the Zanskar Himalaya is a 50- to 55-km-thick (Zanskar Shear Zone to Main Central Thrust at the Kishtwar Window, plan-view; Fig. 2) Neoproterozoic

to Mesozoic metasedimentary sequence of greenschist- to upper-amphibolite-facies schist, gneiss, migmatite, and leucogranite. The metasedimentary rocks of the Greater Himalayan Sequence are inferred to represent metamorphosed Haimanta Group, though they also include younger Mesozoic formations of the Neotethyan shelf (Fig. 2; Honegger *et al.*, 1982; Searle *et al.*, 2007). The Greater Himalayan Sequence was metamorphosed during the late Eocene to Miocene (e.g., Searle *et al.*, 1999a; Vance & Harris, 1999; Walker *et al.*, 1999; Robyr & Lanari, 2020; Štípská *et al.*, 2020). The sequence is bounded to the southwest by a major south-vergent high-strain shear zone, the Main Central Thrust, which places the Greater Himalayan Sequence over the low-grade to unmetamorphosed Proterozoic sedimentary strata of the Lesser Himalayan Sequence (Fig. 1 & 2). Where exposed in the Kishtwar Window (Fig. 2), it is expressed as a condensed, inverted metamorphic sequence (amphibolite to greenschist facies) coincident with a ductile high-strain zone (1.5 to 3 km-wide) showing SW-vergent kinematic indicators (Stephenson *et al.*, 2000, 2001).

Regional geology of the Suru Valley area

The northern part of the Suru Valley area contains the metamorphosed equivalents of the Permian–Mesozoic Lamayuru Complex of the Indus Suture Zone (Honegger *et al.*, 1982), including graphite-rich and/or carbonate-bearing metasedimentary rocks, and metavolcanic rocks. To the south of the Indus Suture Zone, the region contains pelitic to psammitic rocks that are correlated with the Neoproterozoic Haimanta series; as well as metamorphosed carbonate-rich rock and associated metamorphosed volcanic rocks, which are respectively correlated with Mesozoic carbonate and the Permian Panjal Traps (Honegger *et al.*, 1982; Walker, 1999; Searle *et al.*, 2007). A variety of pre-collisional granitoid bodies, subsequently metamorphosed during Himalayan metamorphism, and post-collisional plutonic units formed during Himalayan metamorphism are present in the Suru Valley region. The oldest granitoids, which are recognised across Zanskar, comprise a series of prominent K-feldspar augen gneisses with Cambro-Ordovician magmatic ages (e.g., Pognante *et al.*, 1990). Similar ages are purported for the Suru Valley region, most notably for the Rangdum granite (e.g., Honegger *et al.*, 1982; Noble *et al.*, 2001). Permian granitoid bodies occur at Sankoo, Tongul, Parkachik, and Shafat (*ca.* 284–268 Ma; U-Pb zircon; Noble *et al.*, 2001; Horton & Leech, 2013). Leucogranite formed during Himalayan metamorphism with Miocene ages of crustal melting (20.8 ± 0.3 Ma, U-Pb monazite; Noble & Searle, 1995) is documented around Shafat.

Initial geological mapping of the Suru Valley was undertaken by Honegger *et al.* (1982), Honegger (1983), Searle (1983), Searle & Fryer (1986), Gilbert (1986), Fuchs (1987), Searle *et al.* (1988) and Walker *et al.* (2001), with constraints further east along the Zanskar Valley by Herren (1987), Kundig (1989), Stäubli (1989) and Dèzes *et al.* (1999). The maps of Honegger *et al.* (1982), Honegger (1983), Gilbert (1986), Searle & Fryer (1986), Searle & Rex (1989), Gapais *et al.* (1992), Searle *et al.* (1992) and Walker *et al.* (2001) display a series of kilometer-scale, SW-verging recumbent folds in the Himalayan metamorphic core underlain by a younger lower domal structure. Honegger *et al.* (1982) documented complex folding of Tethyan Mesozoic carbonate and Permian Panjal Traps in the sequence. Searle *et al.* (1992, 1999b) and Walker *et al.* (2001) determined that these structures were bound to the NE of the Greater Himalayan Sequence by the Zanskar Shear Zone. Honegger (1983) mapped a series of discontinuous detachments (equivalent to the Zanskar Shear Zone) between the Greater Himalayan Sequence and the Tethyan Himalayan Sequence, and a fault (termed the 'Zanskar-Sanku-Pindras Thrust') between the Greater Himalayan Sequence–Tethyan Himalayan Sequence and Indus Suture Zone that is dominantly defined by backthrusting. The Zanskar Shear Zone was first described and traced from the Zanskar Valley, NW to the Suru Valley, by Gapais *et al.* (1984), Gilbert (1986), Searle & Fryer (1986), and Herren (1987). To the southwest of the Suru Valley, low-grade sedimentary rocks are juxtaposed above the Greater Himalayan Sequence by either a detachment fault (Honegger, 1983) or a steep, late-stage, NE-vergent backthrust (Warwan backthrust; Searle *et al.*, 1992). This structure is herein referred to as the Warwan fault, and is reportedly exposed at the SW periphery of the mapped region (Fig. 2). The low-grade to unmetamorphosed (meta-)sedimentary rocks in the hanging wall of the fault have been correlated with Mesozoic platform sedimentary rocks (Honegger *et al.*, 1982), Kashmir Tethyan basin strata (Singh *et al.*, 2000), or Proterozoic–Mesozoic Kashmir sedimentary units (Searle *et al.*, 1992, 1999a). The hanging wall units of the Warwan fault can therefore be viewed as belonging to the Tethyan Himalayan Sequence. In this study, mapping by remote sensing affirms this correlation. The Main Central Thrust is not exposed in the mapped area, but it is exposed to the south of the Suru Valley region around the Kishtwar Window (Fig. 2). The trace of isograd surfaces from the Suru Valley region to the Kishtwar window produces a map-scale closure between a right-way-up and inverted metamorphic sequence (Honegger, 1983; Searle & Fryer, 1986).

Previous metamorphic constraints and geochronology of NW India

On average, peak metamorphic pressures from the Himalayan metamorphic core in the Suru Valley area (~6–12 kbar; Fig. S1a) are higher than those recorded in other regions of NW India, including: Kishtwar at ~4–10 kbar (Fig. S1b), Zanskar Valley and Upper Lahaul at ~5–10 kbar (Fig. S1c), and Lahaul and Himachal Pradesh at ~5–9 kbar (Fig. S1d; see locations in Fig. 2). A migmatitic sample from the Gumburanjun dome is an exception, with a high pressure of 11.7 ± 1.0 kbar and 11.8 kbar (no reported error; Dèzes *et al.*, 1999; Robyr, 2002, Fig. S1c). On average, peak metamorphic temperatures in the Suru Valley area (~500–700 °C; Fig. S1a) represent on average a decreased temperature range when compared to all other regions (~500–800 °C; Fig. S1b–d). All *P-T* conditions are constrained through conventional thermobarometry, multi-equilibrium thermobarometry, and/or phase equilibrium modelling (Fig. S1). Differences in the *P-T* conditions of the Suru Valley region agree with observations reporting a dominance of higher-pressure, kyanite-bearing assemblages (e.g., Searle *et al.*, 1992; Walker *et al.*, 2001) in comparison to other regions that are more dominated by lower-pressure, sillimanite-bearing and migmatitic assemblages (e.g., Vannay & Grasemann, 1998; Manickavasagam *et al.*, 1999; Searle *et al.*, 1999b; Stephenson *et al.*, 2000; Robyr, 2002; Finch *et al.*, 2014).

The Himalayan metamorphic core in NW India consistently preserves a record of mid-Eocene to Oligocene prograde–peak metamorphic ages ranging from *ca.* 44–27 Ma (Fig. S2; U-(Th)-Pb zircon, monazite, xenotime, and uraninite; Sm-Nd garnet; Vance & Harris, 1999; Walker *et al.*, 1999; Chambers *et al.*, 2009; Thöni *et al.*, 2012; Horton & Leech, 2013; Stübner *et al.*, 2014; Robyr & Lanari, 2020; Štípská *et al.*, 2020). Few data points from previous studies are available from the Suru Valley region. However, Sm-Nd core–rim garnet ages from kyanite-zone samples give lower Oligocene ages (*ca.* 33–28 Ma; Vance & Harris, 1999), that are consistent with prograde–peak metamorphism within lower structural levels of the Suru Valley region .

LITHOSTRATIGRAPHIC ARCHITECTURE AND GEOLOGICAL MAP

The Suru Valley region exposes a volcanic and siliciclastic dominated lithostratigraphic succession comprising 17 map units. Map units dip gently to the north and north-east and original stratigraphic contacts are structurally transposed. Figure 3 shows a geological map of the re-

gion, and Figure 4 displays associated cross-sections. Lithological units are referenced from these figures. Seven units are assigned to the Indus Suture Zone—which is further subdivided into the Indus Group, the Dras Volcanics, and the Lamayuru Complex—with the remaining units belonging to the Tethyan and Greater Himalayan Sequence. No subdivision between the Tethyan and Greater Himalayan Sequence is shown in Figures 2–4 owing to the lack of a continuous tectonic boundary between these sequences and correlative metamorphosed sedimentary or volcanic lithological units within both sequences (e.g., group A metavolcanic rock; mixed semipelite, metacarbonate, and pelite; and metacarbonate; Figs. 3 and 4; Searle *et al.*, 2007). Representative field photographs of map units are given in Figure 5. Supplemental Text details the methods employed in geological mapping (including the distribution of mapping by fieldwork and remote sensing within the mapped area) and structural and petrographic analysis. This file also includes detailed descriptions of all map units with the exception of the Indus Group molasse, which is the highest-structural unit and is only present in the area mapped with remote sensing. The field-mapped area is outlined by the dashed white box in Figure 3.

The Dras Volcanics (Fig. 5a–b) dominantly comprise extrusive volcanic rocks (basalt and basaltic-andesite), with subordinate epiclastic breccia. They form part of an interpreted island-arc terrane known as the Dras Arc Complex (after Robertson & Degnan, 1994; Bhat *et al.*, 2019a) or Dras-Nindam terrane (after Walsh *et al.*, 2021). Locally, these units are cut by the gabbroic to granodioritic Kargil Intrusives (Honegger *et al.*, 1982; Dietrich *et al.*, 1983; Bhat *et al.*, 2019a; Walsh *et al.*, 2021). The metasedimentary rocks of the Lamayuru Complex (Fig. 5c–e) from deeper to shallower lithostratigraphic levels include: (1) graphitic pelite; (2) mixed pelite, psammite, and semipelite; and (3) mixed graphitic pelite, semipelite, and metacarbonate. This sequence is intercalated with metavolcanic rocks (group B metavolcanic rock; Fig. 5f).

The metasedimentary rocks of the Greater Himalayan Sequence–Tethyan Himalayan Sequence (Fig. 5g–k) from lithostratigraphically deeper to shallower levels include: (1) pelite; (2) a mixed package of psammite, pelite, and semipelite; (3) psammite, locally with preserved cross-stratification; (4) thick-bedded metacarbonate; and (5) a mixed package of semipelite, metacarbonate, and pelite. Like the Lamayuru Complex, the Greater Himalayan Sequence–Tethyan Himalayan Sequence is also intercalated with metavolcanic rocks (group A metavolcanic rock; Fig. 5l). The metamorphosed volcanic rocks present in the Lamayuru Complex and the Greater Himalayan Sequence–Tethyan Himalayan Sequence are distinguished based on

structural position, lithological correlation, and overall lithostratigraphic setting. Both groups are characterized by a fine- to medium-grained silica-poor and ferromagnesian-rich mineral assemblage that includes a combination of actinolite, tremolite, hornblende, albite/plagioclase, chlorite, biotite, epidote, and/or muscovite. This mineral assemblage is consistent with a volcanic and/or subvolcanic rock protolith. The volcano-siliciclastic sequence of the Greater Himalayan Sequence–Tethyan Himalayan Sequence is variably associated with pre-Himalayan age meter- to kilometer-scale granitoids that are metamorphosed to biotite-muscovite syenogranite and garnet-biotite-muscovite granite assemblages (Fig. 5m–n), and intruded by Himalayan-age centimeter- to meter-scale lenses of garnet tourmaline leucogranite (Fig. 5o). Leucogranite occurs as localized $<$ 40-m-thick bodies in the area; migmatite (*sensu stricto*) does not occur in the main study area. *in situ* migmatization (Fig. 5p) occurs ~20 km SSW of Rangdum, outside of the study area shown in Figure 3; detailed field and petrographic observations of a traverse through this zone (Lalung Valley; Fig. 2) are incorporated into the study to ensure that all zones of regional metamorphism are documented.

The progressive change documented from deeper to shallower lithostratigraphic levels in the Himalayan metamorphic core are interpreted to represent laterally continuous regional lithostratigraphic packages. These packages comprise: (1) graphitic pelite; (2) mixed pelite, psammite, and semipelite; and (3) mixed graphitic pelite, semipelite, and metacarbonate of the Lamayuru Complex (Fig. 5c–e). Or, they comprise (1) pelite; (2) mixed psammite, pelite, and semipelite; (3) psammite; (4) metacarbonate; and (5) mixed semipelite, metacarbonate, and pelite of the Greater Himalayan Sequence–Tethyan Himalayan Sequence (Fig. 5g–k). Regional metamorphism and polyphase deformation have reworked the original stratigraphic sequence. Nevertheless, the sequence remains readily discernable for the following reasons. Firstly, folding transposed but did not disaggregate the original lithostratigraphic units and associated sedimentary structures (e.g., Fig. 5h, i). Second, in the absence of large quantities of fluid during regional metamorphism, compositional mass transfer is restricted to the grain and micro-domain scale (Walther & Orville, 1982). Consequently, compositionally defined sedimentary features, such as cross-stratification, graded bedding, and changes in mudstone content in a turbidite succession, remain identifiable following regional metamorphism (e.g., Myers, 2001; Dyck *et al.*, 2019). Such features are readily observed in the Suru Valley area (Fig. 5i).

The macroscale architecture of the study area, shown in Figures 3 and 4, is that of a tightly

folded package of metasedimentary and metavolcanic rocks with the deepest lithostratigraphic units exposed in the center of the mapped area between Panikhar and Tongul due to late open folding. Higher structural levels of the Greater Himalayan Sequence are exposed toward the edge of the mapped area and are marked by the increased abundance of (1) mixed semipelite, metacarbonate, and pelite (pale blue) and (2) group A metavolcanic rocks (dark green). These units correlate to the shallowest lithostratigraphic levels, yet they are also consistently folded as thinner, discontinuous horizons into the lowest structural levels. The eastern and western portions of the map show the transition from the Greater Himalayan Sequence to the Tethyan Himalayan Sequence, across the Zanskar Shear Zone and the possible Warwan fault. The northern portion of the mapped area is underlain by the unmetamorphosed to metamorphosed units of the Indus Suture Zone, which are tectonically juxtaposed against the Greater Himalayan Sequence–Tethyan Himalayan Sequence (no tectonic boundary). These units are similarly deformed by late open folds. Pre-Himalayan granites outcrop at a range of structural levels, from lower structural levels in the southeast at Shafat, to higher levels in the north at Karpokhar.

STRUCTURAL ARCHITECTURE

Five generations of planar and/or linear structural features are identified in the study region. Three penetrative fabrics (S_1–S_3); three linear elements (L_1–L_3); and four macroscale fold generations (F_2–F_5) are documented and then discussed in the context of five interpreted deformation events (D_1–D_5). A summary of the structural features defining these deformation events are presented in Table 1, and Figures S3 & S4 show the show the spatial distribution of recorded planar and linear structural elements across the mapped region. Field photographs documenting examples of planar and linear fabrics are shown in Figure 6, and macroscale fold interference patterns are shown in Figure 7. Finally, a simplified geological map of the region separated into six zones with associated stereonet data for D_1–D_3 planar and linear structural elements is shown in Figure 8.

The nomenclature used to record planar and/or linear structural elements and their associated deformation events keeps track of superposed fabrics and mineral assemblage relationships by locality. These fabrics and associated assemblages represent markers within the context of progressive regional metamorphism and deformation. They most likely developed at different structural levels at various times and do not imply discrete temporal events.

Deformation fabrics (S_1–S_3) in the Suru Valley region are identified in metasedimentary rocks by the alignment of phyllosilicate minerals and flattening of quartz and feldspar. In metavolcanic rocks, they are defined by the preferred orientation of chlorite and biotite, and locally by amphibole mats and plagioclase-quartz aggregate laminations. Fabrics are associated with well-developed lineations (L_1–L_3) defined in metasedimentary rocks by elongate rods of quartz and feldspar and the aspect ratio of phyllosilicate minerals. In metavolcanic rocks, the lineation is defined by the orientation of actinolite, tremolite, and hornblende, and the aspect ratio of chlorite and biotite. Detailed descriptions of fabric-defining metamorphic mineral assemblages for each deformation event are included in the Supplemental Text.

$\mathbf{S_0/S_1/L_1}$

The oldest deformation fabric (S_1) identified in the study area is manifest as a schistosity. S_1 lies parallel or subparallel to the bedding plane (S_0) that is locally preserved in metasedimentary rocks (Fig. 6a). S_1 is associated with a well-developed stretching lineation (L_1). Where minimally disturbed, S_1 dips moderately to the NE, and L_1 plunges to the E. However, S_1 is commonly reoriented by later sequences of deformation, and thus a clear original orientation of early planar elements is rarely preserved (Fig. S3). L_1 is dominantly coaxial to the most penetrative later phases of deformation (D_2 and D_3), and thus is likely less reoriented (Fig. S4).

S_1 is documented in all units except the pelite unit, where a pervasive S_2 is the earliest planar fabric recognized, and the Dras Volcanics. S_1 is best preserved in psammite-rich zones of the mixed psammite, pelite, and semipelite (Fig. 6a). D_1 represents the first phase expressed, which is poorly constrained to have had a NE–SW orientation.

$\mathbf{S_2/L_2/F_2}$

S_2 comprises a crenulation cleavage, which lies axial planar to crenulations of S_1 (Fig. 6a, b) and that dominantly develops into a penetrative schistosity (Fig. 6a). S_2 dips gently to moderately to the NW to NE (locally to the SW and SE; Fig. 6c; Fig. S3). The associated well-developed L_2 plunges to the NW to NE (Fig. S4), though shows an oblique orientation to dip direction, consistent with non-coaxial deformation. Dominant thrust-sense shearing can be observed in augen and/or locally developed C-S fabrics (Fig. 6d).

S_2 is axial planar to the associated folds (F_2; Fig. 6b). F_2 is present as generally type 2 (occasionally type 3 or 1c; Ramsay, 1967), tight-to-isoclinal (rarely close), inclined, overturned, or recumbent, meter- to kilometer-scale folds of the S_1 fabric (Fig. 7). Drag folds and secondary folds are associated with the development of larger folds. Limb thickness, as measured perpendicular to the dip of the axial surface, varies from centimeter-scale to ~3 km across the mapped area. The inter-limb angle of macroscale folds, defined here as those that can be distinguished at map-scale (i.e., approximate wavelength $>$ 200 m), is tight–isoclinal at higher structural levels and decreases to dominantly isoclinal at lower structural levels, where evidence of S_1 is poorly preserved. S_2 and L_2 are coaxial with S_1 and L_1. Shearing and folding of S_1 is interpreted as resulting in S_2. Folding brings S_1 compositional layering progressively into alignment with S_2 (e.g., Fig. 6a).

The best developed kilometer-scale F_2 folds are observed at Karpokhar, Donara, and Tongul (Fig. 3; A-A' and C-C' in Fig. 4). Characteristic examples of F_2 folds are shown in Figures 6a, b, c & 7. The Karpokhar antiform is located directly south of Sankoo at Karpokhar village (Fig. 3); the antiform is an overturned, northeast-plunging, open fold of garnet-biotite-muscovite granite and mixed psammite, pelite, and semipelite (A-A' in Fig. 4 and Fig. 6c). Linked centimeter- to meter-scale asymmetric parasitic F_2 folds are found on both fold limbs, and isoclinal F_2 synforms are developed on the N- and S- side of the antiform (Fig. 3 and A-A' in Fig. 4). A significant contast in competency is inferred between the granite and metasedimentary rocks, with the interpreted higher competency granite causing the fold hinge to be significantly more open than other F_2 folds (Fig. 6c). Despite the open fold hinge, these lithological units have a dominant S_2 (and/or subparallel S_1) fabric that is best developed in the metasedimentary rocks. The southern side of the Karpokhar antiform locally records a moderately to steeply S-dipping S_2 fabric (Fig. 3 and A-A' in Fig. 4), and is interpreted to be characterized by a minor N-dipping blind thrust to accommodate competency variation between the granite and metasedimentary rocks (A-A' in Fig. 4).

The Donara antiform is located directly N of the Donara campsite along Chellong Nala (Fig. 3). It is an kilometer-scale, open, SW-plunging overturned antiform that folds the mixed semipelite, metacarbonate, and pelite; mixed psammite, pelite, and semipelite; interlayered garnet-biotite-muscovite granite and metavolcanic rock group A (A-A' in Fig. 4 and Fig. 7a). A kilometer-scale isoclinal F_2 synform extending from Tanak peak SE of Tongul occurs near

the hinge of the Donara antiform (Fig. 3). The axial traces of these folds start to converge in this area due to later stage warping or folding that is interpreted to relate to movement on the Warwan fault located farther SW (A-A' in Fig. 4 and Fig. 7a).

The Tongul antiform, located just south of Tongul (Fig. 3), is a kilometer-scale, overturned-to-recumbent, isoclinal, NE-plunging antiform developed within the mixed psammite, pelite, and semipelite; mixed semipelite, metacarbonate, and pelite; and group A metavolcanic rock (Fig. 7c). Late open folding (F_4) reorients the Tongul antiform from early SW-vergence (B-B' and C-C' in Fig. 4 and Fig. 7c).

S_2 is the most penetrative structural fabric in the Zanskar Himalaya and it is recognizable at all structural levels and in all lithologies. Large (up to kilometer-scale) F_2 folds are best preserved in the mixed semipelite, metacarbonate, and pelite and/or pure metacarbonate, which deformed in a ductile manner and as such highlights the folding of D_1 fabrics and any subparallel S_0 (e.g., Fig. 7a–c). Due to the intensity of S_2 fabric development, preservation of folding at smaller scales (meter scale) and evidence of crenulation cleavage is best observed in the psammite of the mixed psammite, pelite, and semipelite (e.g. Fig. 6a). S_2, L_2, and F_2 represent the effects of continued NE–SW directed deformation. D_2 fabrics and structures have accommodated significant thickening of the Himalayan metamorphic core through microscale–macroscale isoclinal folding. Thrust fabrics show that significant shearing occurred during D_2.

$\mathbf{S_3/L_3/F_3}$

S_3 comprises a mylonitic fabric (locally displaying C-S or composite C-S-C'), or crenulation cleavage that is axial planar to crenulations of S_1 and S_2. L_3 is associated with a normal sense of shear as identified by C-S-C' fabrics, rotated porphyroblasts, and/or augen (Fig. 6e). An oblique orientation of L_3 to dip direction and evidence of extensional boudins perpendicular to stretching lineations are visible in outcrop, and represent non-coaxial simple shear. S_3 dips gently to moderately to the N to ENE (locally to the NW and SE; Fig. S3), and L_3 plunges towards the ENE (Fig. S4). S_3 and L_3 are broadly coplanar or coaxial with S_2 and L_2. Shearing and/or folding of S_2 are interpreted to result in the development of S_3.

S_3 is axial planar to associated folds (F_3). F_3 is dominantly restricted to the northern area of the map (Fig. 3; Fig. S4). These folds are type 1c (occasionally type 1b or 2; Ramsay, 1967), open to close (variation from gentle to isoclinal as a function of position with respect to

the shear zone), inclined, or overturned, or recumbent, meter-scale (rarely kilometer-scale) folds of S_2 and/or S_1 fabric (Fig. 6f). F_3 folds generally show normal-vergence. A kilometer-scale F_3 antiformal backfold (Barsoo antiform) east of Sankoo, which folds the Dras Volcanics and the underlying Lamayuru Complex, is defined by limbs that are inclined to open, and a ESE-plunging fold axis (B-B' in Fig. 4 and Fig. 6g). Secondary folds are associated with development of this F_3 (Fig. 6g). Another kilometer-scale F_3 antiformal backfold is interpreted from remote sensed mapping north of Tapshah and southwest from Sankoo (Fig. 3, and C-C' in Fig. 4). Limb thickness of the F_3 structures, as measured perpendicular to the dip of the axial surface, varies from the centimeter to meter scale (generally < 5 m), although the Barsoo antiform has a thickness of 2 km.

Three dominant shear zones are documented in the area: (1) the Zanskar Shear Zone, (2) the Dras shear zone (juxtaposing the Dras Volcanics in the NE and Lamayuru Complex in the SW), and (3) the Lamayuru shear zone (juxtaposing the Lamayuru complex in the NE with the units of the Indian slope–shelf to the SW). Shear zones are defined based on footwall-hanging wall relations (with respect tolithostratigraphy and metamorphic grade) and ductile and brittle fabric development. These structures are displayed in Figure 3 and across the lines of section in Figure 4. The term Zanskar Shear Zone solely refers to the intense normal-sense shearing that occurred during exhumation (e.g., Patel *et al.*, 1993), and excludes previous thrust fabrics that likely developed during the early stages of crustal thickening where the Greater Himalayan Sequence was underthrust below the Tethyan Himalayan Sequence (e.g., Patel *et al.*, 1993; Dèzes *et al.*, 1999; Robyr, 2002; Finch *et al.*, 2014). The Dras and Lamayuru shear zones record a heterogeneously distributed zone of polyphase normal-thrust movements that is herein termed the Sankoo fault zone. These polyphase movements initiated prior to the India-Asia collision (e.g., Robertson, 2000). Given the complicated polyphase history across all three of these shear zones, this study focuses on later (dominantly normal-sense) movements that occurred during D_3.

At the highest structural levels of the Greater Himalayan Sequence, in the southeastern portion of the map, S_3 and L_3 are pervasive within an ~3- to 4-km-thick mylonitic fault zone within the footwall of the Zanskar Shear Zone (Figs. S3 & S4), which is dominated by metacarbonate, group A metavolcanic rock, and mixed semipelite, metacarbonate, and pelite. Toward the NE extent of the Zanskar Shear Zone, S_3 and L_3 occur within an ~100-m-thick zone. In these

areas, adjacent to the Zanskar Shear Zone, S_3 is dominantly mylonitic in nature, and displays a transition from ductile to brittle structures as observed by tension gashes crosscutting the shear fabric. In the northern portion of the map, S_3 and F_3 show development of a broad zone of crenulated fabric in the metasedimentary and metavolcanic rock units of the Lamayuru Complex, with a penetrative mylonitic fabric (S_3 and L_3) developed locally (50–250 m in thickness) along the footwall contact of the shear zones (Figs. S3 & S4). Away from these shear zones, S_3 and the associated crenulation lineations are observed within the mixed psammite, pelite, and semipelite. They are commonly displayed in the pelite layers that facilitate the development of crenulations more readily than the more competent psammitic intervals. At the lowest structural levels, S_3 locally displays a strong crenulation cleavage that is developed as a penetrative schistosity.

Normal shearing and movement on the Zanskar Shear Zone and late movement on the Sankoo fault zone in the northern part of the map are interpreted to comprise D_3. Due to the growth of retrograde mineral phases during D_3 (e.g., chlorite and biotite growth along shear bands), D_3 is interpreted as a post-metamorphic peak event. The transition from thrust-sense fabrics in D_2 to normal-sense shear fabrics in D_3 and the coaxial nature of the respective structures can be used as evidence to suggest that D_3 largely involved the reactivation of D_2 structures, with consistent orientation of the major stress direction (overall compressional regime; e.g., Kellett *et al.*, 2019). Observed extensional boudins imply that there may have been both a flattening and an extensional vector, or strike-slip component, resulting in non-ideal simple shearing during development of the Zanskar Shear Zone fabrics, as has been previously suggested (see Walker, 1998; Walker *et al.*, 2001). In contrast, the northern portion of the mapped area displays a wide zone of distributed shearing and folding across the Lamayuru Complex. Late-stage open folding (F_3 backfolds) in this region appears to have overturned faults (e.g., Lamayuru shear zone) and produced apparent normal-sense or thrust-sense movement. Although in parts of the northern area it is possible to distinguish the origin of these movements from early pre-collisional thrusting and subsequent late warping during D_3, it is often difficult. We infer the zone to be characterized by both normal-sense and backthrust movement (thrusting to the NE). Therefore, D_3 can be described as a protracted phase of deformation initially propagating from NE to SW, characterized by normal-sense movement, and later progressing into NE-directed backthrusting.

$\mathbf{F}_4$

F_4 are kilometer-scale, type 3 (Ramsay, 1967), open symmetric, cross-folds. Fold axes plunge gently towards the NE (e.g., between Panikhar and Parkachik in Fig. 3 or zone B in Fig. 8) and SW, with axial surfaces dipping steeply towards the NW or SE. No mesoscale or microscale fabrics are directly associated with F_4, though F_4 structures warp D_1–D_3 structures. Older mineral stretching lineations (L_1–L_3) are minimally affected by the F_4 structures, as fold axes are subparallel to the preexisting lineations (see Table 1 and Fig. S4). L_3 fabric crenulations are often developed near F_4 structures (Fig. 3), and therefore, it is possible that F_4 may be associated with a late D_3 event. Alternatively, D_3 structural elements may represent sites of crustal weakness where further buckling during D_4 is focused. F_4 kilometer-scale open cross-folds of previous fabrics are best observed between Panikhar, Tongul, and Parkachik (Fig. 3, and B-B' and C-C' in Fig. 4).

The southern limbs of F_4 folds are often defined by generations of transposed earlier folds that are now NE-verging structures. This is observed south of Tongul, where multiple fabric generations dip to the S, defining the lower limb of an overturned N-verging F_2 fold (B-B' and C-C' in Fig. 4). Mineral growth-fabric relations indicate that these fabrics are consistent with N- to NE-dipping fabrics found elsewhere in the mapped area. These fabrics are assigned as S_1 and S_2 and indicate that F_4 structures refold previous linear and planar structures and are the direct result of NE-vergent F_2 structures. Importantly, NE-vergent folds in the Suru Valley region do not represent a prolongation of early NE-directed folds and thrusts that predate SW-directed folding and thrusting (cf. Steck, 2003).

$\mathbf{F}_5$

F_5 are late kilometer-scale folds that are open and symmetric with upright/steeply dipping axial surfaces that trend to the NW and/or SE. No mesoscale or microscale fabrics are associated with F_5, and F_5 structures appear to fold D_1–D_3 structures. F_5 folds are best observed in the region between Sangrah and Parkachik (Fig. 3). The S_2 fabrics dip away from the intersection of D_4 and D_5 folds (Fig. S3) and L_2 are perpendicular to the axial surface of F_5 folds (Fig. S4). This results in a crustal doming pattern. D_3 crenulations and planar S_3 observed on the hill between Panikhar and Parkachik are perpendicular to the axis of F_5, and crenulations display normal-sense vergence (i.e., cascading folds), which implies that such generations are likely distinct.

Fold axes are not displayed on areas outside of the main mapping area. However, remote sensing indicates that at the NE and NW portions of the map (Fig. 3), the Tethyan Himalayan Sequence, Lamayuru Complex and intervening Lamayuru shear zone are folded around the axis of large NW–SE-oriented kilometer-scale open synforms. These synformal structures are inferred to be coincident with the D_5 event on the basis of their scale, orientation, symmetrical nature, and inferred timing, which postdate all phases of movement on the Lamayuru shear zone.

Structural zones

The mapped region is separated into six structural zones, with stereonet data displaying planar and linear structural elements from D_1–D_3 (Fig. 8). Zones were selected based on completed transects along valleys and the overall structural architecture.(s) and (c) refer to mineral stretching and crenulation lineations, respectively. Zones are presented and discussed in clockwise order: easternmost zone A displays D_1–D_3 fabrics; central zone B preserves D_2 fabrics warped by late D_4 and D_5 folding; westernmost zones C and D document D_2 and D_3 fabrics; and zones E and F located in the north of the mapped area record D_1 and D_2 fabrics subsequently reoriented by D_3 crenulations and folding. The following observations are summarized with reference to Figure 8:

1. Zone A: Linear and structural planar elements in this zone are co-planar across D_1–D_3. Foliation dips to the NE, and stretching lineations plunge to the ENE. No late folds are present in this zone, as is supported by the consistent orientation of structures and map units.

2. Zone B: Poles to S_2 define a centred cluster that represents a gently dipping S_2 in all directions. $L_2(s)$, $L_2(c)$, and mesoscale F_2 record a strongly bipolar ENE-WSW distribution. These observations are also broadly consistent for the recorded structural and planar elements of D_3. F_4 only weakly reorients the linear elements due to the coaxial orientation of the fold hinge and linear structural elements. The NNW–SSE trending F_5 domal culmination results in the warping and bipolar distribution of the linear structural elements of both D_2 and D_3.

3. Zone C: Poles to S_2 record a distributed girdle. This is not indicative of a fold axis as the local foliation changes from moderately NE-dipping, to steeply dipping, to overturned and SW-dipping (see SW end of A-A' in Fig. 4). Instead, the distribution of S_2 is inferred to

result from the development of the Warwan fault, which produced progressive steepening and overturning of preexisting planar and linear structural elements. The Warwan fault may transect the SW extent of section A-A' or within ~7 km SW of A' (Honegger, 1983; Searle *et al.*, 1992). $L_2(s)$ displays a bipolar E–W plunge. S_3 is characterized in this region by a NW-dipping foliation and $L_3(c)$ varies from W- to N-plunging.

4. Zone D: Poles to S_2 and S_3 define a mean NW-dipping foliation with NW-plunging $L_2(s)$, $L_3(s)$, and $L_3(c)$.

5. Zone E: Poles to S_1 record a poorly distributed girdle defining a W–E-oriented F_3 axial plane. An E-plunging $L_1(s)$ is only weakly disturbed by F_3. Poles to S_2 define a distributed girdle that represents an ENE plunging F_2 that is later disturbed by F_3. F_2 is locally recorded here as a distributed girdle due to a strong competency contrast between the rigid metamorphosed granite south of Sankoo and the surrounding metasedimentary rocks, which yield a fold (Karpokhar antiform) that is both open and overturned (see A-A' in Fig. 4). Subsequent mesoscale F_3 and $L_3(c)$ are documented, with fold axes subparallel to F_2. Due to the coaxial nature, this is represented as a combined F_2/F_3 pole to the girdle plane. A NE-plunging $L_2(s)$, $L_2(c)$, and mesoscale F_2 are weakly reoriented by F_3. D_3 planar and linear structural elements define a NE-dipping S_3 with an ENE-plunging $L_3(s)$ and bipolar E–W distribution of $L_3(c)$ and F_3. D_3 planar and linear structural elements are locally warped around late F_5.

6. Zone F: Poles to S_1 and S_2 record a distributed girdle that defines a W–E-oriented F_3 axial plane. An ESE-plunging $L_1(s)$ and E-plunging $L_2(s)$ are only weakly reoriented by F_3. D_3 is characterized in this zone by an E-dipping S_3 and ENE-plunging $L_3(s)$, $L_3(c)$, and F_3. S_3 appears to be consistent around the hinge and limbs of the antiform, which indicates that the fabric is either synchronous or postdates D_3 (Fig. S3). The axial plane of the antiform is coaxial with mesoscale F_3, supporting a kilometer-scale F_3 (backfold) interpretation.

METAMORPHIC ARCHITECTURE

Given the widespread distribution of both pelite and metabasite in the study area, the relationship of progressive fabric development (as outlined above) with respect to the prograde growth of metamorphic index minerals can be constrained using both rock types. Bulk compo-

sition is known to control the timing of porphyroblast growth in any one rock type; therefore, observations are restricted to rock types of similar bulk composition (e.g., pelite and semipelite rather than psammite). The objective is to constrain the relative timing of mineral growth during metamorphic peak with respect to the penetrative deformation events outlined above and illustrated by photomicrographs in Figure 9, and then summarized in Figure 10. The relative timing of growth of additional metamorphic mineral phases is detailed in the Suppelemental Text. These observations are then compared to relationships between the trace of metamorphic mineral isograds and mesoscale–macroscale lithotectonic features, as documented in Figures 3, 4, 11 and 12. Index minerals can be associated with varying assemblages during a prograde–retrograde metamorphic cycle, which further enables the recognition of different generations of mineral growth (i.e. I, II, and III).

Pelite index minerals

The pelitic component of the Himalayan metamorphic core displays a complete Barrovian metamorphic sequence from chlorite zone (greenschist facies) to sillimanite+K-feldspar zone (upper-amphibolite facies; Fig. 11). An increase in grade is observed moving structurally down-section from the Zanskar Shear Zone to the migmatitic zone exposed in the Lalung Valley 20 km SSW of Rangdum (Fig. 2 & 3), followed by a decrease in grade moving farther south and/or west towards the Warwan fault (Honegger, 1983; Searle *et al.*, 1992) or Main Central Thrust zone (Stephenson *et al.*, 2000, 2001).

Chlorite is the first Barrovian index mineral observed in the pelitic component of the Suru Valley region. Chlorite locally occurs as small (submillimeter) porphyroblasts in the sheared rocks belonging to the Zanskar Shear Zone and associated normal-sense shear zones. Where present in the low-grade rocks near Sankoo and Rangdum (Fig. 3), tabular chlorite defines S_1 and is reoriented parallel to S_2 (chlorite I). Chlorite porphyroblasts are wrapped by S_3 and preserve cleavage domains perpendicular to the mylonitic fabric and are interpreted as having been originally aligned with S_1 or S_2. Taken as a set, these observations suggest that chlorite grew syn-D_1, and growth continued during the early stages of D_2. Retrogressive chlorite (chlorite II) is also associated with C-S-C' fabrics that developed along S_3 shear bands.

The biotite isograd is marked by the entrance of submillimeter- to millimeter-scale poikiloblasts of biotite in graphitic pelite (Lamayuru Complex) near the Dras shear zone and in the

mixed metacarbonate, semipelite, and pelite (Greater Himalayan Sequence–Tethyan Himalayan Sequence) near the Zanskar Shear Zone. Dominantly tabular subhedral–euhedral biotite grains are aligned with S_2 (biotite I). At higher grades biotite poikiloblasts overgrow the S_2 fabric and preserve matrix-concordant inclusion trails (biotite II, Figure 9a). These observations suggest that biotite commenced growth syn-D_2 and growth and recrystallization continued post-D_2. Retrogressive biotite growth was coincident with garnet breakdown and is locally also associated with S_3 C'-fabrics (biotite III).

Garnet occurs as subhedral to euhedral poikiloblasts that occasionally overgrow isoclinal F_2 microfolds. Garnet cores typically display spiral or concordant inclusion trails with respect to the main S_2 fabric (garnet I, Fig. 9b; Fig. S6a). Generally, inclusion-poor rims that overgrow the S_2 fabric are also present at staurolite-grade and above (garnet II). Where the S_2 fabric is crenulated by D_3, inclusions in the garnet porphyroblasts appear discordant to the developing S_3 fabric (Fig. S6b). In localities where S_3 has become dominant, S_3 wraps both phases of garnet growth and inclusion trails are discordant to the main fabric. These observations suggest that most garnet growth occurred syn- to post-D_2 and prior to D_3.

Staurolite occurs as subhedral to euhedral tabular to rounded grains and is found near the garnet rims (garnet I & II are locally resorbed) or as matrix poikiloblasts. In high-Al pelite (which is generally found adjacent to mixed semipelite, metacarbonate, and pelite), matrix staurolite locally displays a shape preferred orientation parallel to S_2-aligned micas, and likely nucleates mimetically on such phyllosilicate minerals (Fig. S7a; e.g., Patrick & Lieberman, 1988; Gibson, 1993). In such samples, staurolite dominantly extinguishes along the long axis, parallel to phyllosilicate grain extinction, which implies possible structural control from earlier mica. S_2-aligned staurolite commonly displays matrix-concordant graphitic inclusion trails, with no evidence of rotation of prismatic staurolite after growth. In all other pelitic samples, staurolite crosscuts the S_2 fabric and preserves S_2-concordant inclusion trails (Figure 9c). No distinct alignment of the long axis of staurolite with respect to L_2 is visible in outcrop (Fig. S6c). S_3 wraps around staurolite porphyroblasts and is associated with post-peak mineral assemblages. These observations suggest that staurolite growth dominantly occurred post-D_2, with localized syn-D_2 and/or post-tectonic mimetic growth occurring in high-Al pelite.

Kyanite poikiloblasts occasionally show examples of growth coincident with staurolite breakdown. However, staurolite remains present in many kyanite-bearing samples (e.g., Pattison &

Spear, 2018). Kyanite is observed adjacent to garnet rims (garnet I & II are locally resorbed) or as discrete matrix phases. Kyanite locally lies within the S_2 fabric (Fig. S7b) and crosscuts the S_2 fabric in all other samples (kyanite I, Fig. 9d). Where it lies within the fabric, as observed in high-Al pelite layers, kyanite appears to preferentially overgrow white mica and thus may represent mimetic growth (Fig. S7b; e.g., Spry, 1963; Harte & Johnson, 1969). When present, S_3 fabrics wrap around kyanite porphyroblasts (kyanite I). No distinct alignment of the long axis of kyanite with respect to L_2 is visible in outcrop (Fig. S6c). A later stage of kyanite growth (kyanite II) is also preserved, coincident with garnet breakdown in certain sillimanite-zone samples. Locally, larger kyanite crystals are aligned to S_3, whereas smaller skeletal grains appear to crosscut the fabric. This suggests decompression and breakdown of garnet initiation following growth of post-D_2 garnet (garnet II) but prior to and/or during D_3. These observations suggest that kyanite growth dominantly occurred post-D_2 and pre-D_3 (kyanite I) with secondary/late growth occurring coincident with garnet breakdown (inferred as broadly concurrent with D_3, kyanite II). Localized syn-D_2 and/or post-tectonic mimetic growth is also recorded in high-Al pelite.

Where kyanite and sillimanite coexist, sillimanite typically appears to nucleate on biotite and muscovite as fibrous mats (fibrolite) or is found within garnet corona associated with biotite (biotite III) and plagioclase. With increasing grade, sillimanite becomes prismatic and lies both within and crosscuts S_2 (Figure 9e). Locally, alignment of the long axis of sillimanite with the principal mineral stretching directions is visible in outcrop, though generally sillimanite shows a random distribution with respect to L_2. Biotite and muscovite at these grades dominantly lie within S_2 and are aligned to L_2, which makes it likely that alignment of sillimanite to S_2 and L_2 represents epitaxial nucleation (Fig. S7c; e.g., Chinner, 1961; Carmichael, 1969; Yardley, 1977). Therefore, sillimanite growth therefore initiated post-D_2 or syn-D_3. The dominant phase of growth is inferred to have developed during decompression when the Zanskar Shear Zone was active (Searle *et al.*, 1992), which is consistent with syn-D_3 growth of kyanite II or sillimanite following garnet breakdown.

The highest-grade index mineral in metasedimentary rocks is K-feldspar stable with sillimanite. The crystallization of K-feldspar appears coincident with *in situ* small-scale (centimeter to tens of centimeter) partial melting. Leucosomes appear either concordant with the S_2 fabric or crosscut the fabric as part of a stockwork. Leucosomes are characterized by the mineral

assemblage quartz-K-feldspar-plagioclase-sillimanite-garnet-biotite. Sillimanite is dominantly prismatic and shows similar relationships to S_2 as described for the sillimanite zone. Garnet in these rocks is found in both the paleosome and the leucosome, with the mineral core often defined by an inclusion-poor earlier growth phase that is consistent with microstructural characteristics of lower-grade garnet. The rim is rich in inclusions of sillimanite that display no consistent orientation (garnet III) and wrap resorbed previous phases of growth. Leucosomes are also host to larger (~1–5 mm) garnet grains (garnet III) that preserve coarse-grained quartz in lobate embayments and inclusions that are inferred to develop during dehydration melting (Waters, 2001).

Mineral growth in the higher-temperature range of the Barrovian sequence (staurolite to sillimanite+K-feldspar zone) shows relationships to the main regional fabric (S_2), which implies dominantly post-D_2 growth, whereas mineral growth at lower grades shows mineral-fabric relationships supporting growth syn- to post-D_2. Taken as a set, these observations document that peak temperature mineral growth outlasted development of the dominant (S_2) regional fabrics.

Metabasite index minerals

Mineral assemblages in metabasite also show a systematic change with increasing metamorphic grade (e.g., Bégin, 1992; Starr *et al.*, 2020). The following prograde sequence is observed: actinolite-albite-chlorite-epidote (± tremolite), hornblende-actinolite-albite-epidote (± chlorite), hornblende-actinolite-plagioclase-epidote, hornblende-plagioclase (± epidote), garnet-hornblende-plagioclase, clinopyroxene-hornblende-plagioclase (± K-feldspar). Broadly, these changes define actinolite, hornblende, oligoclase, and garnet+plagioclase zones (Fig. 12).

Actinolite nucleates as acicular grains at the lowest grade observed. At lower-greenschist facies actinolite mats define a weak S_1 and actinolite grains a weak L_1. Where D_2 crenulates S_1, actinolite grains largely crosscut or show a very weak alignment with the stretching lineation (L_2; Fig. S6d). Similarly, at lower-greenschist facies, S_2 is weakly defined by mats of actinolite and plagioclase-quartz aggregate laminations. Once transitional greenschist- to amphibolite-facies conditions are reached (as defined by Starr *et al.*, 2020), actinolite defines L_2 and S_2, although there are multiple occurrences where the amphibole crystals crosscut the dominant planar and linear structural elements. Where S_3 fabrics are present, actinolite grains are always folded

and reoriented by D_3 to define S_3 and L_3 (Fig. S6e). All mineral growth-fabric relationships outlined for actinolite also apply to tremolite, where it is present. These observations suggest that actinolite and tremolite growth is syn-D_1, syn- to post-tectonic with respect to D_1 and D_2 (Figure 9f) and pre-D_3.

The first appearance of hornblende in metabasic rocks occurs between the biotite and garnet isograds constrained in adjacent metasedimentary rock units, though the volumetrically-dominant amphibole at these grades remains actinolite (Figs. 11, 12). Actinolite in metabasic rocks largely disappears after the staurolite isograd in adjacent metasedimentary rock units (Figs. 11, 12). Hornblende and plagioclase are the dominant minerals in metabasic rocks at amphibolite-facies. Hornblende first occurs as elongate needles on the S_2 foliation plane and is dominantly misoriented with respect to L_2, especially in the transitional greenschist–amphibolite facies (Fig. S6d). As grade increases into the amphibolite-facies domain, hornblende shows increasing alignment with L_2 (Fig. S6f). Ultimately, hornblende both lies in and overgrows the S_2 fabric (Figure 9g). Where S_3 is developed, matrix hornblende is folded by F_3 microfolds, and S_3 wraps around hornblende porphyroblasts. Matrix hornblende is reoriented parallel to L_3 (Fig. S6e). Porphyroblastic hornblende also occurs within supracrustal volcano-sedimentary layers associated with metabasite flows. In these layers, hornblende overgrows the S_2 fabric (Figure 9h). These observations suggest that hornblende growth is syn- to post-D_2 and reoriented during D_3.

At mid-amphibolite grade, garnet porphyroblasts appear in metabasic rocks of the Himalayan metamorphic core that are associated with hornblende and plagioclase. This occurs between the staurolite and kyanite isograds in the metasedimentary rock sequence (Figs. 11, 12). Garnet grows across the hornblende-defined S_2 fabric (Figure 9i) or appears to be wrapped by hornblende, developing strain caps and strain shadows around the porphyroblast. S_3 is deflected around garnet porphyroblasts. Garnet in the metabasite sequence is interpreted to have grown syn- to post-D_2 and prior to D_3.

Rare examples of kyanite in metabasic rock occur as part of the assemblage hornblende-plagioclase-kyanite. Kyanite appears to overgrow S_2 (Figure 9j); however, no examples of an S_3 fabric are documented with such assemblages. Kyanite in the metabasite sequence is interpreted to have grown post-D_2.

The highest-grade zone of the Himalayan metamorphic core shows bulk composition varia-

tion within metabasite, which locally includes clinopyroxene with hornblende corona. No clear relationships between fabric and mineral growth are observed. Clinopyroxene-hornblende (± garnet) assemblages are also noted by Honegger (1983) and Pognante & Lombardo (1989).

Relationship of peak metamorphic minerals to penetrative fabrics

Figure 10 summarizes the relationship of metamorphic mineral growth relative to penetrative fabric development in the Suru Valley region. The principal observations are that: (1) the lower-grade minerals (chlorite–garnet) consistently show evidence of syn-D_2 growth, (2) all metamorphic minerals except chlorite (i.e., biotite to sillimanite+K-feldspar) document post-D_2 growth, (3) amphibolite-grade pelitic minerals (i.e., staurolite-sillimanite) initiated growth post-D_2, and (4) all metamorphic minerals, excluding sillimanite and K-feldspar, and late growth of chlorite, biotite, and kyanite, terminated growth prior to the development of D_3 fabric. Notably, where present, the apparent alignment of staurolite and kyanite relative to the S_2 fabric could represent mimetic nucleation on fabric-defining phyllosilicate minerals (Fig. S7a, b; e.g., Spry, 1963; Harte & Johnson, 1969; Patrick & Lieberman, 1988; Gibson, 1993). S_2- and L_2-aligned fibrolitic and prismatic sillimanite, where present, is interpreted as epitaxial nucleation on fabric-defining micas (Fig. S7c; e.g., Chinner, 1961; Carmichael, 1969; Yardley, 1977).

Isograds

The relationships between the trace of metamorphic mineral isograds and mesoscale to macroscale lithotectonic features also inform a discussion of prograde mineral growth and regional deformation. The relationship of the trace of isograds to D_1 structures is not directly considered as linear and planar features are generally only preserved at the microscale and mesoscale. However, as S_1 is subparallel to the original bedding (S_0), the subsequently deformed lithostratigraphic sequence (a feature that can be readily viewed at map scale) is interpreted to be representative of transposed D_1 architecture. Figures 3, 4, and 11 show the trace of the pelitic isograds in both map and cross-section view. Figure 12 shows the interpreted trace of the metabasic isograds in map view. Using this 3-D perspective of the metamorphic culmination within the study area, the following observations can be made:

1. The trace of the biotite isograd is subparallel to the lithostratigraphy, S_2, axial surfaces of F_2 folds, and D_3 features (Fig. 3 and A-A', B-B' and D-D' in Fig. 4). Specifically, the biotite isograd is aligned with the D_3 shear zones, and where D_3 structural elements

are not pervasive the biotite isograd is parallel to major lithostratigraphic contacts, S_2, and the axial surface of F_2 (although the isograd is not folded around these folds). The garnet isograd is broadly parallel to D_2 structural elements when in proximity to the Zanskar Shear Zone or normal-sense structures of the Sankoo fault zone (Fig. 3 and all sections in Fig. 4). Away from these normal-sense shear zones the garnet isograd varies from subparallel to strongly discordant to lithostratigraphic contacts, S_2, and the axial surfaces of F_2 folds. The crosscutting nature of the garnet isograd is best observed in the western section of the map along Shanshin Nala (Fig. 3). These observations suggest that in the biotite zone, the peak metamorphic assemblages and D_2 planar structural features developed concurrently. In contrast, in the garnet zone, the peak metamorphic assemblages appear to be locally concurrent with regional D_2 structural elements in some regions, yet clearly postdate D_2 elsewhere (Fig. 11), with the establishment of the garnet isograd reached after the development of F_2. These inferences match microscale observations: both syn- and post-tectonic growth of garnet is observed in microstructures (Fig. 9b), and garnet grains are documented overgrowing isoclinal microfolding of the S_1 fabrics. The trace of the garnet isograd is interpreted to be parallel to both the Zanskar Shear Zone and associated D_3 movement on shear zones of the Sankoo fault zone due to the reactivation and/or refolding of D_2 structures during D_3.

2. The discordance between the thermal peak of metamorphism and the structural architecture of the Himalayan metamorphic core is best observed at higher metamorphic grades with the trace of the kyanite and sillimanite isograds in Figures 3 and 11. In the western section of the map, just west of Panikhar and between Shanshin Nala and Chellong Nala, the kyanite isograd cuts up-section, across F_2 structures and lithostratigraphic contacts. The trace of the sillimanite isograd shows a large discordance to the axial surface of F_2 structures and lithostratigraphic contacts. This is particularly obvious north of Parkachik in Figure 3. In Figure 4 (cross-sections B-B' and C-C'), at high angles the sillimanite isograd truncates the axial surface of F_2 structures and lithostratigraphic units near Tongul and Panikhar. These observations strongly suggest the development of peak metamorphic assemblage at kyanite and sillimanite grade and the establishment of the related isograds after D_2.

3. The relative structural spacing between isograds is generally independent of whether the

isograds are aligned or crosscut lithostratigraphy and D_2 planar features. However, across the mapped region, the distance between isograds is notably more condensed in the eastern section between Parkachik to Rangdum, which is defined by D_3 reactivation of D_2 structural features, in comparison to the northern and northwestern portions of the map, defined by D_3 crenulation, folding and local reactivation of D_1 and D_2 structural features (Figs. 3 and 11; Figs. S3 and S4). These observations suggest prominent tectonic thinning adjacent to zones defined by D_3 reactivation of earlier structural features (i.e., near the Zanskar Shear Zone).

4. Isograds of all grades (including peak kyanite and sillimanite fabrics) are folded around the axis of late open folds. This includes the F_4 folds and the axis of large NNW-SSE trending open folds (F_5), and thus outlines a broad D_4 and D_5 domal culmination (Fig. 3, and B-B' and C-C' in Fig. 4).

5. In the metavolcanic rock sequence, the hornblende and oligoclase isograds are notably discordant to transposed lithostratigraphy in the western section of the mapped area (Fig. 12). However, like the garnet isograd in the metasedimentary sequence, the trace of the hornblende and oligoclase isograds are parallel with the plane of the Zanskar Shear Zone and associated normal-sense shear zones of the Sankoo fault zone. Integrating the observations made for equivalent greenschist- to amphibolite-facies isograds in the metasedimentary sequence, the syn- to post-D_2 development of hornblende in outcrop and thin-section (Figs. 9g,h; Figs. S6d–f), and the observations based on the metabasic isograds, suggests that the latter isograds were established syn- to post-D_2, and prior to D_3.

6. In the metabasic isograd sequence, the hornblende isograd occurs between biotite and garnet isograds, oligoclase between the garnet and staurolite isograds, and the garnet+plagioclase isograd occurs at or between the staurolite and kyanite isograds (Figs. 11 & 12).

Combined, these observations document the final establishment of the metamorphic isograds (and thus the thermal culmination) in the later stages of shortening, transposition and thickening of the lithostratigraphic sequence, concurrent with the development of D_2 structures at lower grades and following formation of the D_2 structures at higher grades. The biotite and garnet isograds from the metasedimentary rock sequence and the hornblende and oligoclase isograds from the metavolcanic rock sequence are subparallel with the plane of the Zanskar Shear Zone

(where it is adjacent to this structure), which implies that at least these grades predate the development of features associated with D_3. D_4 and D_5 structures are observed to modify all regionally mapped metamorphic isograds, which documents that all mineral isograds in the map area were established prior to D_4 and D_5. Outside of the map area, in the Lalung Valley, SSW of Rangdum (Fig. 2), only one transect was undertaken into the sillimanite+K-feldspar zone, and therefore relevant observations of the trace of this isograd relative to D_2–D_5 structures are not available. However, the mapped trace of the sillimanite+K-feldspar isograd reported in Honegger (1983) suggests that this isograd is also discordant to transposed lithostratigraphy and thereby D_1 and D_2 structures.

DISCUSSION AND TECTONIC IMPLICATIONS

The extensive higher-pressure, and likely older, assemblages that developed in the Suru Valley area, make it an advantageous location for studying the early tectonometamorphic architecture of the predominantly sillimanite-grade Himalayan metamorphic core (e.g., Searle *et al.*, 1992; Walker *et al.*, 2001). Results presented here highlight how field geological maps, structural cross-sections, and detailed observations of fabric development and metamorphic mineral growth can be used to constrain the sequence of crustal thickening, metamorphism and exhumation in a collisional mountain belt. Specifically, four aspects of Himalayan metamorphic core evolution are considered below: (1) how folding and thereby crustal-thickening is accommodated in the crust during the early stages of orogenesis; (2) how the growth of peak metamorphic assemblages relates to deformation at the macroscale, mesoscale, and microscale; (3) how the tectonometamorphic architecture of the Himalayan metamorphic core documented along the Suru Valley area compares along strike; and (4) the broader implications for our understanding of orogenic processes.

Mechanisms of crustal thickening and burial during orogenesis

Thickening of crust on the Indian margin following the collision of India and Asia is dominantly accommodated by SW-vergent folding and thrusting along NE-dipping shear and thrust zones (Fig. 13a, b; Honegger *et al.*, 1982; Honegger, 1983; Searle, 1983; Gilbert, 1986; Searle & Fryer, 1986; Searle & Rex, 1989; Gapais *et al.*, 1992; Searle *et al.*, 1992, 1999a; Walker *et al.*, 1999; Wyss *et al.*, 1999; Hodges, 2000; Stephenson *et al.*, 2000, 2001; Walker *et al.*, 2001; Wiesmayr & Grasemann, 2002). SW-vergent deformation is expressed in the Suru Valley region as planar

and/or linear structural features associated with D_1 and D_2. Pervasive folding and thrusting, which thickened the Himalayan metamorphic core, characterizes the D_2 event (Fig. 13b). The following features of F_2 structures can be emphasized: they are tight to isoclinal and involve different lithological units of varying competencies; the folds are perpendicular in attitude to the shortening direction where they are not disrupted by later refolding, and they are documented from the macroscale to the microscale. Furthermore, the folds display significant amplitude, and fold the shallowest lithostratigraphic levels into the lowest structural levels. These characteristics imply that the confining stresses exerted by plate convergence during orogenesis were both pervasive and penetrative across the region at all scales. Although F_2 structures are observed in most units, strain is preferentially distributed into less competent lithologies that undergo enhanced ductile deformation. Less competent units (e.g., pelite) dominantly preserve microscale F_2, whereas more competent mixed units (e.g., mixed semipelite, metacarbonate, and pelite) preserve folds at all scales. Subparallel planar and linear structural elements from D_1 through D_3 imply a continuous sequence of deformation with a consistent orientation of the major stress direction from early- to late-structures (Table 1). The oblique orientation of mineral stretching lineations to the dip direction during these deformation phases implies that there was non-coaxial ductile deformation, as inferred across other areas of NW India (e.g., Patel *et al.*, 1993; Walker *et al.*, 1999; Wyss *et al.*, 1999; Stephenson *et al.*, 2000; Wiesmayr & Grasemann, 2002; Vannay *et al.*, 2004). Thickening of the crust occurred principally during D_2 and created the dominant deformation fabric in the region. Although some thickening of the crust was accommodated by F_4 and F_5 structures, these are discrete open features that clearly postdate the main prograde–peak regional metamorphism of the Suru Valley area.

Relationship between lithostratigraphy, fabric development, macroscale deformation and metamorphism in the Himalayan metamorphic core

The observations presented in this study indicate that final establishment of peak metamorphic mineral assemblages and conditions occurred after extensive penetrative deformation of the lithostratigraphic sequence during D_1 and D_2 and prior to D_3 (summarized in Table 2). Isograds are generally subparallel to transposed lithostratigraphy at lower grades where they are brought into alignment along D_3 structures (Fig. 13c). In the Suru Valley area, isograds are discordant across lithostratigraphic contacts and early folds (Fig. 14a), particularly in the western section of the map (Fig. 3), as is also noted by Honegger *et al.* (1982). The same broad

structure of isograds can be observed in both the pelitic (Fig. 11) and metabasic (Fig. 12) rock sequences. As with any isograd mapping, subtle changes in bulk chemistry (e.g., variation in $X_{\mathrm{Mg}} = \frac{Mg}{Mg+Fe^{2+}}$ or Al-content) could also exert a control on isograd spacing. Given that the relative structural spacing of the isograds is consistent, regardless of whether they are parallel to or crosscut lithostratigraphic contacts, the trace of the isograds would appear to be controlled by the overall thermal structure rather than the effects of bulk rock chemistry. Tectonic thinning during D_3, and crustal scale folding during D_4 and D_5, disturbed the overall pattern (Fig. 13c, d). However, due to the localized and/or open nature of these later deformation phases, any discordance between the isograds and transposed lithostratigraphic contacts must be early.

Given the lack of substantial plutonic bodies of Cenozoic age in the study area, tectonic thickening of the crust during D_1 and D_2, accommodated through folding and thrusting (Fig. 13b), and the increase in radiogenic heat available from thickened crust, are interpreted as having been the dominant cause of metamorphism within the orogenic pile. Peak metamorphism in the Suru Valley area is constrained to being synchronous with to postdating the development of regional fabrics associated with crustal thickening during D_2, as documented from the macroscale to microscale (Fig. 14). The documentation of post-tectonic metamorphic assemblages throughout the study area implies that crustal thickening in the Zanskar Himalaya principally occurred early in the orogenic cycle.

Crustal-scale folding and domal culminations

The final stage of deformation in the Suru Valley region is expressed as crustal-scale folding (i.e. D_4 and D_5), producing dome and basin culminations of the preexisting structural and metamorphic architecture (Fig. 13d). In particular, domal structures may have played a significant role in the exhumation of high-grade rocks of the Himalayan metamorphic core. A variety of emplacement mechanisms have been suggested for domal culminations in the Himalaya including diapirism, structural interference patterns, isostatic uplift in the footwall of an extensional detachment, compressional core complexes, thrust duplex formation, and/or surficial erosion (see discussion in Kundig, 1989; Searle *et al.*, 1992; Robyr *et al.*, 2006; Horton *et al.*, 2015; Searle & Lamont, 2019). Domal structures across Zanskar appear to be coincident with crustal exhumation along the South Tibetan Detachment System and Main Central Thrust and/or postdate such events (e.g., Kundig, 1989; Stephenson *et al.*, 2001; Robyr *et al.*, 2006). Kundig (1989)

suggested that domes originate from local syn-metamorphic movement relating to tectonic uplift from the Main Central Thrust and Zanskar Shear Zone. Similarly, Searle *et al.* (1992) suggested that domes could be thrust-related culminations that splay off the Main Central Thrust (e.g., Burg *et al.*, 1984). Although such interpretations may be relevant elsewhere, they seem unlikely to apply in the Suru Valley area, where the domal culminations have a symmetrical structure and the final structures appear to postdate shear zone movement. The bipolar NE-SW distribution of L_2 in the Suru domal culmination (Fig. S4) can only be reasonably explained by a kilometer-scale open F_5, with F_4 only minimally reorienting L_2 given its coaxial orientation (Table 1). We propose that domal culminations in the Suru Valley area dominantly result from structural interference patterns of high-angle fold axial traces (F_4 and F_5; Ramsay, 1962, 1967). Consequently, the D_2 fabrics that best outline the domal culmination, predate the formation of the dome itself, rather than being linked to its formation (cf. Gilbert, 1986; Gapais *et al.*, 1992; Searle *et al.*, 1992). Similar observations are also documented with the cross-folding of the Sankoo granite (F_2, Karpokhar antiform, and F_5) that resulted in a domal culmination with a type 1 interference pattern (Ramsay, 1967), which is outlined by the metamorphic foliations, stretching lineations, and isograds in this area (Figs. 3 and 4; Figs. S3 and S4). Gilbert (1986) reported these same observations for the Sankoo granite.

Given that the western Himalaya is dominated by NE- to -SW-directed compressional tectonics, a high-angle (NW–SE oriented) phase of shortening is required to produce a superposition of folds that results in a domal interference pattern (Robyr *et al.*, 2006). It is possible that following accommodation of a consistent major stress direction during exhumation of the Himalayan metamorphic core, the accumulation of subsequent strain to the polydeformed terrain may have locally necessitated alternate vectors and/or variations in strain to be exerted orthogonal to the regional strike of the mountain belt (e.g., formation of map-scale F_4 cross-folds). Reports of deformation orthogonal to the principal stress axes (i.e., NW–SE- to N–S-oriented deformation) and cross-folding of earlier fold generations are reported in Himachal Pradesh (Pandey *et al.*, 2003).

The axes of D_5 folds are perpendicular to the primary stress axes of the mountain belt and are best observed trending between Stakpa and Tongul in the main mapped region (Fig. 3). Mapping by remote sensing also highlights inferred F_5 folds at the NE and NW of the mapped region where the contacts between the Tethyan Himalayan Sequence, Lamayuru Complex, and

Dras Volcanics, as well as the trace of faults along the Lamayuru and Dras shear zones, appear folded around the axis of large NW–SE, kilometer-scale, open synforms (fold axes not shown on Fig. 3). Late NW–SE folds are similarly proposed across NW India by Thakur (1981). Steck (2003) inferred the Suru dome to have formed during the late Pliocene to Holocene. Domal culmination in the Kishtwar Window to the southwest is also proposed to have resulted from a late, kilometer-scale, N–S-oriented antiform that produced a symmetrical pattern and postdated movement on the Main Central Thrust zone (Stephenson *et al.*, 2001). Therefore, it is reasonable to infer that late NW–SE-oriented folding of the Suru Valley area and Kishtwar Window relate to the same event, as suggested by Honegger (1983).

The cooling history of rocks from the Shafat region was calculated by Searle *et al.* (1999a) and shows rapid cooling between 21 and 18.5 Ma (with exhumation rates of 6–10 mm a^{-1}). This is calculated by fitting a cooling curve to K-Ar and $^{40}Ar/^{39}Ar$ ages from hornblende, biotite, and muscovite; and a leucogranite U-Pb monazite age from Noble & Searle (1995). This model assumes that leucogranite crystallisation coincides with sillimanite-grade (M_2) metamorphic peak (~650 °C) through the closure temperature for muscovite and biotite in the Ar system down to ~300 °C (Searle *et al.*, 1999a). This age range overlaps with postulated timing for normal-sense shearing on the Zanskar Shear Zone (Finch *et al.*, 2014; Dèzes *et al.*, 1999). Kumar *et al.* (1995) also document uplift at slower rates from apatite fission-track ages between 5–1 Ma in samples from the Suru domal culmination (with exhumation rates of $\leq$ 0.33 mm a^{-1}) and Kishtwar Window ($\leq$ 3.6 mm a^{-1}). Late uplift along a N–S-oriented domal axis had a significant impact on the current architecture of the Suru Valley and Kishtwar regions. Therefore, it may be reasonable to suggest that the domal structures initiated during uplift along the Zanskar Shear Zone, and were subsequently accentuated by late F_5 folding.

Implications for Himalayan tectonics and orogenic processes

The Himalayan metamorphic core in the Zanskar Himalaya preserves early fabrics and structures that formed at millimeter- to kilometer-scales (D_1 and D_2; Fig. 14) by significant SW-directed crustal thickening following the initial collision of India and Asia. Relationships between prograde–peak metamorphic growth and these early fabrics show that thickening of the crust, through folding and thrusting, followed by thermal relaxation (Fig. 13b, 14a), caused thermal peak in peak-pressure assemblages prior to development of South Tibetan Detachment System-related exhumation fabrics (Fig. 10, 13c). Later assemblages (i.e. sillimanite and post-peak

kyanite II) formed during decompression from peak pressures and are associated with the development of these exhumation fabrics.

The preserved architecture of the Suru Valley region is typical of Barrovian metamorphic systems where burial and crustal thickening occurs faster than thermal equilibration, which yields clockwise *P-T* paths (England & Thompson, 1984; Weller *et al.*, 2013) and predominantly late- to post-tectonic mineral growth (Brodie & Rutter, 1985; Stüwe, 2007; Brown, 2009). Consistent with the interpretation of this study, these characteristics reflect a thermal response to rapid thickening rather than rapid exhumation (Brown, 2009). The Suru Valley region also documents other classical examples of collisional orogenesis, including polyphase deformation; non-coaxial plane strain (Dewey *et al.*, 1998); late-orogenic, long-wavelength folding (Lucas, 1989; Lucas & Byrne, 1992); and a complete Barrovian metamorphic isograd sequence. In addition, the occurrence of metabasic isograds interspersed with or alternating with the pelitic isograd sequence yields a finer documentation of the metamorphic architecture and evolution of greenschist- to amphibolite-facies assemblages. The consistency in the spacing and map pattern of the isograd sequence in each rock type (Figs. 11 & 12) emphasizes a thermal architecture that is relevant to tectonothermal processes at the regional scale rather than one controlled by local variations in bulk composition.

The Himalayas are frequently suggested to exhibit significant along-strike homogeneity, as inferred from the impressive continuity of structures along the ~2500 km length. However, the orogen also features variations in the nature of the dominant regional fabric and diachroneity in the timing of metamorphism relative to regional deformation. Therefore, understanding the specific nature of the fabrics and their associated tectonostructural context as conducted in this study, is key to constraining the metamorphic architecture of the Himalayan metamorphic core. In contrast to the Suru Valley region, numerous studies of the Himalayan metamorphic core in other parts of the orogen record a dominance of pre- and/or syn-tectonic growth of peak-pressure and peak-temperature metamorphic assemblages relative to the main regional fabric: Western Himalaya (Kundig, 1989; Pognante *et al.*, 1993; Stephenson *et al.*, 2000; Finch *et al.*, 2014; Phukon *et al.*, 2019); Central Himalaya (Cottle *et al.*, 2007; Jessup *et al.*, 2008; Larson *et al.*, 2010; Yakymchuk & Godin, 2012; Montomoli *et al.*, 2015; Thakur *et al.*, 2015; Braden *et al.*, 2017; Iaccarino *et al.*, 2017a,b; Soucy La Roche *et al.*, 2018; Carosi *et al.*, 2019; Montemagni *et al.*, 2019; Soucy La Roche *et al.*, 2019; Dyck *et al.*, 2020); and Eastern Himalaya

(Goswami *et al.*, 2009; Groppo *et al.*, 2012; Kellett *et al.*, 2013; Smit *et al.*, 2014; Chakraborty *et al.*, 2016; Zhang *et al.*, 2018; Kalita *et al.*, 2022). Although the dominant regional fabric in each locality is not directly correlative with those observed in this study, most areas of the Himalayan metamorphic core preserve metamorphic conditions and associated tectonostructural relationships that are indicative of processes associated with decompression and exhumation (e.g., Goscombe *et al.*, 2018). The observed orogen-parallel heterogeneity in the preserved timing of peak assemblages relative to regional deformation possibly reflects varying crustal exposure, driven by differences in the timing, rates, and/or spatial distribution of exhuming fault systems. Notably, the Suru Valley region exhibits less metamorphism associated with exhumation-driven fabrics and the cessation of a near-continuous detachment system. Along-strike variation may also result from differences in rates of thickening and radiogenic heating, which are also crucial parameters in determining *P-T* history, or from the structure of the bounding plates, such as passive margin stratigraphy. Such complexity is the hallmark of continental tectonics, which departs significantly from the simple kinematics of plate tectonics (England & Jackson, 1989; Copley & Weller, 2024). In this sense, it is the apparent continuity of structures along-strike that is perhaps the most remarkable aspect of Himalayan tectonics.

CONCLUSIONS

A comprehensive analysis of the relationship between lithostratigraphic units, folds, faults, deformation fabrics, metamorphic isograds, and the relative timing of porphyroblast growth within the Suru Valley area of the Zanskar Himalaya of NW India enables a thorough documentation of the tectonometamorphic evolution of the Himalayan metamorphic core. Deciphering the 3-D geology of the region is based on a new 1:50,000-scale geological map of the Suru Valley area, associated structural cross-sections, field observations at kilometer- to millimeter-scale, and petrographic analysis. The findings presented here highlight five main phases of deformation with all but one deformation phase oriented parallel to the strike of the mountain chain in NW India.

The oldest deformation phase, D_1, manifests as a relic greenschist-facies fabric subparallel to S_0. This phase records incipient NE–SW directed deformation linked with the early stage of collision between India and Asia. D_2 formed by penetrative crenulation of preexisting D_1 fabrics and resulted in formation of the dominant regional fabric, which is defined by greenschist-

to amphibolite-facies mineral assemblages. D_2 lineations record associated SW-vergent thrust-sense deformation. During D_3, earlier fabrics were reactivated during exhumation of the Greater Himalayan Sequence in the footwall of the Zanskar Shear Zone, an along-strike structure equivalent to the South Tibetan Detachment. D_3 fabrics associated with the Zanskar Shear Zone are mylonitic and lineations record normal-sense shearing. In the northern part of the mapped area, the Greater Himalayan Sequence and Tethyan Himalayan Sequence are juxtaposed against the Indus Suture Zone by a set of long-lived fault structures that record polyphase deformation. Normal-sense D_3 fabrics are also developed in this region, yet are defined by a crenulation cleavage (locally penetrative) and macroscale to mesoscale folding. The variation in the nature of D_3 is interpreted to represent a transition from exhumation along the Zanskar Shear Zone to backfolding and backthrusting towards the NE. Lastly, D_4 and D_5 are characterized by open kilometer-scale folding of planar features and some linear features associated with previous deformation events.

The relationship of mineral isograd surfaces and metamorphic porphyroblast growth relative to the suite of deformation fabrics constrains the metamorphic evolution of this region. Isograd surfaces exhibit varying relationships to D_2 planar structural elements, ranging from subparallel to crosscutting. Peak metamorphic phases, ranging from greenschist to upper-amphibolite facies in both pelitic and metabasic lithologies, are synchronous with or postdate D_2 fabrics. Tectonic thinning adjacent to D_3 normal faults telescopes the isograds and reorients isogradic surfaces into parallelism with the faults. D_3 fabrics are documented as postdating prograde–peak garnet, staurolite, kyanite, and hornblende porphyroblasts and are observed to realign actinolite and hornblende parallel to linear structural elements. Finally, D_4 and D_5 structures are observed to modify all regionally mapped mineral isograds. These observations indicate that thermal peak metamorphism was reached after the dominant phase of deformation (D_2) and that peak pressure kyanite-grade conditions preceded movement on the Zanskar Shear Zone (D_3).

As a whole, the new dataset highlights that peak metamorphic conditions in the Zanskar Himalaya are primarily attained following crustal thickening of the Indian margin, rather than predominantly influenced by processes occurring during decompression and exhumation of the Himalayan metamorphic core, as is documented for other areas along strike. Variable levels of crustal exposure, as a result of the discontinuous nature and/or reduced expression of exhuming fault systems, may account for the preservation of this unique record. These results are

consistent with classical characteristics of collisional orogenesis including implied clockwise P-T paths, polyphase deformation, and a complete Barrovian metamorphic isograd sequence supplemented by complementary metabasic isograds. Commensurate with the intricate spatial and temporal distribution of deformation and metamorphism during continental tectonics, datasets over a range of structural levels and large length scales are necessary to decipher their inherent complexity.

ACKNOWLEDGEMENTS

This work forms part of I.P. Cawood's doctoral research project, which was funded by the Natural Environment Research Council (NERC; grant NE/L002612/1) with funding support for fieldwork and equipment genesrously provided by the Geological Society of London (Mike Coward Fund); Department of Earth Sciences, University of Oxford (Burdett-Coutts); and Worcester College, University of Oxford. We extend significant thanks to Hamish Stirling and Jordy De Vries for assistance during fieldwork, and Jonathan Wells for thin section preparation. We thank journal reviewers Aaron J. Martin and Sean P. Long; Geological Survey of Canada internal reviewer Daniele Regis; and Editor Mihai Ducea for suggestions that greatly improved both the clarity and content of the material presented. This is Natural Resources Canada contribution no. 20230265.

REFERENCES

Ambrose, T., K. Larson, C. Guilmette, J. Cottle, H. Buckingham, & S. Rai (2015), Lateral extrusion, underplating, and out-of-sequence thrusting within the Himalayan metamorphic core, Kanchenjunga, Nepal, *Lithosphere*, 7(4), 441–464, doi:10.1130/L437.1.

An, W., X. Hu, E. Garzanti, J.-G. Wang, & Q. Liu (2021), New Precise Dating of the India-Asia Collision in the Tibetan Himalaya at 61 Ma, *Geophysical Research Letters*, 48(3), e2020GL090,641, doi:10.1029/2020GL090641.

Baud, A., M. Gaetani, E. Garzanti, E. Fois, A. Nicora, & A. Tintori (1984), Geological observations in southeastern Zanskar and adjacent Lahul area (northwestern Himalaya), *Eclogae Geologicae Helvetiae*, 77(1), 161–197.

Bégin, N. J. (1992), Contrasting mineral isograd sequences in metabasites of the Cape Smith Belt, northern Québec, Canada: Three new bathograds for mafic rocks, *Journal of Metamorphic Geology*, 10(5), 685–704, doi:10.1111/j.1525-1314.1992.tb00115.x.

Bhat, I. M., T. Ahmad, & D. V. S. Rao (2019a), Petrology and Geochemistry of Mafic Intrusive Rocks from the Sapi-Shergol Ophiolitic Mélange, Indus Suture Zone, Western Ladakh: Constraints on Petrogenesis and Tectonic Setting, *The Journal of Geology*, 127(5), 543–566, doi:10.1086/704254.

Bhat, I. M., T. Ahmad, & D. V. Subba Rao (2019b), The tectonic evolution of the Dras arc complex along the Indus Suture Zone, western Himalaya: Implications for the Neo-Tethys Ocean geodynamics, *Journal of Geodynamics*, 124, 52–66, doi:10.1016/j.jog.2019.01.015.

Bhat, I. M., H. Chauhan, T. Ahmad, & R. A. Dar (2023), Geochemistry and petrogenesis of ophiolitic rocks from the Indus Suture Zone (ISZ), Ladakh Himalaya: Insights for depleted mantle beneath an intra-oceanic island arc complex, *International Geology Review*, doi:10.1080/00206814.2023.2185824.

Braden, Z., L. Godin, & J. M. Cottle (2017), Segmentation and rejuvenation of the Greater Himalayan sequence in western Nepal revealed by in situ U–Th/Pb monazite petrochronology, *Lithos*, 284–285, 751–765, doi:10.1016/J.LITHOS.2017.04.023.

Brodie, K. H., & E. H. Rutter (1985), On the Relationship between Deformation and Metamorphism, with Special Reference to the Behavior of Basic Rocks, in Metamorphic Re-

actions: Kinetics, Textures, and Deformation, edited by A. B. Thompson & D. C. Rubie, Advances in Physical Geochemistry, pp. 138–179, Springer, New York, NY, doi:10.1007/978-1-4612-5066-1_6.

Brown, M. (2009), Metamorphic patterns in orogenic systems and the geological record | - https://www.lyellcollection.org/doi/full/10.1144/SP318.2, *Geological Society, London, Special Publications*, 318, 37–74.

Burchfiel, B. C., C. Zhiliang, K. V. Hodges, L. Yuping, L. H. Royden, D. Changrong, & X. Jiene (1992), The South Tibetan Detachment System, Himalayan Orogen: Extension Contemporaneous With and Parallel to Shortening in a Collisional Mountain Belt, *The South Tibetan Detachment System, Himalayan Orogen: Extension Contemporaneous With and Parallel to Shortening in a Collisional Mountain Belt*, 269, 41, doi:10.1130/SPE269-p1.

Burg, J. P., M. Brunel, D. Gapais, G. M. Chen, & G. H. Liu (1984), Deformation of leucogranites of the crystalline Main Central Sheet in southern Tibet (China), *Journal of Structural Geology*, 6(5), 535–542, doi:10.1016/0191-8141(84)90063-4.

Carmichael, D. M. (1969), On the mechanism of prograde metamorphic reactions in quartz-bearing pelitic rocks, *Contributions to Mineralogy and Petrology*, 20(3), 244–267, doi:10.1007/BF00377479.

Carosi, R., C. Montomoli, & S. Iaccarino (2018), 20 years of geological mapping of the metamorphic core across Central and Eastern Himalayas, *Earth-Science Reviews*, 177, 124–138, doi:10.1016/J.EARSCIREV.2017.11.006.

Carosi, R., C. Montomoli, S. Iaccarino, & D. Visonà (2019), Structural evolution, metamorphism and melting in the Greater Himalayan Sequence in central-western Nepal, *Geological Society, London, Special Publications*, 483(1), 305–323, doi:10.1144/SP483.3.

Chakraborty, S., R. Anczkiewicz, F. Gaidies, D. Rubatto, N. Sorcar, K. Faak, D. Mukhopadhyay, & S. Dasgupta (2016), A review of thermal history and timescales of tectonometamorphic processes in Sikkim Himalaya (NE India) and implications for rates of metamorphic processes, *Journal of Metamorphic Geology*, 34(8), 785–803, doi:10.1111/jmg.12200.

Chambers, J., M. Caddick, T. Argles, M. Horstwood, S. Sherlock, N. Harris, R. Parrish, & T. Ahmad (2009), Empirical constraints on extrusion mechanisms from the upper margin

of an exhumed high-grade orogenic core, Sutlej valley, NW India, *Tectonophysics*, 477(1-2), 77–92, doi:10.1016/J.TECTO.2008.10.013.

Chinner, G. A. (1961), The Origin of Sillimanite in Glen Clova, Angus, *Journal of Petrology*, 2(3), 312–323, doi:10.1093/petrology/2.3.312.

Clift, P. D., P. J. Degnan, R. Hannigan, & J. Blusztajn (2000), Sedimentary and geochemical evolution of the Dras forearc basin, Indus suture, Ladakh Himalaya, India, *GSA Bulletin*, 112(3), 450–466.

Clift, P. D., A. Carter, M. Krol, & E. Kirby (2002), Constraints on India-Eurasia collision in the Arabian Sea region taken from the Indus Group, Ladakh Himalaya, India, *Geological Society, London, Special Publications*, 195, 97–116.

Copley, A., & O. M. Weller (2024), Modern-style continental tectonics since the early Archean, *Precambrian Research*, 403, 107,324, doi:10.1016/j.precamres.2024.107324.

Corfield, R. I., & M. P. Searle (2000), Crustal shortening estimates across the north Indian continental margin, Ladakh, NW India, *Geological Society, London, Special Publications*, 170(1), 395–410, doi:10.1144/GSL.SP.2000.170.01.21.

Cottle, J. M., M. J. Jessup, D. L. Newell, M. P. Searle, R. D. Law, & M. S. A. Horstwood (2007), Structural insights into the early stages of exhumation along an orogen-scale detachment : The South Tibetan Detachment System , Dzakaa Chu section , Eastern Himalaya, *Journal of Structural Geology*, 29(11), 1781–1797, doi:10.1016/j.jsg.2007.08.007.

Cottle, J. M., M. P. Searle, M. S. A. Horstwood, & D. J. Waters (2009), Timing of Midcrustal Metamorphism, Melting, and Deformation in the Mount Everest Region of Southern Tibet Revealed by U(-Th)-Pb Geochronology, *The Journal of Geology*, 117(6), 643–664, doi:10.1086/605994.

Cottle, J. M., K. P. Larson, & D. A. Kellett (2015), How does the mid-crust accommodate deformation in large, hot collisional orogens? A review of recent research in the Himalayan orogen, *Journal of Structural Geology*, 78, 119–133, doi:10.1016/j.jsg.2015.06.008.

DeCelles, P. G., P. Kapp, G. E. Gehrels, & L. Ding (2014), Paleocene-Eocene foreland basin evolution in the Himalaya of southern Tibet and Nepal: Implications for the age of initial India-Asia collision, *Tectonics*, 33(5), 824–849, doi:10.1002/2014TC003522.

Dewey, J. F., R. E. Holdsworth, & R. A. Strachan (1998), Transpression and transtension zones, *Geological Society, London, Special Publications*, 135(1), 1–14, doi:10.1144/GSL.SP.1998.135.01.01.

Dèzes, P. J., J. C. Vannay, A. Steck, F. Bussy, & M. Cosca (1999), Synorogenic extension: Quantitative constraints on the age and displacement of the Zanskar shear zone (northwest Himalaya), *GSA Bulletin*, 111(3), 364–374, doi:10.1130/0016-7606(1999)111⟨0364:SEQCOT⟩2.3.CO;2.

Dietrich, V. J., W. Frank, & K. Honegger (1983), A Jurassic-Cretaceous island arc in the Ladakh-Himalayas, *Journal of Volcanology and Geothermal Research*, 18(1), 405–433, doi:10.1016/0377-0273(83)90018-5.

Dyck, B., M. St-Onge, M. P. Searle, N. Rayner, D. Waters, & O. M. Weller (2019), Protolith lithostratigraphy of the greater Himalayan series in Langtang, Nepal: Implications for the architecture of the Northern Indian margin, *Geological Society Special Publication*, 483(1), 281–304, doi:10.1144/SP483.9.

Dyck, B., D. J. Waters, M. R. St-Onge, & M. P. Searle (2020), Muscovite dehydration melting: Reaction mechanisms, microstructures, and implications for anatexis, *Journal of Metamorphic Geology*, 38(1), 29–52, doi:10.1111/JMG.12511.

England, P., & J. Jackson (1989), Active Deformation of the Continents, *Annual Review of Earth and Planetary Sciences*, 17(Volume 17, 1989), 197–226, doi:10.1146/annurev.ea.17.050189.001213.

England, P. C., & A. B. Thompson (1984), Pressure–Temperature–Time Paths of Regional Metamorphism I. Heat Transfer during the Evolution of Regions of Thickened Continental Crust, *Journal of Petrology*, 25(4), 894–928, doi:10.1093/petrology/25.4.894.

Epard, J.-L., & A. Steck (2004), The Eastern prolongation of the Zanskar Shear Zone (Western Himalaya), *Eclogae Geologicae Helvetiae*, 97, 193–212, doi:10.1007/s00015-004-1116-7.

Finch, M., P. Hasalová, R. F. Weinberg, & C. M. Fanning (2014), Switch from thrusting to normal shearing in the Zanskar shear zone, NW Himalaya: Implications for channel flow, *GSA Bulletin*, 126(7-8), 892–924, doi:10.1130/B30817.1.

Fuchs, G. (1982), The geology of Western Zanskar, *Jahrbuch der Geologischen Bundesanstalt*, 125(1-2), 1–50.

Fuchs, G. (1987), The Geology of Southern Zanskar (Ladakh) - Evidence for the Autochthony of the Tethys Zone of the Himalaya, *Jahrbuch der Geologischen Bundesanstalt*, 130(4), 465–491.

Gaetani, M., & E. Garzanti (1991), Multicyclic History of the Northern India Continental Margin (Northwestern Himalaya), *The American Association of Petroleum Geologists Bulletin*, 75(9), 1427–1446.

Gaetani, M., R. Casnedi, E. Fois, E. Garzanti, F. Jadoul, A. Nicora, & A. Tintori (1986), Stratigraphy of the Tethys Himalaya in Zanskar, Ladakh, *Rivista Italiana di Paleontologia e Stratigrafia*, 91(4), 443–478.

Gapais, D., E. Gilbert, & A. Pecher (1984), Structures et trajectoires de déformation dans la zone de suture de l'Indus-Tsangpo en Himalaya du Ladakh, région de la Suru, *Comptes Rendus de l'Académie des Sciences*, 299(4), 179–182.

Gapais, D., A. Pêcher, E. Gilbert, & M. Ballèvre (1992), Synconvergence spreading of the Higher Himalaya Crystaline in Ladakh, *Tectonics*, 11(5), 1045–1056.

Garzanti, E., & T. Van Haver (1988), The indus clastics: Forearc basin sedimentation in the Ladakh Himalaya (India), *Sedimentary Geology*, 59(3), 237–249, doi:10.1016/0037-0738(88)90078-4.

Garzanti, E., A. Baud, & G. Mascle (1987), Sedimentary record of the northward flight of india and its collision with eurasia (ladakh himalaya, India), *Geodinamica Acta*, 1(4-5), 297–312, doi:10.1080/09853111.1987.11105147.

Gibson, R. (1993), When is a hornfels not a hornfels? Metapelitic rocks from the lower Witwatersrand Supergroup, Vredefort Dome, South Africa, *South African Journal of Geology*.

Gilbert, E. (1986), Évolution structurale d'une chaine de collision : Structures et déformation dans le nord de la plaque indienne en Himalaya du Ladakh (cristallin du haut Himalaya et séries téthysiennes), These de doctorat, Poitiers.

Goscombe, B., D. Gray, & M. Hand (2006), Crustal architecture of the Himalayan metamorphic front in eastern Nepal, *Gondwana Research*, 10(3-4), 232–255, doi:10.1016/j.gr.2006.05.003.

Goscombe, B., D. Gray, & D. A. Foster (2018), Metamorphic response to collision in the Central Himalayan Orogen, *Gondwana Research*, 57, 191–265, doi:10.1016/j.gr.2018.02.002.

Goswami, S., S. K. Bhowmik, & S. Dasgupta (2009), Petrology of a non-classical Barrovian inverted metamorphic sequence from the western Arunachal Himalaya, India, *Journal of Asian Earth Sciences*, 36(4-5), 390–406, doi:10.1016/J.JSEAES.2009.07.006.

Green, O. R., M. P. Searle, R. I. Corfield, & R. M. Corfield (2008), Cretaceous-Tertiary Carbonate Platform Evolution and the Age of the India-Asia Collision along the Ladakh Himalaya (Northwest India), *The Journal of Geology*, 116(4), 331–353, doi:10.1086/588831.

Groppo, C., F. Rolfo, & A. Indares (2012), Partial Melting in the Higher Himalayan Crystallines of Eastern Nepal: The Effect of Decompression and Implications for the 'Channel Flow' Model, *Journal of Petrology*, 53(5), 1057–1088, doi:10.1093/PETROLOGY/EGS009.

Harte, B., & M. R. W. Johnson (1969), Metamorphic history of Dalradian rocks in Glens Clova, Esk and Lethnot, Angus, Scotland, *Scottish Journal of Geology*, 5(1), 54–80, doi:10.1144/sjg05010054.

Heim, A., & A. Gansser (1939), Central Himalaya: Geological Observations of the Swiss Expedition 1936, vol. LXXIII, Denkschriften der Schweizerischen Naturforschenden Gesellschaft.

Herren, E. (1987), Zanskar shear zone : Northeast-southwest extension within the Higher Himalayas (Ladakh, India), *Geology*, 15, 409–413.

Hodges, K. V. (2000), Tectonics of the Himalaya and Southern Tibet from two perspectives, *GSA Bulletin*, 112(3), 324–350, doi:10.1130/0016-7606(2000)112⟨324:TOTHAS⟩2.0.CO;2.

Honegger, K. (1983), Struktur und Metamorphose des Zaskar/Kristallins, Suru Ladakh, Ph.D. thesis, E.T.H., Zurich.

Honegger, K., V. Dietrich, W. Frank, A. Gansser, M. Thöni, & V. Trommsdorff (1982), Magmatism and metamorphism in the Ladakh Himalayas (the Indus-Tsangpo suture zone), *Earth and Planetary Science Letters*, 60(2), 253–292, doi:10.1016/0012-821X(82)90007-3.

Honegger, K., P. Le Fort, G. Mascle, & J. L. Zimmermann (1989), The blueschists along the Indus Suture Zone in Ladakh, NW Himalaya, *Journal of Metamorphic Geology*, 7(1), 57–72, doi:10.1111/J.1525-1314.1989.TB00575.X.

Horton, F., & M. L. Leech (2013), Age and origin of granites in the Karakoram shear zone and Greater Himalaya Sequence, NW India, *Lithosphere*, 5(3), 300–320, doi:10.1130/L213.1.

Horton, F., J. Lee, B. Hacker, M. Bowman-Kamaha'o, & M. Cosca (2015), Himalayan gneiss dome formation in the middle crust and exhumation by normal faulting: New geochronology of Gianbul dome, northwestern India, *Bulletin of the Geological Society of America*, 127(1-2), 162–180, doi:10.1130/B31005.1.

Hu, X., E. Garzanti, T. Moore, & I. Raffi (2015), Direct stratigraphic dating of India-Asia collision onset at the Selandian (middle Paleocene, 59 ± 1 Ma), *Geology*, 43, 859–862, doi: 10.1130/g36872.1.

Hughes, N. C., P. M. Myrow, S. Peng, & D. M. Banerjee (2018), The Parahio Formation of the Tethyan Himalaya: The type section, thickness, lithostratigraphy and biostratigraphy of the best characterised Cambrian succession in the Indian subcontinent, *Journal of the Palaeontological Society of India*, 63(1), 1–18.

Hughes, N. C., P. M. Myrow, S. Peng, & D. M. Banerjee (2019), The Parahio Formation of the Tethyan Himalaya: Further consideration of a case history in lithostratigraphy, *Journal of the Palaeontological Society of India*, 64(2), 275–282.

Iaccarino, S., C. Montomoli, R. Carosi, H.-J. Massonne, A. Langone, & D. Visonà (2015), Pressure–temperature–time–deformation path of kyanite-bearing migmatitic paragneiss in the Kali Gandaki valley (Central Nepal): Investigation of Late Eocene–Early Oligocene melting processes, *Lithos*, 231, 103–121, doi:10.1016/j.lithos.2015.06.005.

Iaccarino, S., C. Montomoli, R. Carosi, H. J. Massonne, & D. Visonà (2017a), Geology and tectono-metamorphic evolution of the Himalayan metamorphic core: Insights from the Mugu Karnali transect, Western Nepal (Central Himalaya), *Journal of Metamorphic Geology*, 35(3), 301–325, doi:10.1111/JMG.12233.

Iaccarino, S., C. Montomoli, R. Carosi, C. Montemagni, H. J. Massonne, A. Langone, A. K. Jain, & D. Visonà (2017b), Pressure-Temperature-Deformation-Time Constraints on the South Tibetan Detachment System in the Garhwal Himalaya (NW India), *Tectonics*, 36(11), 2281–2304, doi:10.1002/2017TC004566.

Inger, S. (1998), Timing of an extensional detachment during convergent orogeny: New Rb-Sr

geochronological data from the Zanskar shear zone, northwestern Himalaya, *Geology*, 26(3), 223–226, doi:10.1130/0091-7613(1998)026⟨0223:TOAEDD⟩2.3.CO;2.

Jain, A., R. Manickavasagam, & S. Singh (1999), Collision tectonics in the NW Himalaya: deformation, metamorphism, emplacement of leucogranite along Beas-Parbati Valleys, Himachal Pradesh, *Gondwana Research Group Memoir*, 6, 3–37.

Jessup, M. J., J. M. Cottle, M. P. Searle, R. D. Law, D. L. Newell, R. J. Tracy, & D. J. Waters (2008), P-T-t-D paths of Everest Series schist, Nepal, *Journal of Metamorphic Geology*, 26(7), 717–739, doi:10.1111/J.1525-1314.2008.00784.X.

Kalita, P., P. Phukon, T. K. Goswami, T. Imayama, & H. B. Srivastava (2022), Chemical mass transport during deformation and metamorphism: Insights from the Main Central Thrust and its footwall of Western Arunachal Himalaya, NE India, *Lithos*, 416–417, 106,641, doi: 10.1016/J.LITHOS.2022.106641.

Kellett, D. A., & D. Grujic (2012), New insight into the South Tibetan detachment system: Not a single progressive deformation, *Tectonics*, 31(2), doi:10.1029/2011TC002957.

Kellett, D. A., D. Grujic, I. Coutand, J. Cottle, & M. Mukul (2013), The South Tibetan detachment system facilitates ultra rapid cooling of granulite-facies rocks in Sikkim Himalaya, *Tectonics*, 32(2), 252–270, doi:10.1002/tect.20014.

Kellett, D. A., J. M. Cottle, & M. Smit (2014), Eocene deep crust at Ama Drime, Tibet: Early evolution of the Himalayan orogen, *Lithosphere*, 6(4), 220–229, doi:10.1130/L350.1.

Kellett, D. A., J. M. Cottle, & K. P. Larson (2019), The South Tibetan detachment system: History, advances, definition and future directions, *Geological Society Special Publication*, 483(1), 377–400, doi:10.1144/SP483.2.

Khan, A., M. Jan, B. Windley, J. Tarney, & M. Thirlwall (1989), The Chilas Mafic-Ultramafic Igneous Complex; The root of the Kohistan Island Arc in the Himalaya of northern Pakistan, *Geological Society of America Special Paper*, 232, doi:10.1130/SPE232-p75.

Khanal, G. P., J. M. Wang, K. P. Larson, F. Y. Wu, S. M. Rai, J. G. Wang, & L. Yang (2021), Eocene Metamorphism and Anatexis in the Kathmandu Klippe, Central Nepal: Implications for Early Crustal Thickening and Initial Rise of the Himalaya, *Tectonics*, 40(4), e2020TC006,532, doi:10.1029/2020TC006532.

Kohn, M. J. (2014), Himalayan Metamorphism and Its Tectonic Implications, *Annual Review of Earth and Planetary Sciences*, 42(1), 381–419, doi:10.1146/annurev-earth-060313-055005.

Kumar, A., N. Lal, A. K. Jain, & R. B. Sorkhabi (1995), Late Cenozoic - Quaternary Thermo-Tectonic History of Higher Himalayan Crystalline (HHC) in Kishtwar- Padar-Zanskar region, NW Himalaya: Evidence from Fission Track Ages, *Geological Society of India*, 45(4), 375–391.

Kundig, R. (1989), Domal structures and high-grade metamorphism in the Higher Himalayan Crystalline, Zanskar Region, north-west Himalaya, India, *Journal of Metamorphic Geology*, 7, 43–55.

Larson, K. P., & L. Godin (2009), Kinematics of the Greater Himalayan sequence, Dhaulagiri Himal: Implications for the structural framework of central Nepal, *Journal of the Geological Society, London*, 166, 25–43, doi:10.1144/0016-76492007-180.

Larson, K. P., L. Godin, & R. A. Price (2010), Relationships between displacement and distortion in orogens: Linking the Himalayan foreland and hinterland in central Nepal, *GSA Bulletin*, 122(7-8), 1116–1134, doi:10.1130/B30073.1.

Long, S., & N. Mcquarrie (2010), Placing limits on channel flow : Insights from the Bhutan Himalaya, *Earth and Planetary Science Letters*, 290(3-4), 375–390, doi:10.1016/j.epsl.2009.12.033.

Lucas, S. B. (1989), Structural evolution of the Cape Smith Thrust Belt and the role of out-of-sequence faulting in the thickening of mountain belts, *Tectonics*, 8(4), 655–676, doi:10.1029/TC008i004p00655.

Lucas, S. B., & T. Byrne (1992), Footwall involvement during arc-continent collision, Ungava orogen, northern Canada, *Journal of the Geological Society*, 149(2), 237–248, doi:10.1144/gsjgs.149.2.0237.

Manickavasagam, R., A. Jain, S. Singh, & A. Asokan (1999), Metamorphic evolution of the north-west Himalaya, India: Pressure-temperature data, inverted metamorphism, and exhumation in the Kashmir, Himachal, and Garhwal Himalayas, *Special Paper of the Geological Society of America*, 328, 179–198, doi:10.1130/0-8137-2328-0.179.

Martin, A. J. (2016), A review of definitions of the Himalayan Main Central Thrust, *International Journal of Earth Sciences*, doi:10.1007/s00531-016-1419-8.

Martin, A. J. (2017), A review of Himalayan stratigraphy, magmatism, and structure, *Gondwana Research*, 49, 42–80, doi:10.1016/j.gr.2017.04.031.

Metcalf, K., & P. Kapp (2017), The Yarlung suture mélange, Lopu Range, southern Tibet: Provenance of sandstone blocks and transition from oceanic subduction to continental collision, *Gondwana Research*, 48, 15–33, doi:10.1016/j.gr.2017.03.002.

Montemagni, C., C. Montomoli, S. Iaccarino, R. Carosi, A. K. Jain, H. J. Massonne, & I. M. Villa (2019), Dating protracted fault activities: Microstructures, microchemistry and geochronology of the Vaikrita Thrust, Main Central Thrust zone, Garhwal Himalaya, NW India, *Geological Society, London, Special Publications*, 481(1), 127–146, doi:10.1144/SP481.3.

Montomoli, C., R. Carosi, & S. Iaccarino (2015), Tectonometamorphic discontinuities in the Greater Himalayan Sequence: A local or a regional feature?, in Tectonics of the Himalaya, vol. 412, edited by S. Mukherjee, R. Carosi, P. A. Van Der Beek, B. K. Mukherjee, & D. M. Robinson, pp. 25–41, Geological Society, London, Special Publications.

Myers, J. S. (2001), Protoliths of the 3.8-3.7 Ga Isua greenstone belt, West Greenland, *Precambrian Research*, 105, 129–141.

Myrow, P. M., K. Snell, N. Hughes, T. Paulsen, N. Heim, & S. Parcha (2006), Cambrian Depositional History of the Zanskar Valley Region of the Indian Himalaya: Tectonic Implications, *Journal of Sedimentary Research*, 76, 364–381, doi:10.2110/jsr.2006.020.

Nanda, M. M., & M. P. Singh (1976), Stratigraphy and sedimentation of the Zanskar area, Ladakh and adjoining parts of the Lahaul region of Himachal Pradesh, *Himalayan Geol.*, 6, 365–388.

Noble, S. R., & M. P. Searle (1995), Age of crustal melting and leucogranite formation from U-Pb zircon and monazite dating in the western Himalaya, Zanskar, India, *Geology*, 23(12), 1135–1138, doi:10.1130/0091-7613(1995)023⟨1135:AOCMAL⟩2.3.CO;2.

Noble, S. R., M. P. Searle, & C. B. Walker (2001), Age and Tectonic Significance of Permian Granites in Western Zanskar, High Himalaya, *The Journal of Geology*, 109(1), 127–135, doi: 10.1086/317966.

Pandey, A., N. Virdi, & V.K.Gairola (2003), Evolution of structural fabrics and deformation

events in the Kulu-Rampur and Larji Window zones, NW Himalaya, India., *Himalayan Geology*, 24, 1–21.

Parsons, A. J., K. Hosseini, R. Palin, & K. Sigloch (2020), Geological, geophysical and plate kinematic constraints for models of the India-Asia collision and the post-Triassic central Tethys oceans, *Earth-Science Reviews*, 202(January), 103,084, doi:10.1016/j.earscirev.2020.103084.

Patel, R. C., S. Singh, A. Asokan, R. M. Manickavasagam, & A. K. Jain (1993), Extensional tectonics in the Himalayan orogen, Zanskar, NW India, *Himalayan Tectonics*, 74, 445–459.

Patrick, B. E., & J. E. Lieberman (1988), Thermal overprint on blueschists of the Seward Peninsula: The Lepontine in Alaska, *Geology*, 16(12), 1100, doi:10.1130/0091-7613(1988)016⟨1100:TOOBOT⟩2.3.CO;2.

Pattison, D. R. M., & F. S. Spear (2018), Kinetic control of staurolite–Al2SiO5 mineral assemblages: Implications for Barrovian and Buchan metamorphism, *Journal of Metamorphic Geology*, 36(6), 667–690, doi:10.1111/jmg.12302.

Phukon, P., K. Sen, P. C. Singh, A. Sen, H. B. Srivastava, & S. Singhal (2019), Characterizing anatexis in the Greater Himalayan Sequence (Kumaun, NW India) in terms of pressure, temperature, time and deformation, *Lithos*, 344–345, 22–50, doi:10.1016/J.LITHOS.2019.04.018.

Pognante, U., & B. Lombardo (1989), Metamorphic evolution of the High Himalayan Crystallines in SE Zanskar, India, *Journal of Metamorphic Geology*, 7(1), 9–17, doi:10.1111/J.1525-1314.1989.TB00571.X.

Pognante, U., D. Castelli, P. Benna, G. Genovese, F. Oberli, M. Meier, & S. Tonarini (1990), The crystalline units of the High Himalayas in the Lahul-Zanskar region (northwest India): Metamorphic-tectonic history and geochronology of the collided and imbricated Indian plate, *Geological Magazine*, 127(2), 101–116, doi:10.1017/S0016756800013807.

Pognante, U., P. Benna, & P. L. Fort (1993), High-pressure metamorphism in the High Himalayan Crystallines of the Stak valley, northeastern Nanga Parbat-Haramosh syntaxis, Pakistan Himalaya, *Geological Society Special Publication*, 74, 161–172, doi:10.1144/GSL.SP.1993.074.01.12.

Ramsay, J. G. (1962), The Geometry and Mechanics of Formation of "Similar" Type Folds, *The Journal of Geology*, 70(3), 309–327, doi:10.1086/626821.

Ramsay, John. G. (1967), Folding and Fracturing of Rocks, McGraw-Hill, New York.

Raz, U., & K. Honegger (1989), Magmatic and tectonic evolution of the Ladakh Block from field studies, Tech. rep.

Reuber, I., R. Montigny, & R. Thuizat (1989), K-Ar ages of ophiolites and arc volcanics of the Indus suture zone : Clues on the early evolution of the Neo-Tethys, doi:10.5169/SEALS-166398.

Robertson, A. (1998), Rift-related sedimentation and volcanism of the north-Indian margin inferred from a Permian-Triassic exotic block at Lamayuru, Indus suture zone (Ladakh Himalaya) and regional comparisons, *Journal of Asian Earth Sciences*, 16, 159–172.

Robertson, A., & P. Degnan (1994), The Dras arc Complex: Lithofacies and reconstruction of a Late Cretaceous oceanic volcanic arc in the Indus Suture Zone, Ladakh Himalaya, *Sedimentary Geology*, 92, 117–145.

Robertson, A., & I. Sharp (1998), Mesozoic deep-water slope/rise sedimentation and volcanism along the North-Indian passive margin: Evidence from the Karamba Complex, Indus suture zone (Western Ladakh Himalaya), *Journal of Asian Earth Sciences*, 16, 195–215.

Robertson, A. H., & P. J. Degnan (1993), Sedimentology and tectonic implications of the Lamayuru Complex: Deep-water facies of the Indian passive margin, Indus Suture Zone, Ladakh Himalaya, *Geological Society Special Publication*, 74, 299–321, doi:10.1144/GSL.SP.1993.074.01.21.

Robertson, A. H. F. (2000), Formation of melanges in the Indus Suture Zone, Ladakh Himalaya by successive subduction-related, collisional and post-collisional processes during Late Mesozoic-Late Tertiary time, *Tectonics of the Nanga Parbat Syntaxis and the Western Himalaya*, 170, 333–374.

Robyr, M. (2002), Thrusting, Extension and Doming in the High Himalaya of Lahul Zanskar Area (NW India): Structural and Pressure-Temperature Constraints, vol. 40, 127–127 pp., Section des Sciences de la Terre, Université de Lausanne.

Robyr, M., & P. Lanari (2020), Kinematic, Metamorphic, and Age Constraints on the Miyar

Thrust Zone: Implications for the Eohimalayan History of the High Himalayan Crystalline of NW India, *Tectonics*, 39(11), 1–24, doi:10.1029/2020TC006379.

Robyr, M., B. R. Hacker, & J. M. Mattinson (2006), Doming in compressional orogenic settings: New geochronological constraints from the NW Himalaya, *Tectonics*, 25(2), 1–19, doi:10.1029/2004TC001774.

Searle, M. P. (1983), Stratigraphy, structure and evolution of the Tibetan–Tethys zone in Zanskar and the Indus suture zone in the Ladakh Himalaya, *Transactions of the Royal Society of Edinburgh: Earth Sciences*, 73, 205–219, doi:10.1017/S0263593300009688.

Searle, M. P., & B. J. Fryer (1986), Garnet, tourmaline and muscovite-bearing leucogranites, gneisses and migmatites of the Higher Himalayas from Zanskar, Kulu, Lahoul and Kashmir, *Geological Society, London, Special Publications*, 19(1), 185–201, doi:10.1144/GSL.SP.1986.019.01.10.

Searle, M. P., & T. N. Lamont (2019), Compressional metamorphic core complexes, low-angle normal faults and extensional fabrics in compressional tectonic settings, *Geological Magazine*, 157(1), 101–118, doi:10.1017/S0016756819000207.

Searle, M. P., & A. J. Rex (1989), Thermal model for the Zanskar Himalaya, *Journal of Metamorphic Geology*, 7(1), 127–134, doi:10.1111/j.1525-1314.1989.tb00579.x.

Searle, M. P., D. J. W. Cooper, & A. J. Rex (1988), Collision tectonics of the Ladakh-Zanskar Himalaya, *Philosophical Transactions of the Royal Society A: Mathematical, Physical & Engineering Sciences*, 326, 117–150, doi:10.1098/rsta.1988.0082.

Searle, M. P., K. T. Pickering, & D. J. W. Cooper (1990), Restoration and evolution of the intermontane Indus molasse basin, Ladakh Himalaya, India, *Tectonophysics*, 174, 301–314, doi:10.1016/0040-1951(90)90327-5.

Searle, M. P., D. J. Waters, D. C. Rex, & R. N. Wilson (1992), Pressure, temperature and time constraints on Himalayan metamorphism from eastern Kashmir and western Zanskar, *Journal - Geological Society (London)*, 149(5), 753–773, doi:10.1144/gsjgs.149.5.0753.

Searle, M. P., D. J. Waters, M. W. Dransfield, B. J. Stephenson, C. B. Walker, J. D. Walker, & D. C. Rex (1999a), Thermal and mechanical models for the structural and metamorphic

evolution of the Zanskar High Himalaya, *Geological Society, London, Special Publications*, 164(1), 139–156, doi:10.1144/GSL.SP.1999.164.01.08.

Searle, M. P., S. R. Noble, A. J. Hurford, & D. C. Rex (1999b), Age of crustal melting, emplacement and exhumation history of the Shivling leucogranite, Garhwal Himalaya, *Geological Magazine*, 136(5), 513–525, doi:10.1017/S0016756899002885.

Searle, M. P., B. Stephenson, J. Walker, & C. Walker (2007), Restoration of the Western Himalaya: Implications for Metamorphic Protoliths, Thrust and Normal Faulting, and Channel Flow Models, *Episodes*, 30(4), 242–257.

Searle, M. P., R. D. Law, L. Godin, K. P. Larson, M. J. Streule, J. M. Cottle, & M. J. Jessup (2008), Defining the Himalayan Main Central Thrust in Nepal, *Journal of the Geological Society*, 165(2), 523–534, doi:10.1144/0016-76492007-081.

Shellnutt, J. G. (2018), The Panjal Traps, *Geological Society, London, Special Publications*, 463, 59–86, doi:10.1144/SP463.4.

Sinclair, H. D., & . N. Jaffey (2001), Sedimentology of the Indus Group, Ladakh, northern India: Implications for the timing of initiation of the palaeo-Indus River, Tech. rep.

Singh, R., J. S. Jamwal, & K. Singh (2000), Geology of Part of Warwan Valley, Doda District, Kashmir Himalaya, *Journal Geological Society of India*, 56, 651–659.

Sinha, A. K., & R. Upadhyay (1993), Mesozoic neo-tethyan pre-orogenic deep marine sediments along the Indus–Yarlung Suture, Himalaya, *Terra Nova*, 5(3), 271–281, doi:10.1111/J.1365-3121.1993.TB00258.X.

Smit, M. A., B. R. Hacker, & J. Lee (2014), Tibetan garnet records early Eocene initiation of thickening in the Himalaya, *Geology*, 42(7), 591–594, doi:10.1130/G35524.1.

Soucy La Roche, R., L. Godin, & J. L. Crowley (2018), Reappraisal of emplacement models for Himalayan external crystalline nappes: The Jajarkot klippe, western Nepal, *GSA Bulletin*, 130(5-6), 1041–1056, doi:10.1130/B31799.1.

Soucy La Roche, R., L. Godin, J. M. Cottle, & D. A. Kellett (2019), Tectonometamorphic evolution of the tip of the Himalayan metamorphic core in the Jajarkot klippe, west Nepal, *Journal of Metamorphic Geology*, 37(2), 239–269, doi:10.1111/JMG.12459.

Spry, A. (1963), The chronological analysis of crystallization and deformation of some Tasmanian

Precambrian rocks, *Journal of the Geological Society of Australia*, 10(1), 193–208, doi:10.1080/00167616308728540.

St-Onge, M. R., N. Rayner, & M. P. Searle (2010), Zircon age determinations for the Ladakh batholith at Chumathang (Northwest India): Implications for the age of the India-Asia collision in the Ladakh Himalaya, *Tectonophysics*, 495(3-4), 171–183, doi:10.1016/j.tecto.2010.09.010.

Starr, P. G., D. R. M. Pattison, & D. E. Ames (2020), Mineral assemblages and phase equilibria of metabasites from the prehnite–pumpellyite to amphibolite facies, with the Flin Flon Greenstone Belt (Manitoba) as a type example, *Journal of Metamorphic Geology*, 38(1), 71–102, doi:10.1111/jmg.12513.

Stäubli, A. (1989), Polyphase metamorphism and the development of the Main Central Thrust, *Journal of Metamorphic Geology*, 7, 73–93.

Steck, A. (2003), Geology of the NW Indian Himalaya, *Eclogae Geologicae Helvetiae*, 96, 147–196, doi:10.5169/seals-169014.

Stephenson, B. J., D. J. Waters, & M. P. Searle (2000), Inverted metamorphism and the Main Central Thrust: Field relations and thermobarometric constraints from the Kishtwar Window, NW Indian Himalaya, *Journal of Metamorphic Geology*, 18(5), 571–590, doi:10.1046/j.1525-1314.2000.00277.x.

Stephenson, B. J., M. P. Searle, D. J. Waters, & D. C. Rex (2001), Structure of the Main Central Thrust zone and extrusion of the High Himalayan deep crustal wedge, Kishtwar–Zanskar Himalaya, *Journal of the Geological Society*, 158(4), 637–652, doi:10.1144/jgs.158.4.637.

Štípská, P., P. Závada, S. Collett, A. R. Kylander-Clark, B. R. Hacker, A. S. Tabaud, & M. Racek (2020), Eocene migmatite formation and diachronous burial revealed by petrochronology in NW Himalaya, Zanskar, *Journal of Metamorphic Geology*, 38(6), 655–691, doi:10.1111/JMG.12534.

Stübner, K., D. Grujic, R. R. Parrish, N. M. Roberts, A. Kronz, J. Wooden, & T. Ahmad (2014), Monazite geochronology unravels the timing of crustal thickening in NW Himalaya, *Lithos*, 210–211, 111–128, doi:10.1016/j.lithos.2014.09.024.

Stüwe, K. (2007), Geodynamics of the Lithosphere, 2nd ed., Springer, Berlin, Heidelberg, doi: 10.1007/978-3-540-71237-4.

Thakur, S. S., c. S. C. Patel, & c. A. K. Singh (2015), A P-T pseudosection modelling approach to understand metamorphic evolution of the Main Central Thrust Zone in the Alaknanda valley, NW Himalaya, *Contributions to Mineralogy and Petrology*, 170(2), doi: 10.1007/s00410-015-1159-y.

Thakur, V. C. (1981), Regional framework and geodynamic evolution of the Indus-Tsangpo suture zone in the Ladakh Himalayas, *Earth and Environmental Science Transactions of The Royal Society of Edinburgh*, 72(2), 89–97, doi:10.1017/S0263593300009925.

Thakur, V. C. (1998), Structure of the Chamba nappe and position of the Main Central Thrust in Kashmir Himalaya, *Journal of Asian Earth Sciences*, 16(2-3), 269–282.

Thöni, M., C. Miller, C. Hager, B. Grasemann, & M. Horschinegg (2012), New geochronological constraints on the thermal and exhumation history of the Lesser and Higher Himalayan Crystalline Units in the Kullu-Kinnaur area of Himachal Pradesh (India), *Journal of Asian Earth Sciences*, 52, 98–116, doi:10.1016/j.jseaes.2012.02.015.

Vance, D., & N. Harris (1999), Timing of prograde metamorphism in the Zanskar Himalaya, *Geology*, 27(5), 395–398.

Vannay, J.-C., & B. Grasemann (1998), Inverted metamorphism in the High Himalaya of Himachal (NW India) : Phase equilibria versus thermobarometry, *Schweizerische Mineralogische und Petrographische Mitteilungen*, 78(1), 107–132, doi:10.5169/SEALS-59277.

Vannay, J.-C., B. Grasemann, M. Rahn, W. Frank, A. Carter, V. Baudraz, & M. Cosca (2004), Miocene to Holocene exhumation of metamorphic crustal wedges in the NW Himalaya: Evidence for tectonic extrusion coupled to fluvial erosion, *Tectonics*, 23(1), doi: 10.1029/2002TC001429.

Vannay, J.-C. C., & A. Steck (1995), Tectonic evolution of the High Himalaya in Upper Lahul (NW Himalaya, India), *Tectonics*, 14(2), 253–263, doi:10.1029/94TC02455.

Walker, C. B. (1999), The tectonothermal evolution of the High Himalaya in the Suru Valley, NW Zanskar with constraints from metamorphic modelling, Ph.D. thesis, University of Oxford.

Walker, C. B., M. P. Searle, & D. J. Waters (2001), An integrated tectonothermal model for the

evolution of the high Himalaya in Western Zanskar with constraints from thermobarometry and metamorphic modeling, *Tectonics*, 20(6), 810–833, doi:10.1029/2000TC001249.

Walker, J. D. (1998), The Structural and Metamorphic Evolution of the High Himalayan Slab in SE Zanskar and NW Lahaul, Ph.D. thesis, University of Oxford.

Walker, J. D., M. W. Martin, S. A. Bowring, M. P. Searle, D. J. Waters, & K. V. Hodges (1999), Metamorphism, Melting, and Extension: Age Constraints from the High Himalayan Slab of Southeast Zanskar and Northwest Lahaul, *The Journal of Geology*, 107(4), 473–495, doi:10.1086/314360.

Walsh, J. M. J., S. Buckman, A. P. Nutman, & R. Zhou (2021), The significance of Upper Jurassic felsic volcanic rocks within the incipient, intraoceanic Dras Arc, Ladakh, NW Himalaya, *Gondwana Research*, 90, 199–219, doi:10.1016/j.gr.2020.11.007.

Walther, J. V., & P. M. Orville (1982), Volatile production and transport in regional metamorphism, *Contributions to Mineralogy and Petrology*, 79, 252–257, doi:10.1007/BF00371516.

Wang, J.-M., J.-J. Zhang, K. Liu, B. Zhang, X.-X. Wang, S. Rai, & M. Scheltens (2016), Spatial and temporal evolution of tectonometamorphic discontinuities in the central Himalaya: Constraints from P–T paths and geochronology, *Tectonophysics*, 679, 41–60, doi:10.1016/j.tecto.2016.04.035.

Waters, D. J. (2001), The significance of prograde and retrograde quartz-bearing intergrowth microstructures in partially melted granulite-facies rocks, *Lithos*, 56(1), 97–110, doi:10.1016/S0024-4937(00)00061-X.

Waters, D. J. (2019), Metamorphic constraints on the tectonic evolution of the High Himalaya in Nepal: The art of the possible, *Geological Society London, Special Publication*, 483, doi:10.1144/sp483-2018-187.

Webb, A. A. G., A. Yin, T. M. Harrison, J. Célérier, G. E. Gehrels, C. E. Manning, & M. Grove (2011), Cenozoic tectonic history of the Himachal Himalaya (northwestern India) and its constraints on the formation mechanism of the Himalayan orogen, *Geosphere*, 7(4), 1013–1061, doi:10.1130/GES00627.1.

Weller, O. M., M. R. St-Onge, D. J. Waters, N. Rayner, M. P. Searle, S.-L. Chung, R. M. Palin, Y.-H. Lee, & X. Xu (2013), Quantifying Barrovian metamorphism in the Danba Structural

Culmination of eastern Tibet, *Journal of Metamorphic Geology*, 31(9), 909–935, doi:10.1111/jmg.12050.

Weller, O. M., C. M. Mottram, M. R. St-Onge, C. Möller, R. Strachan, T. Rivers, & A. Copley (2021), The metamorphic and magmatic record of collisional orogens, *Nature Reviews Earth & Environment*, 2(11), 781–789, doi:10.1038/s43017-021-00218-z.

Whitney, D. L., & B. W. Evans (2010), Abbreviations for names of rock-forming minerals, *American Mineralogist*, 95(1), 185–187, doi:10.2138/am.2010.3371.

Wiesmayr, G., & B. Grasemann (2002), Eohimalayan fold and thrust belt: Implications for the geodynamic evolution of the NW-Himalaya (India), *Tectonics*, 21(6), 8–1–8–18, doi:10.1029/2002TC001363.

Wu, F. Y., P. D. Clift, & J. H. Yang (2007), Zircon Hf isotopic constraints on the sources of the Indus Molasse, Ladakh Himalaya, India, *Tectonics*, 26(2), doi:10.1029/2006TC002051.

Wyss, M., J. Hermann, & A. L. Steck (1999), Structural and metamorphic evolution of the northern Himachal Himalaya, NW India (Spiti-eastern Lahul-Parvati valley traverse), *Eclogae Geologicae Helvetiae*, 92, 3–44.

Yakymchuk, C., & L. Godin (2012), Coupled role of deformation and metamorphism in the construction of inverted metamorphic sequences: An example from far-northwest Nepal, *Journal of Metamorphic Geology*, 30(5), 513–535, doi:10.1111/J.1525-1314.2012.00979.X.

Yardley, B. W. D. (1977), The nature and significance of the mechanism of sillimanite growth in the Connemara schists, Ireland, *Contributions to Mineralogy and Petrology*, 65(1), 53–58, doi:10.1007/BF00373570.

Yin, A. (2006), Cenozoic tectonic evolution of the Himalayan orogen as constrained by along-strike variation of structural geometry, exhumation history, and foreland sedimentation, *Earth-Science Reviews*, 76(1-2), 1–131, doi:10.1016/j.earscirev.2005.05.004.

Zhang, L., Y. Ye, & S. Qin (2018), Water in the Thickened Lower Crust of the Eastern Himalayan Orogen, *Journal of Earth Sci-ence*, 29(5), 1040, doi:10.1007/s12583-018-0880-7.

Zhu, D.-C., Q. Wang, Z.-D. Zhao, S.-L. Chung, P. A. Cawood, Y. Niu, S.-A. Liu, F.-Y. Wu, & X.-X. Mo (2015), Magmatic record of India-Asia collision, *Scientific Reports*, 5(1), 14,289, doi:10.1038/srep14289.

Zhu, D.-C., Q. Wang, S.-L. Chung, P. A. Cawood, & Z.-D. Zhao (2019), Gangdese magmatism in southern Tibet and India–Asia convergence since 120 Ma, *Geological Society, London, Special Publications*, 483(1), 583–604, doi:10.1144/SP483.14.

FIGURE CAPTIONS

Figure 1: Simplified geological map of the Himalaya with location of the Suru Valley field area (Fig. 3) and the NW India map (Fig. 2). Modified from Parsons *et al.* (2020), with NW India constrained by Steck (2003)

.

Figure 2: Simplified geological map of NW India modified from Steck (2003), with adjustments to Suru Valley region (rectangular box) based on Figure 3. Completed transect through the Lalung Valley is shown by the small rhomboid box. MZB = Main Zanskar Backthrust, WF = Warwan fault, SD = Sangla Detachment, MCT = Main Central Thrust, MBT = Main Bounary Thrust.

Figure 3: 1:50,000-scale geological map of the Himalayan metamorphic core of the Suru Valley region, NW India, displaying the southern extent of the Indus Suture Zone and and Tethyan Himalayan Sequence, and upper portion of the Greater Himalayan Sequence. The white dashed line represents the limit of field mapping with regions outside this area constrained by remote-sensed mapping.

Figure 4: Vertical cross-sections of the Suru Valley region. Lines of section are shown in Fig. 3. Sections display lithological contacts, mineral isograds, and major faults and folds 1.5 km above and below topography to better represent the complicated structure of the region. Lighter shading represents rocks that have passed above the erosion surface. Cross-sections A-A' B-B' and C-C' are aligned to cross over points as viewed on the geological map, but D-D' does not cross over other sections.

Figure 5: Field photographs of the Dras Volcanics, Indus Suture Zone and Tethyan Himalayan Sequence-Greater Himalayan Sequence lithological units of NW India; c–e and g–k = deeper to shallower lithostratigraphic levels variably intruded by f, l–o. *in situ* partial melting of pelitic layers in h forms p. HCS—Hummocky cross-stratification, GHS—Greater Himalayan Sequence, THS—Tethyan Himalayan Sequence.

Figure 6: mesoscale field photos of planar and linear features formed during D_1–D_3. a) centimeter-scale S_1 fabric deformed by D_2 to form an axial planar S_2; b) meter-scale isoclinal folding of transposed S_1 fabric by F_2 to develop axial planar S_2; c) kilometer-scale folding of S_1 fabrics by Karpokhar antiform F_2 fold, subsequent fabric development produces penetrative S_2 fabric on fold limbs; d) thrust-sense augen and mylonitic S_2 fabric formed during D_2; e) normal-sense augen and mylonitic S_3 fabric, through reactivation of S_2 during D_3; f) centimeter- to meter-scale F_3 folds with sharp hinge zones deforming S_2 fabric; and g) kilometer-scale panorama of Barsoo antiformal backfold, a SE-plunging F_3 structure (fold hinge further to the N), normal movement is inferred on the lower limb, as documented on the Dras shear zone, which becomes overturned and transitions to a NE-directed backthrust.

Figure 7: Annotated panoramic field photographs of macroscale folds. Lithological colors match those in the legend of Figure 3 and 4. a) Oblique perspective of the Donara antiform at the river confluence along Chellong Nala, view to the N. b) Intersecting F_2 and F_4 folds above Parkachik glacier, view to the ESE. Geometry and lithology of rocks below glacier inferred from observed structures and rock units bounding the glacier. c) View above Tongul over to Parkachik metagranite and intersecting F_2 and F_4 folds; the Tongul antiform extends from the SE peaks to underlying Nun in the center of the panorama, view to the S. Original panoramic photographs with no annotation are included in the Supplemental Material.

Figure 8: Simplified geological map of the Suru Valley area, NW India, with D_1–D_3 planar and linear structural data separated into six zones with stereonets. Insufficient D_1 linear and planar elements were recorded in Zones B, C, and D ($n = \leq 3$) to warrant structural interpretations from corresponding stereonets. For lithostratigraphy and symbols refer to Figure 3.

Figure 9: Mineral growth–deformation relationships. (a) Biotite porphyroblast overgrowing S_2 fabric outlined by matrix parallel graphite inclusion trails. (b) Garnet porphyroblasts recording syn- to post-D_2 growth as documented by graphite and ilmenite inclusion trails. (c) Staurolite overgrowing S_2 fabric. (d) Kyanite porphyroblast documenting post-D_2 growth, crosscutting the S_2 foliation. (e) Fibrolitic and prismatic sillimanite overgrowing S_2. (f) Actinolite defining and overgrowing S_2 fabric, indicating syn- to post-D_2 growth. (g) Hornblende both aligned and overgrowing the S_2 fabric, indicating syn- to post-D_2 growth. (h) Hornblende porphyroblast in volcano-sedimentary rock overgrowing S_2 fabric. (i) Garnet porphyroblast overgrowing S_2 fabric. (j) Kyanite porphyroblast overgrowing the S_2 fabric. Bt—biotite, Grt—garnet, Ms—muscovite, St—staurolite, Ky—kyanite, Sil—sillimanite, Act—actinolite, Rt—rutile, Hbl—hornblende after Whitney & Evans (2010).

Figure 10: Summary of fabric development vs. mineral growth in the Suru Valley area, NW India, for metasedimentary and metavolcanic rocks. Faded edges on left and/or right side of bars indicate initiation and/or termination of growth, and are undefined with respect to preceding and subsequent deformation phases.

Figure 11: Form-line map of major lithological, tectonic and metamorphic features of the Suru Valley area, overlain with the distribution of metasedimentary rock mineral assemblages as constrained through petrographic and hand lens observations across samples and field outcrops. Retrogressive mineral phases are excluded. Grid references are truncated, with the final three zeros omitted.

Figure 12: Form-line map of major lithological, tectonic, and metamorphic features of the Suru Valley area showing metavolcanic rock mineral assemblages as constrained through both petrographic and hand lens observations across samples and field outcrops. Retrogressive mineral phases are excluded. Optical methods were used to determine plagioclase composition. In outcrop a composition of albite is assumed at sub-amphibolite-facies, and $> 10\%$ anorthite (plagioclase) at amphibolite facies. Samples with more quartz than Na-feldspar are not used to define isograd surfaces. Grid references are truncated, with the final three zeros omitted.

Figure 13: Schematic mid-crustal block diagrams summarizing the tectonic evolution of the Suru Valley region: a) prior to initiation of India-Asia collision; b) thermal equilibration following progression of D_2 from high to low structural levels; c) D_3 reactivation and exhumation of the sequence, coincident with sillimanite-grade metamorphism; and d) D_4 and D_5 kilometer-scale open warping of the earlier established lithological, tectonic, and metamorphic architecture. Effects of late D_3 backthrusting are preserved along the Dras, Lamayuru, and Zanskar shear zones. GHS—Greater Himalayan Sequence; ISZ—Indus Suture Zone; THS—Tethyan Himalayan Sequence.

Figure 14: Schematic summary of the macroscale to microscale relationship between deformation and metamorphism in pelitic and metabasic rocks at thermal peak (post-D_2). a) Macroscale mid-crustal schematic cross-section displaying thermal equilibration after isoclinal F_2 folding of metasedimentary and metavolcanic rock layers. b) Mesoscale isoclinal F_2 fold of garnet amphibolite (metabasite) and kyanite-staurolite schist (pelite) showing crenulation cleavage defined by S_2. The long-axis of hornblende, kyanite, and staurolite show no consistent orientation with respect to the L_2 stretching lineation. c) Characteristic microscale relations between peak porphyroblast phases and S_2 fabric. In pelite, garnet documents a syn-D_2 core, defined by quartz and Ti-oxides, and post-D_2 rim crosscutting the micaceous S_2 fabric. Kyanite and staurolite overgrow S_2, which is defined by matrix concordant inclusion trails and no warping of external matrix fabric. For metabasite, aligned biotite, laminated hornblende, and quartzo-feldspathic layers produce the dominant S_2 fabric, locally with cross-cutting hornblende and biotite. Garnet overgrows S_2.

[1] Supplemental Material. Text includes a section on methods, detailed descriptions of lithostratigraphic units, observations of fabric-defining metamorphic mineral assemblages and extra mineral growth-deformation fabric relationships. Figures S1–S7 consist of collated pressure-temperature and geochronological datasets from previous studies across NW India, simplified geological maps highlighting different sets of structural data and additional field and petrographic photographs that illustrate the relationship between mineral growth and the development of deformation fabrics. Please visit https://doi.org/10.1130/GSAB.S.25768581 to access the supplemental material; contact editing@geosociety.org with any questions.

Fig. 1

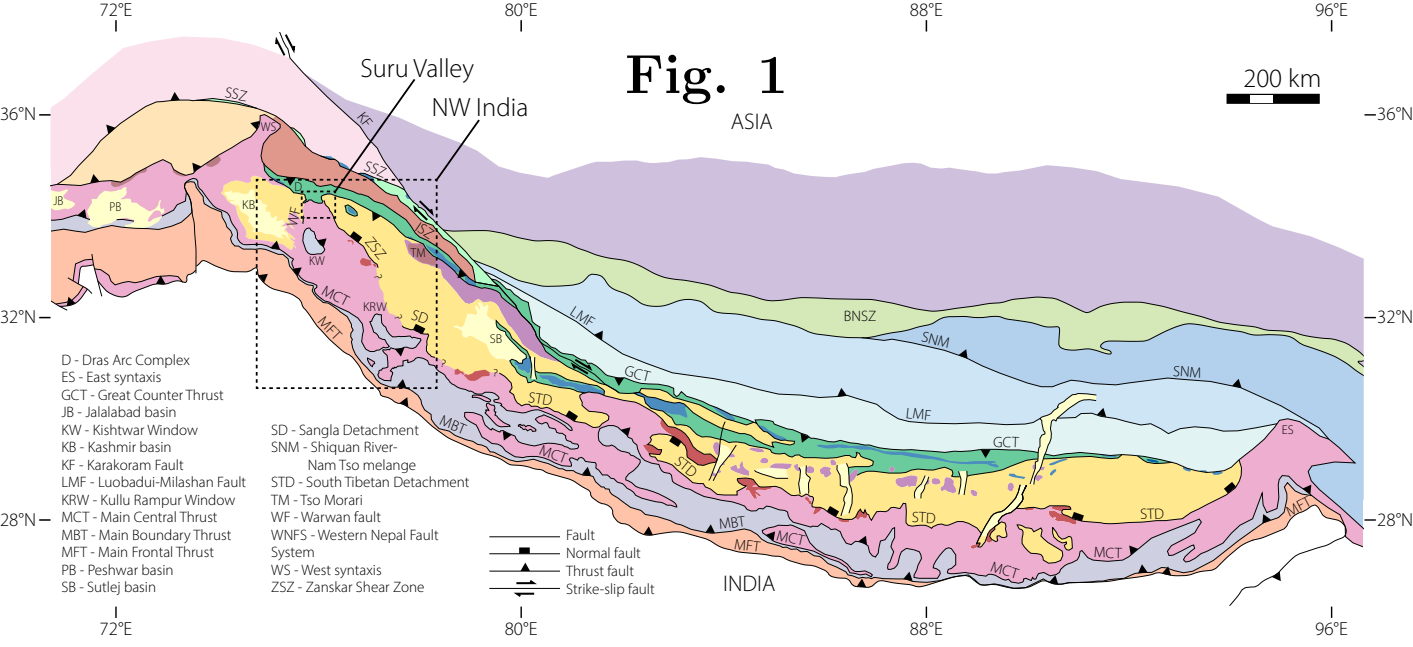

- Himalayan leucogranite
- Tethyan Himalayan Sequence (THS)
- Greater Himalayan Sequence (GHS)
- Lesser Himalayan Sequence (LHS)
- Subhimalayan Zone (SZ)
- gneissic/granitic domes (GHS)
- blueschist-eclogite
- ophiolite
- Indus Suture Zone (ISZ)
- Cenozoic basin fill
- Karakoram block
- Shyok Suture Zone (SSZ)
- Kohistan block
- Ladakh block
- Qiangtang block
- Bangong-Nujiang Suture Zone (BNSZ)
- North Lhasa block
- Central Lhasa block
- South Lhasa block

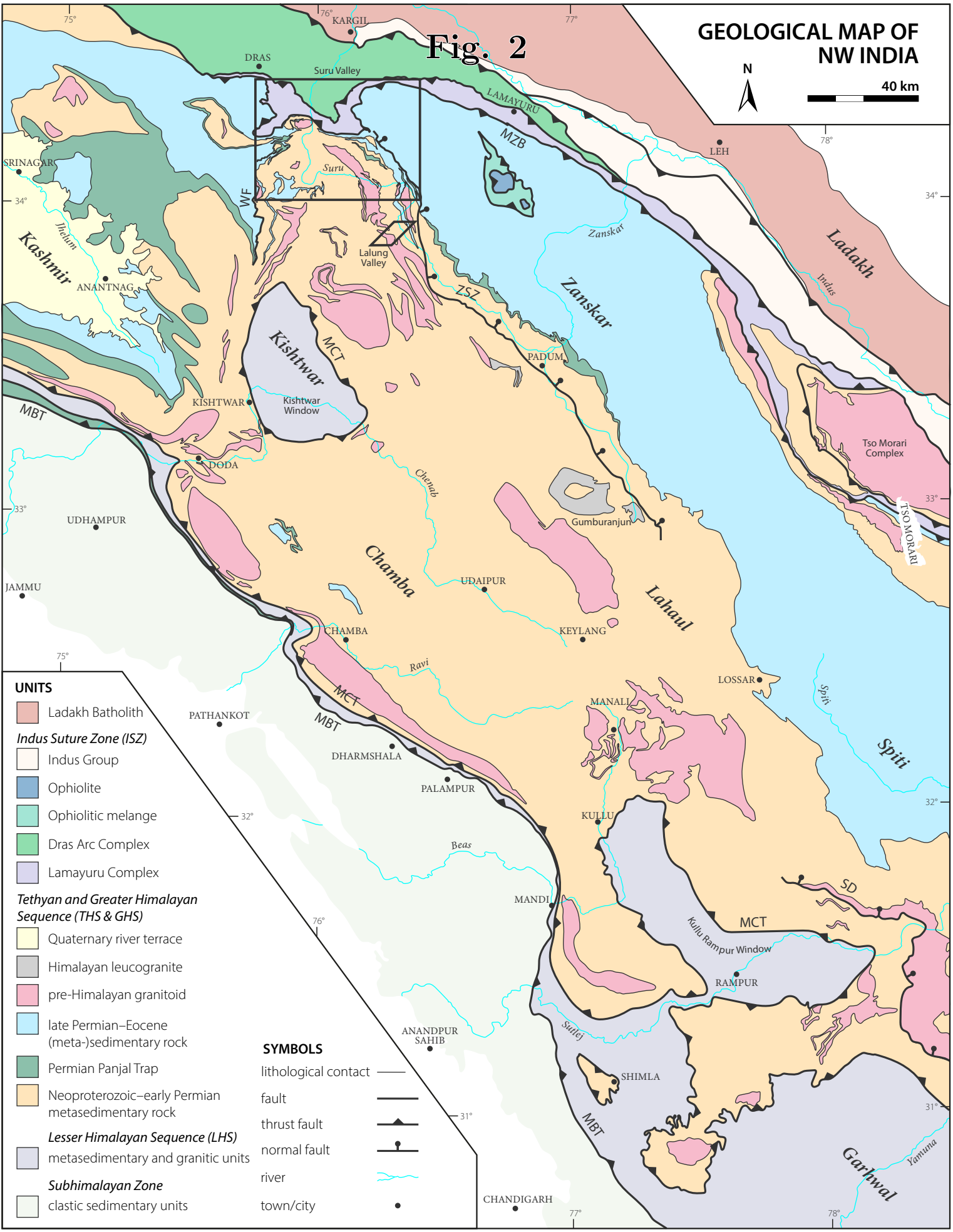
GEOLOGICAL MAP OF NW INDIA
Fig. 2
N
40 km
KARGIL
DRAS
Suru Valley
LAMAYURU
MZB
LEH
SRINAGAR
Suru
WF
Jhelum
Kashmir
ANANTNAG
Lalung Valley
LSZ
Zanskar
Ladakh
Indus
Kishtwar
MCT
PADUM
KISHTWAR
Kishtwar Window
MBT
DODA
Chenab
Tso Morari Complex
TSO MORARI
UDHAMPUR
Gumburanjun
JAMMU
Chamba
UDAIPUR
Lahaul
CHAMBA
KEYLANG
Ravi
LOSSAR
Spiti
MANALI
PATHANKOT
MCT
MBT
DHARMSHALA
PALAMPUR
KULLU
Beas
SD
MANDI
MCT
Kullu Rampur Window
RAMPUR
ANANDPUR SAHIB
Sutlej
SHIMLA
MBT
Garhwal
Yamuna
CHANDIGARH
UNITS
Ladakh Batholith
Indus Suture Zone (ISZ)
Indus Group
Ophiolite
Ophiolitic melange
Dras Arc Complex
Lamayuru Complex
Tethyan and Greater Himalayan Sequence (THS & GHS)
Quaternary river terrace
Himalayan leucogranite
pre-Himalayan granitoid
late Permian–Eocene (meta-)sedimentary rock
Permian Panjal Trap
Neoproterozoic–early Permian metasedimentary rock
Lesser Himalayan Sequence (LHS)
metasedimentary and granitic units
Subhimalayan Zone
clastic sedimentary units
SYMBOLS
lithological contact
fault
thrust fault
normal fault
river
town/city

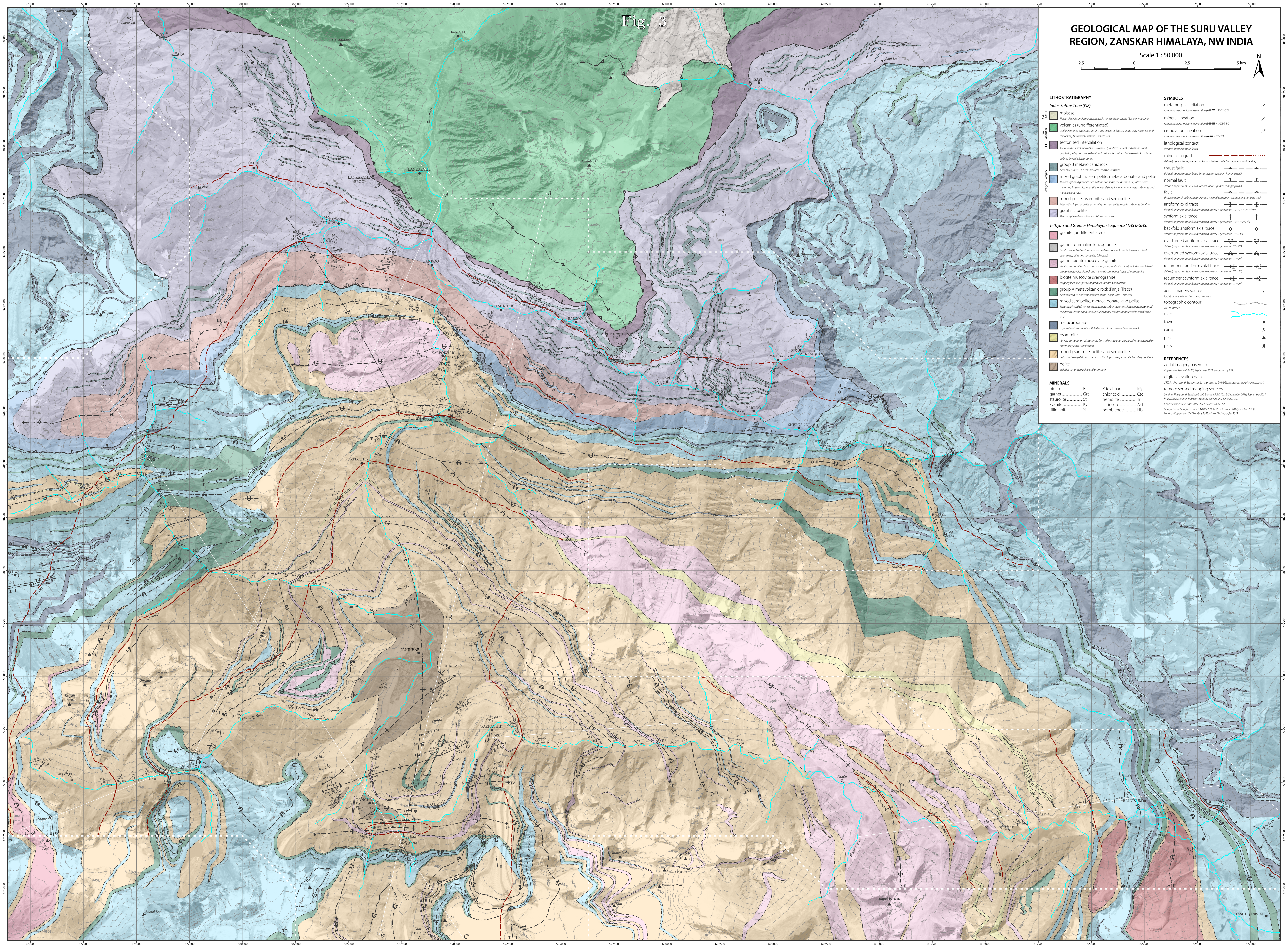
Fig. 3
GEOLOGICAL MAP OF THE SURU VALLEY REGION, ZANSKAR HIMALAYA, NW INDIA
Scale 1 : 50 000
2.5 0 2.5 5 km
N
LITHOSTRATIGRAPHY
Indus Suture Zone (ISZ)
Indus Gp.
molasse
Fluvio-alluvial conglomerate, shale, siltstone and sandstone (Eocene–Miocene).
Dras volcanics
volcanics (undifferentiated)
Undifferentiated andesites, basalts, and epiclastic breccia of the Dras Volcanics, and minor Kargil Intrusives (Jurassic–Cretaceous).
tectonised intercalation
Tectonised intercalation of Dras volcanics (undifferentiated), radiolarian chert, graphitic pelite, and group B metavolcanic rocks contacts between blocks or lenses defined by faults/shear zones.
Lamayuru Complex
group B metavolcanic rock
Actinolite schists and amphibolites (Triassic–Jurassic).
mixed graphitic semipelite, metacarbonate, and pelite
Metamorphosed graphite-rich silstone and shale; metacarbonate; intercalated metamorphosed calcareous siltstone and shale. Includes minor metacarbonate and metavolcanic rocks.
mixed pelite, psammite, and semipelite
Alternating layers of pelite, psammite, and semipelite. Locally carbonate bearing.
graphitic pelite
Metamorphosed graphite-rich silstone and shale.
Tethyan and Greater Himalayan Sequence (THS & GHS)
granite (undifferentiated)
garnet tourmaline leucogranite
Ex-situ products of metamorphosed sedimentary rocks. Includes minor mixed psammite, pelite, and semipelite (Miocene).
garnet biotite muscovite granite
Varying composition from monzo- to syenogranite (Permian), includes xenoliths of group A metavolcanic rock and minor discontinuous layers of leucogranite.
biotite muscovite syenogranite
Megacrystic K-feldspar syenogranite (Cambro-Ordovician).
group A metavolcanic rock (Panjal Traps)
Actinolite schists and amphibolites of the Panjal Traps (Permian).
mixed semipelite, metacarbonate, and pelite
Metamorphosed silstone and shale; metacarbonate; intercalated metamorphosed calcareous siltstone and shale. Includes minor metacarbonate and metavolcanic rocks.
metacarbonate
Layers of metacarbonate with little or no clastic metasedimentary rock.
psammite
Varying composition of psammite from arkosic to quartzitic locally characterized by hummocky cross stratification.
mixed psammite, pelite, and semipelite
Pelitic and semipelitic tops present as thin layers over psammite. Locally graphite-rich.
pelite
Includes minor semipelite and psammite.
MINERALS
biotite .... Bt
garnet .... Grt
staurolite .... St
kyanite .... Ky
sillimanite .... Si
K-feldspar .... Kfs
chloritoid .... Ctd
tremolite .... Tr
actinolite .... Act
hornblende .... Hbl
SYMBOLS
metamorphic foliation
roman numeral indicates generation (I/II/III = 1st/2nd/3rd)
mineral lineation
roman numeral indicates generation (I/II/III = 1st/2nd/3rd)
crenulation lineation
roman numeral indicates generation (II/III = 2nd/3rd)
lithological contact
defined, approximate, inferred
mineral isograd
defined, approximate, inferred, unknown (mineral listed on high temperature side)
thrust fault
defined, approximate, inferred (ornament on apparent hanging wall)
normal fault
defined, approximate, inferred (ornament on apparent hanging wall)
fault
thrust or normal; defined, approximate, inferred (ornament on apparent hanging wall)
antiform axial trace
defined, approximate, inferred; roman numeral = generation (II/IV/V = 2nd/4th/5th)
synform axial trace
defined, approximate, inferred; roman numeral = generation (II/IV = 2nd/4th)
backfold antiform axial trace
defined, approximate, inferred; roman numeral = generation (III = 3rd)
overturned antiform axial trace
defined, approximate, inferred; roman numeral = generation (II= 2nd)
overturned synform axial trace
defined, approximate, inferred; roman numeral = generation (II = 2nd)
recumbent antiform axial trace
defined, approximate, inferred; roman numeral = generation (II = 2nd)
recumbent synform axial trace
defined, approximate, inferred; roman numeral = generation (II = 2nd)
aerial imagery source
fold structure inferred from aerial imagery
topographic contour
200 m interval
river
town
camp
peak
pass
REFERENCES
aerial imagery basemap
Copernicus Sentinel-2 L1C; September 2021, processed by ESA.
digital elevation data
SRTM 1-Arc second; September 2014, processed by USGS. https://earthexplorer.usgs.gov/.
remote sensed mapping sources
Sentinel Playground, Sentinel-2 L1C, Bands 4,3,2 & 12,4,2; September 2019, September 2021. https://apps.sentinel-hub.com/sentinel-playground, Sinergise Ltd.
Copernicus Sentinel data 2017-2022, processed by ESA.
Google Earth, Google Earth V 7.3.4.8642. (July 2013, October 2017; October 2019). Landsat/Copernicus, CNES/Airbus 2023, Maxar Technologies 2023.

Fig. 4

LITHOSTRATIGRAPHY

Indus Suture Zone (ISZ)

Dras volcanics

- volcanics (undifferentiated)
  Undifferentiated andesites, basalts, and epiclastic breccia of the Dras Volcanics, and minor Kargil Intrusives (Jurassic–Cretaceous)
- tectonised intercalation
  Tectonised intercalation of Dras volcanics (undifferentiated), radiolarian chert, graphitic pelite, and group B metavolcanic rocks contacts between blocks or lenses defined by faults/shear zones

Lamayuru Complex

- group B metavolcanic rock
  Actinolite schists and amphibolites (Triassic–Jurassic)
- mixed graphitic semipelite, metacarbonate, and pelite
  Metamorphosed graphite rich siltstone and shale; metacarbonate; intercalated metamorphosed calcareous siltstone and shale. Includes minor metacarbonate and metavolcanic rocks
- mixed pelite, psammite, and semipelite
  Alternating layers of pelite and psammite or semipelite horizons
- graphitic pelite
  Metamorphosed graphite-rich silstone and shale

Tethyan and Greater Himalayan Sequence (THS & GHS)

- granite (undifferentiated)
- garnet tourmaline leucogranite
  Ex-situ products of metamorphosed sedimentary rocks. Includes minor mixed psammite, pelite, and semipelite (Miocene)
- garnet biotite muscovite granite
  Varying composition from monzo- to syenogranite (Permian), includes xenoliths of group A metavolcanic rock and minor discontinuous layers of leucogranite
- biotite muscovite syenogranite
  Megacrystic K-feldspar syenogranite (Cambro-Ordovician)
- group A metavolcanic rock (Panjal Traps)
  Actinolite schists and amphibolites of the Panjal Traps (Permian)
- mixed semipelite, metacarbonate, and pelite
  Metamorphosed silstone and shale; metacarbonate; intercalated metamorphosed calcareous siltstone and shale. Includes minor metacarbonate and metavolcanic rocks
- metacarbonate
  Layers of metacarbonate with little or no clastic metasedimentary rock
- psammite
  Varying composition of psammite from arkosic to quartzitic locally characterized by hummocky cross stratification
- mixed psammite, pelite, and semipelite
  Pelitic and semipelitic tops present as thin layers over psammite. Locally graphite rich
- pelite
  Includes minor semipelite and psammite

SYMBOLS

- apparent dip
  roman numeral indicates generation (I/II/III= 1st/2nd/3rd)
- geological contact
  below topography, aerial
- mineral isograd
  below topography, aerial; mineral listed on high temperature side
- fault
  below topography, aerial; arrows indicate normal or thrust-sense throw
- antiform axial trace
  defined, approximate, inferred; roman numeral = generation (I/II/IV = 2nd/4th/5th)
- synform axial trace
  defined, approximate, inferred; roman numeral = generation (II/IV = 2nd/4th)
- backfold antiform axial trace
  defined, approximate, inferred; roman numeral = generation (III = 3rd)
- overturned antiform axial trace
  defined, approximate, inferred; roman numeral = generation (II = 2nd)
- overturned synform axial trace
  defined, approximate, inferred; roman numeral = generation (II = 2nd)
- recumbent antiform axial trace
  defined, approximate, inferred; roman numeral = generation (II = 2nd)
- recumbent synform axial trace
  defined, approximate, inferred; roman numeral = generation (II = 2nd)

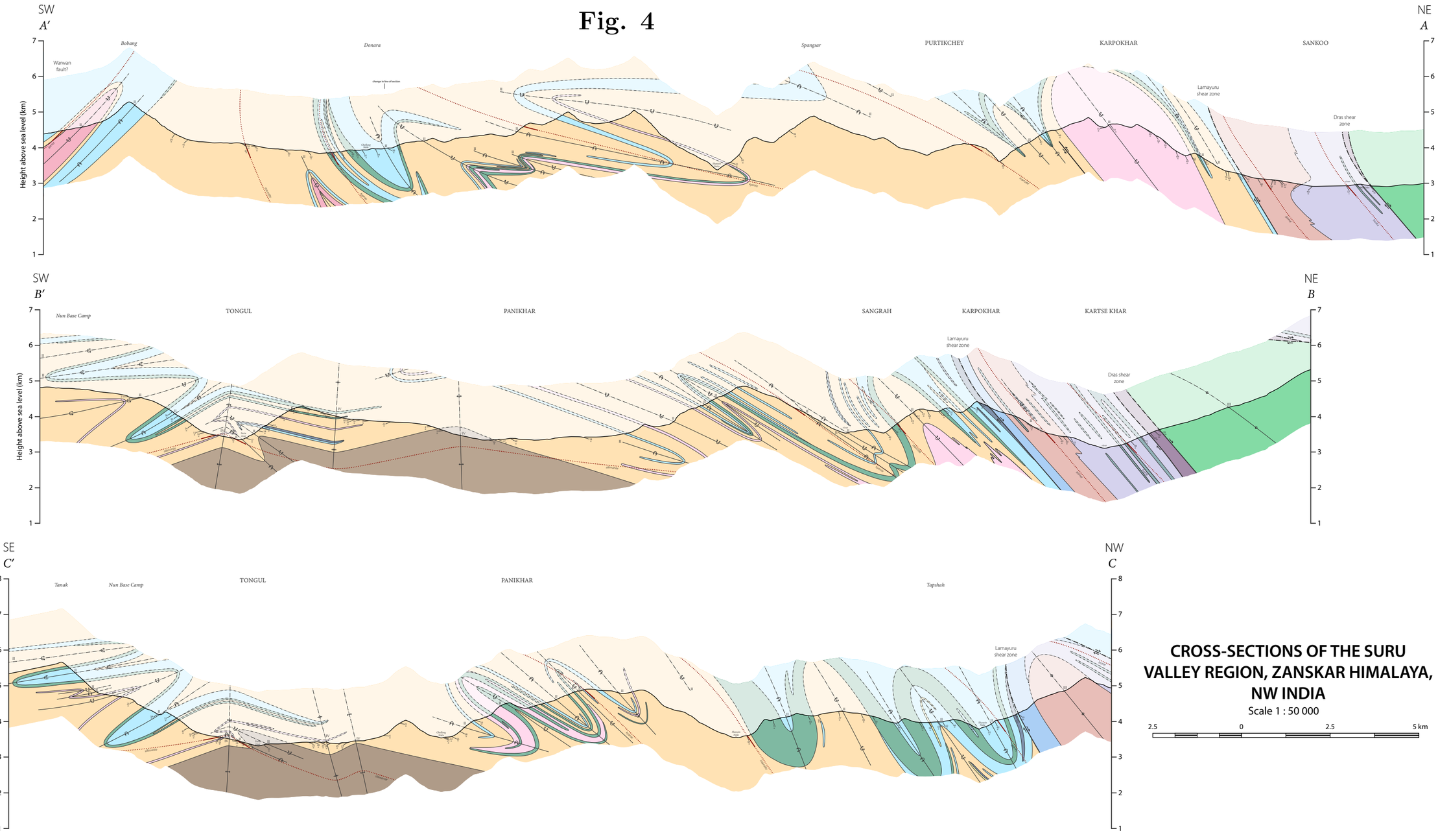

CROSS-SECTIONS OF THE SURU VALLEY REGION, ZANSKAR HIMALAYA, NW INDIA

Scale 1 : 50 000

2.5 0 2.5 5 km

NOTES

A-A′ notes:

- *Small scale folding in Lamayuru Group lithologies represent minor F_3 folds as described in text. The change in S_2 from NE-dipping to SW-dipping reflects F_3 fold structures, with developing S_4 consistently shallowly NE dipping.*
- *Warwan fault located at A′ as suggested by Honegger (1983) or anywhere from this point to 7 km SW as may be inferred from remote sensed mapping.*

B-B′ notes:

- *Small scale folding in Lamayuru Group lithologies represent minor F_3 folds as described in text.*
- *The large overturned F_3 fold and localised inversion of the sequence to place Lamayuru complex above the Dras Volcanics is inferred from the trend of the Dras shear zone N of Shispur and remote sensed mapping. It is supported by the sections of Gilbert (1986), Honegger (1983), and Steck (2003). This is likely a larger equivalent of the minor F3 folds displayed in A-A′. Normal sense movement on the shear zone is warped by the backfold into alligirment with NE-directed backthrusting.*

C-C′ notes:

- *The faults on the NW side of the section display composite normal- and thrust-sense movement, these structures originated as thrust faults, therefore although the structures are folded, the zones reactivated by normal-sense movement post-date the F2 folding.*
- *The folding of the Lamayuru fault is constrained by remote sensed mapping and interpretations of Honegger (1983).*

D-D′ notes:

- *Subsurface leucogranite is constrained by dominance of cm-scale intrusions of leucogranite in host mixed psammite, pelite, and semipelite at surface localities.*

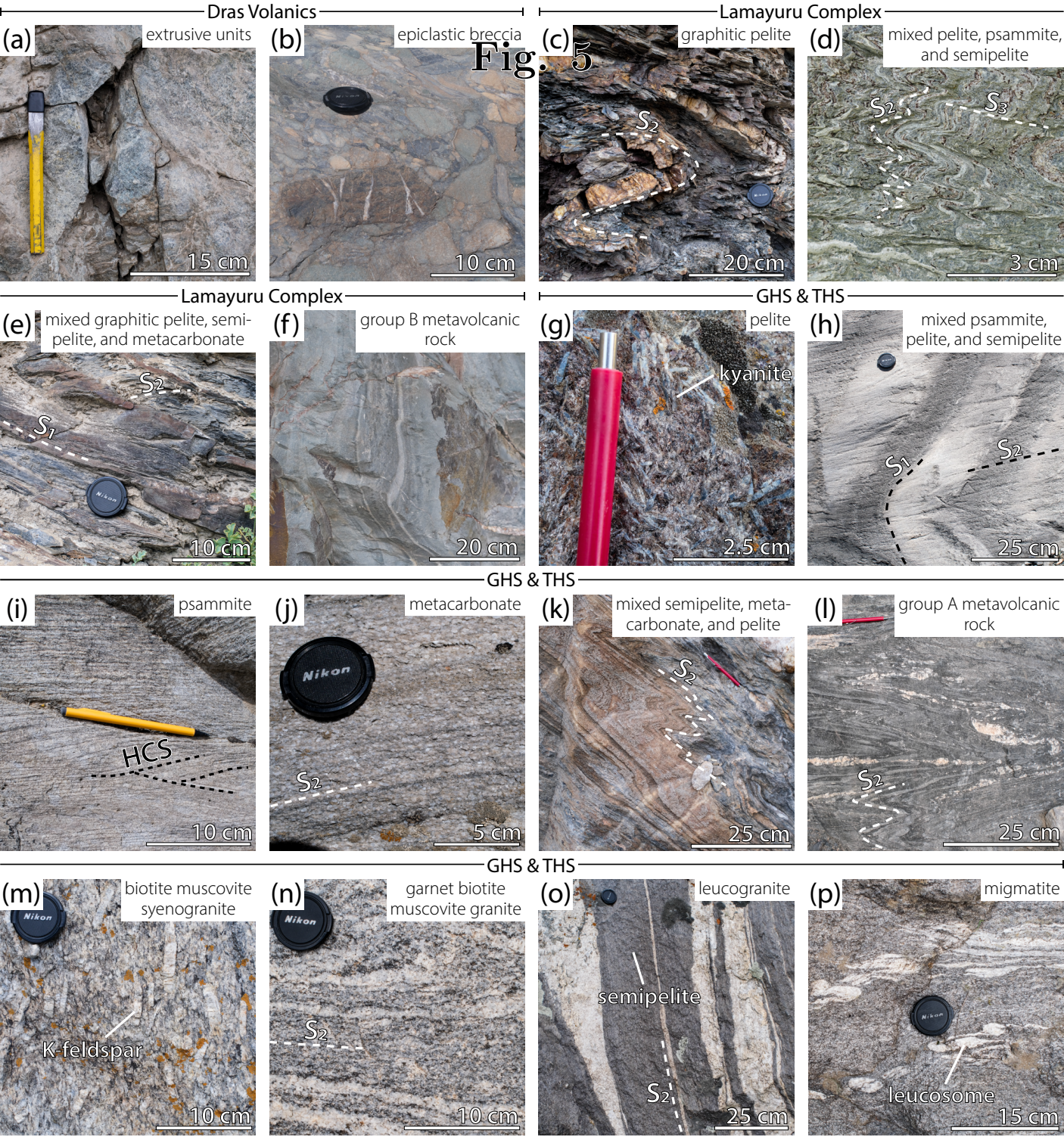
Fig. 5
Dras Volanics
Lamayuru Complex
Lamayuru Complex
GHS & THS
GHS & THS
GHS & THS
(a)
extrusive units
15 cm
(b)
epiclastic breccia
10 cm
(c)
graphitic pelite
S2
20 cm
(d)
mixed pelite, psammite, and semipelite
S2
S3
3 cm
(e)
mixed graphitic pelite, semi-pelite, and metacarbonate
S2
S1
10 cm
(f)
group B metavolcanic rock
20 cm
(g)
pelite
kyanite
2.5 cm
(h)
mixed psammite, pelite, and semipelite
S1
S2
25 cm
(i)
psammite
HCS
10 cm
(j)
metacarbonate
S2
5 cm
(k)
mixed semipelite, meta-carbonate, and pelite
S2
25 cm
(l)
group A metavolcanic rock
S2
25 cm
(m)
biotite muscovite syenogranite
K-feldspar
10 cm
(n)
garnet biotite muscovite granite
S2
10 cm
(o)
leucogranite
semipelite
S2
25 cm
(p)
migmatite
leucosome
15 cm

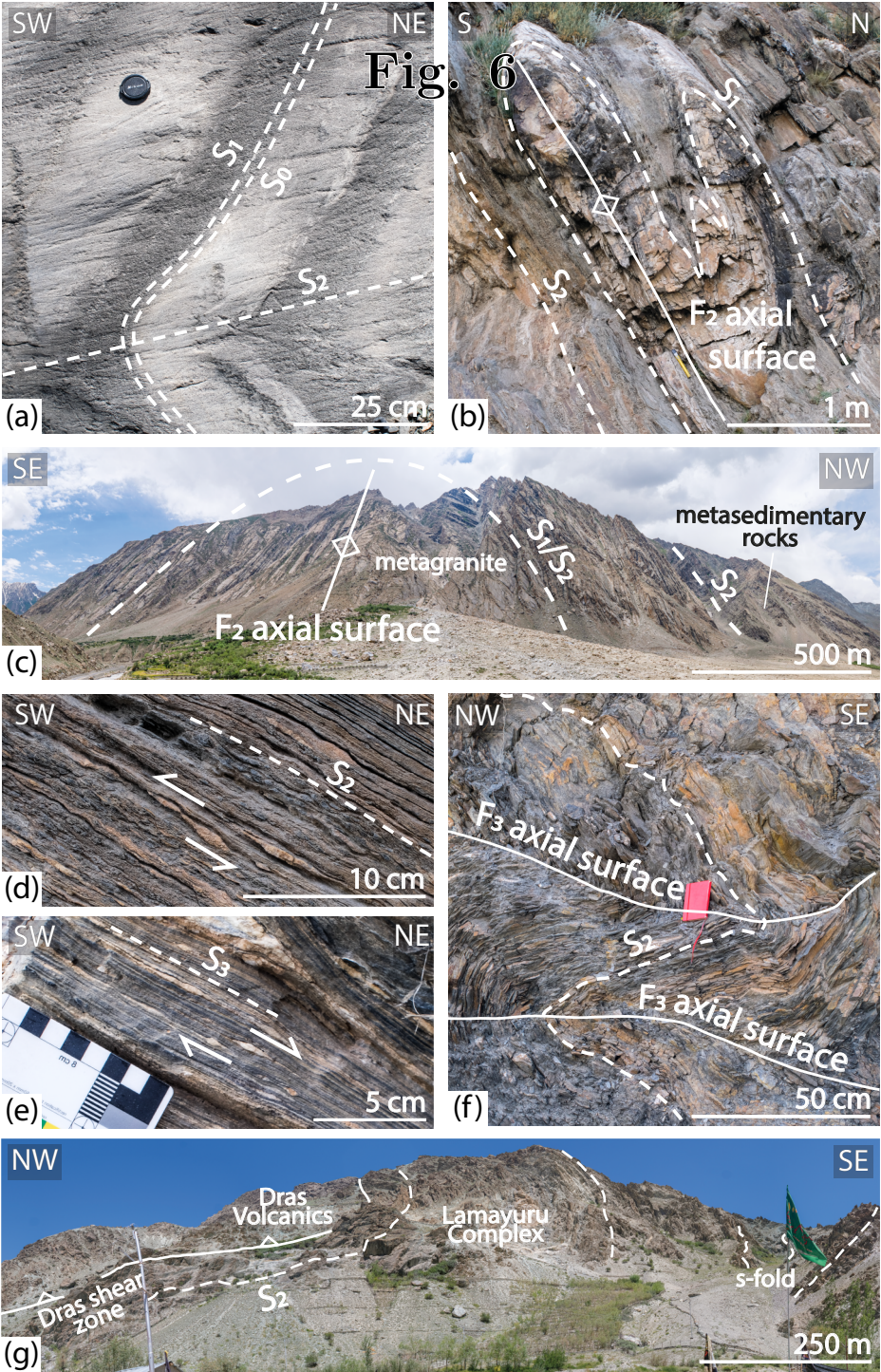
Fig. 6
SW
NE
S1
S0
S2
25 cm
(a)
S
N
S1
S2
F2 axial surface
1 m
(b)
SE
NW
metasedimentary rocks
metagranite
S1/S2
S2
F2 axial surface
500 m
(c)
SW
NE
S2
10 cm
(d)
SW
NE
S3
5 cm
(e)
NW
SE
F3 axial surface
S2
F3 axial surface
50 cm
(f)
NW
SE
Dras Volcanics
Lamayuru Complex
Dras shear zone
S2
s-fold
250 m
(g)

Fig. 7

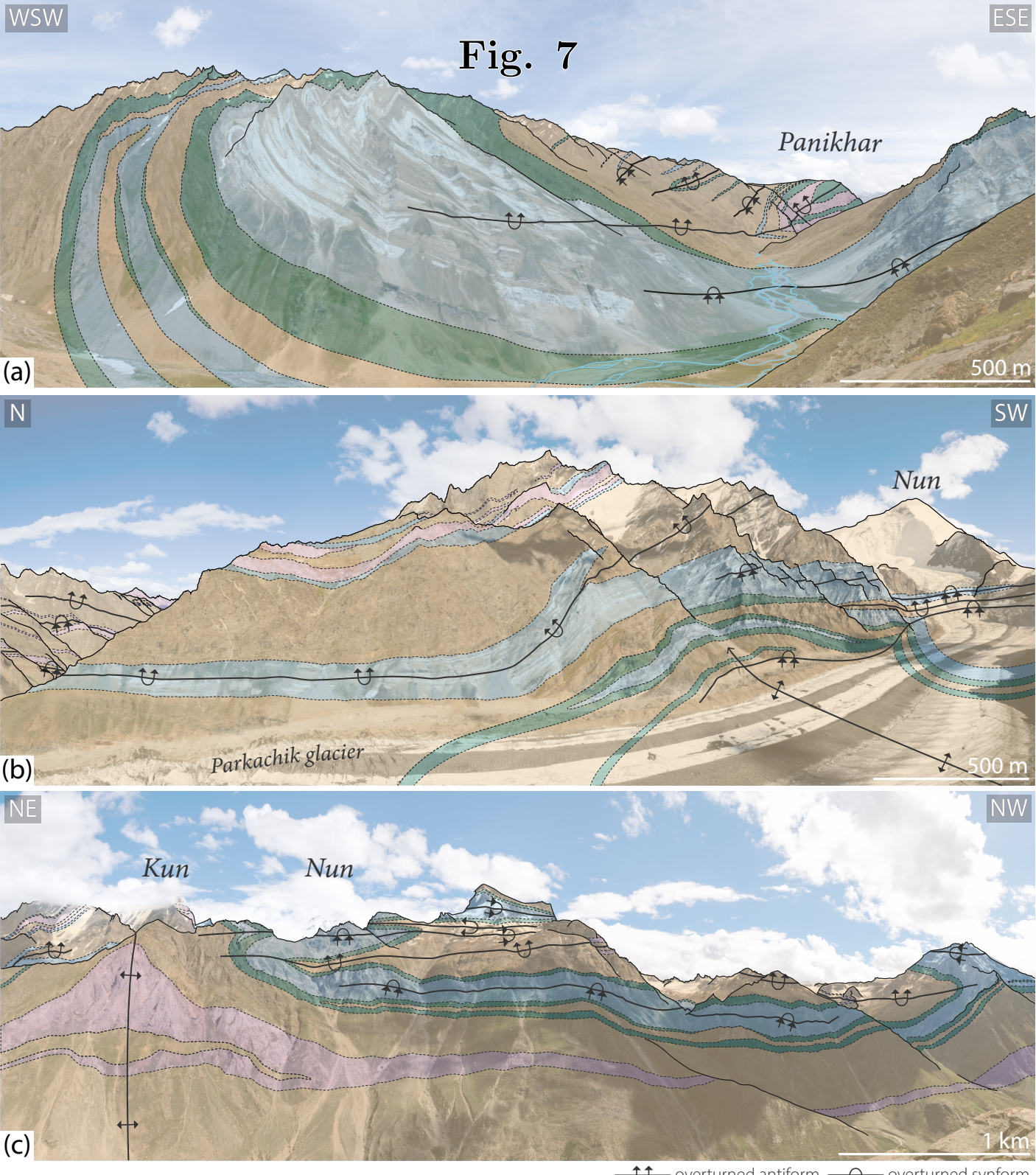
WSW
ESE
Panikhar
(a)
500 m
N
SW
Nun
Parkachik glacier
(b)
500 m
NE
NW
Kun
Nun
(c)
1 km
garnet biotite muscovite granite
group A metavolcanic rock
mixed semipelite, metacarbonate, and pelite
mixed psammite, pelite, and semipelite
overturned antiform
recumbent antiform
antiform
overturned synform
recumbent synform
lithological contact

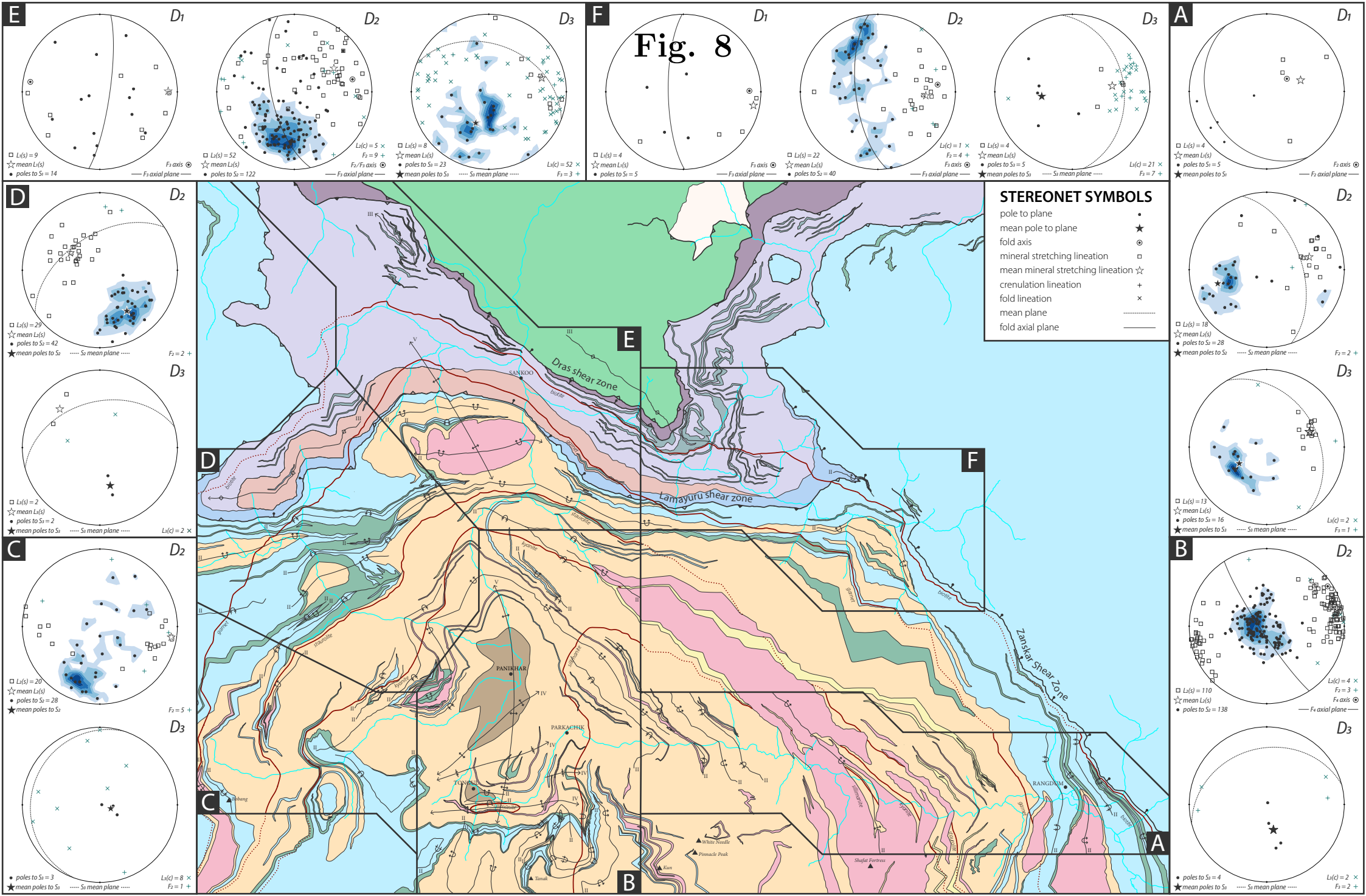
Fig. 8
E
D₁
D₂
D₃
F
A
D
C
B
STEREONET SYMBOLS
pole to plane
mean pole to plane
fold axis
mineral stretching lineation
mean mineral stretching lineation
crenulation lineation
fold lineation
mean plane
fold axial plane
Dras shear zone
Lamayuru shear zone
Zanskar Shear Zone
SANKOO
PANIKHAR
PARKACHIK
TONGDE
RANGDUM
Tanak
White Needle
Pinnacle Peak
Kun
Shafat Fortress
biotite
garnet
staurolite
kyanite
sillimanite
L₁(s) = 9
mean L₁(s)
poles to S₁ = 14
F₁ axis
F₁ axial plane
L₂(s) = 52
mean L₂(s)
poles to S₂ = 122
L₂(c) = 5
F₂ = 9
F₂/F₃ axis
F₃ axial plane
L₃(s) = 8
mean L₃(s)
poles to S₃ = 23
mean poles to S₃
S₃ mean plane
L₃(c) = 52
F₃ = 3
L₁(s) = 4
mean L₁(s)
poles to S₁ = 5
L₂(s) = 22
mean L₂(s)
poles to S₂ = 40
L₂(c) = 1
F₂ = 4
F₃ axis
L₃(s) = 4
mean L₃(s)
poles to S₃ = 5
mean poles to S₃
L₃(c) = 21
F₃ = 7
L₂(s) = 29
mean L₂(s)
poles to S₂ = 42
mean poles to S₂
F₂ = 2
L₃(s) = 2
mean L₃(s)
poles to S₃ = 2
L₃(c) = 2
L₂(s) = 20
mean L₂(s)
poles to S₂ = 28
F₂ = 5
poles to S₃ = 3
L₃(c) = 8
F₂ = 1
L₁(s) = 4
mean L₁(s)
poles to S₁ = 5
L₂(s) = 18
mean L₂(s)
poles to S₂ = 28
L₃(s) = 13
mean L₃(s)
poles to S₃ = 16
L₃(c) = 2
F₃ = 1
L₂(s) = 110
mean L₂(s)
poles to S₂ = 138
L₂(c) = 4
F₂ = 3
F₄ axis
F₄ axial plane
poles to S₃ = 4
L₃(c) = 2
F₃ = 2

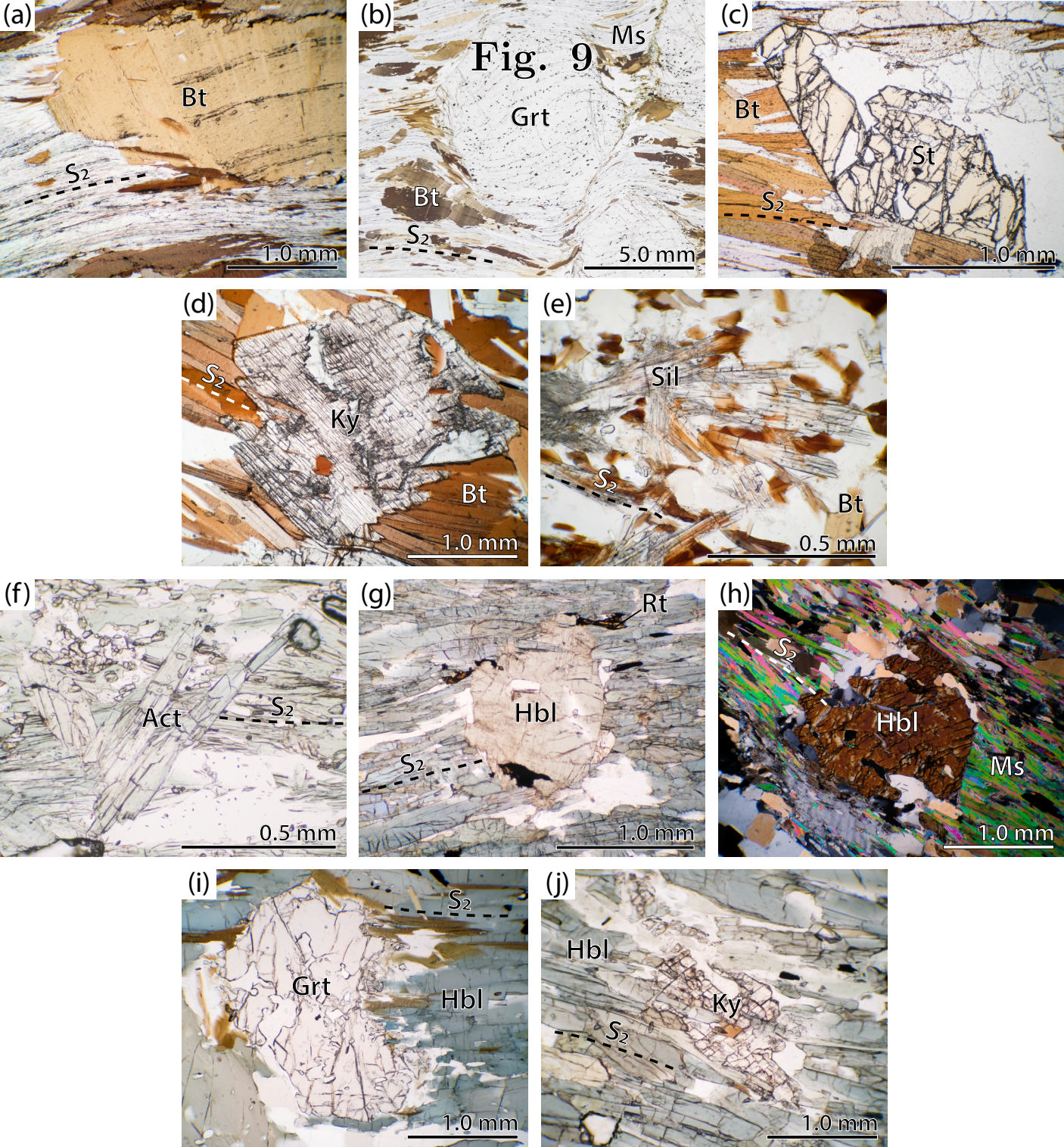
(a)
Bt
S2
1.0 mm
(b)
Fig. 9
Ms
Grt
Bt
S2
5.0 mm
(c)
Bt
St
S2
1.0 mm
(d)
S2
Ky
Bt
1.0 mm
(e)
Sil
S2
Bt
0.5 mm
(f)
Act
S2
0.5 mm
(g)
Rt
Hbl
S2
1.0 mm
(h)
S2
Hbl
Ms
1.0 mm
(i)
S2
Grt
Hbl
1.0 mm
(j)
Hbl
Ky
S2
1.0 mm

Fig. 10

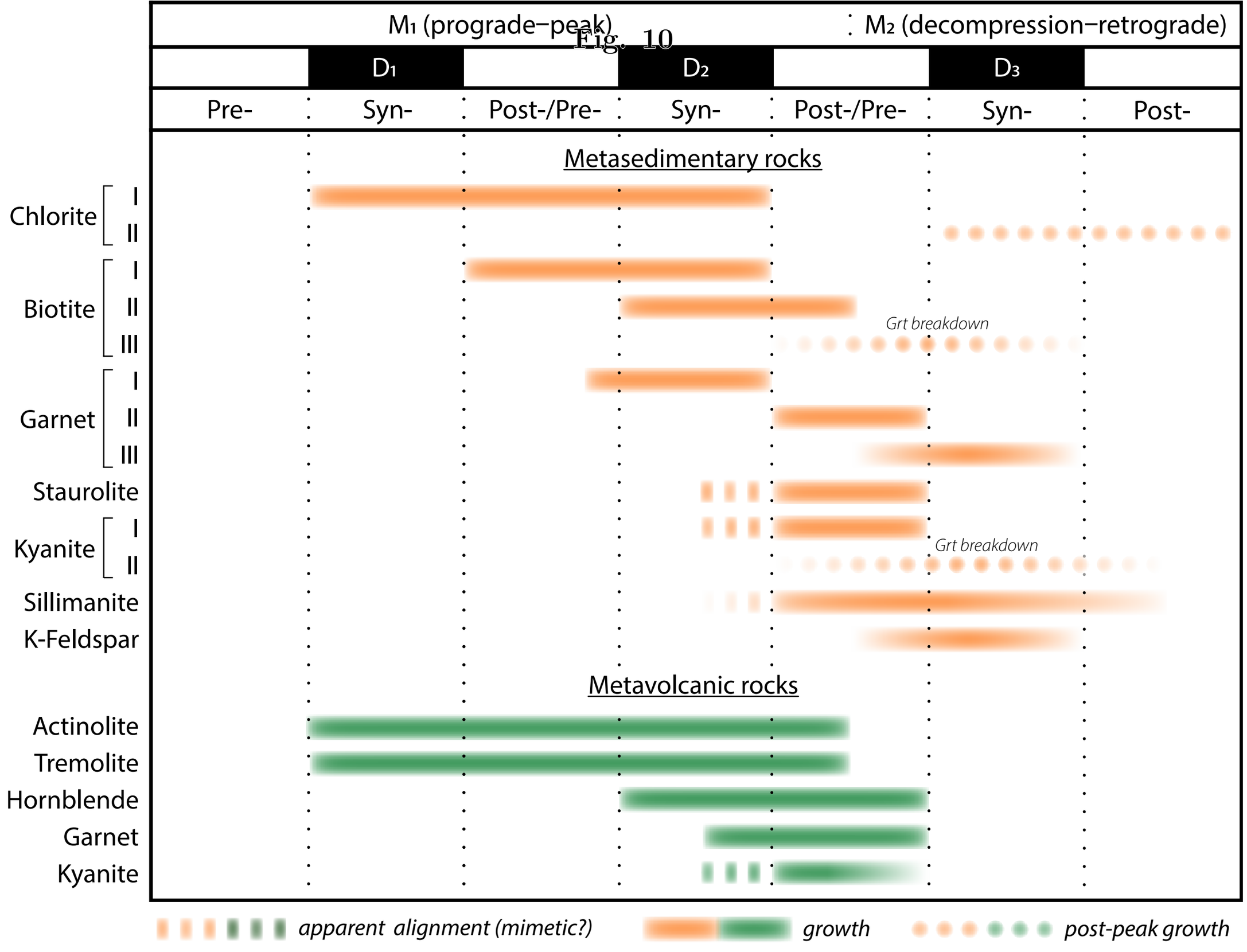
M1 (prograde–peak)
M2 (decompression–retrograde)
D1
D2
D3
Pre-
Syn-
Post-/Pre-
Syn-
Post-/Pre-
Syn-
Post-
Metasedimentary rocks
Chlorite
I
II
Biotite
I
II
III
Grt breakdown
Garnet
I
II
III
Staurolite
Kyanite
I
II
Grt breakdown
Sillimanite
K-Feldspar
Metavolcanic rocks
Actinolite
Tremolite
Hornblende
Garnet
Kyanite
apparent alignment (mimetic?)
growth
post-peak growth

Fig. 11

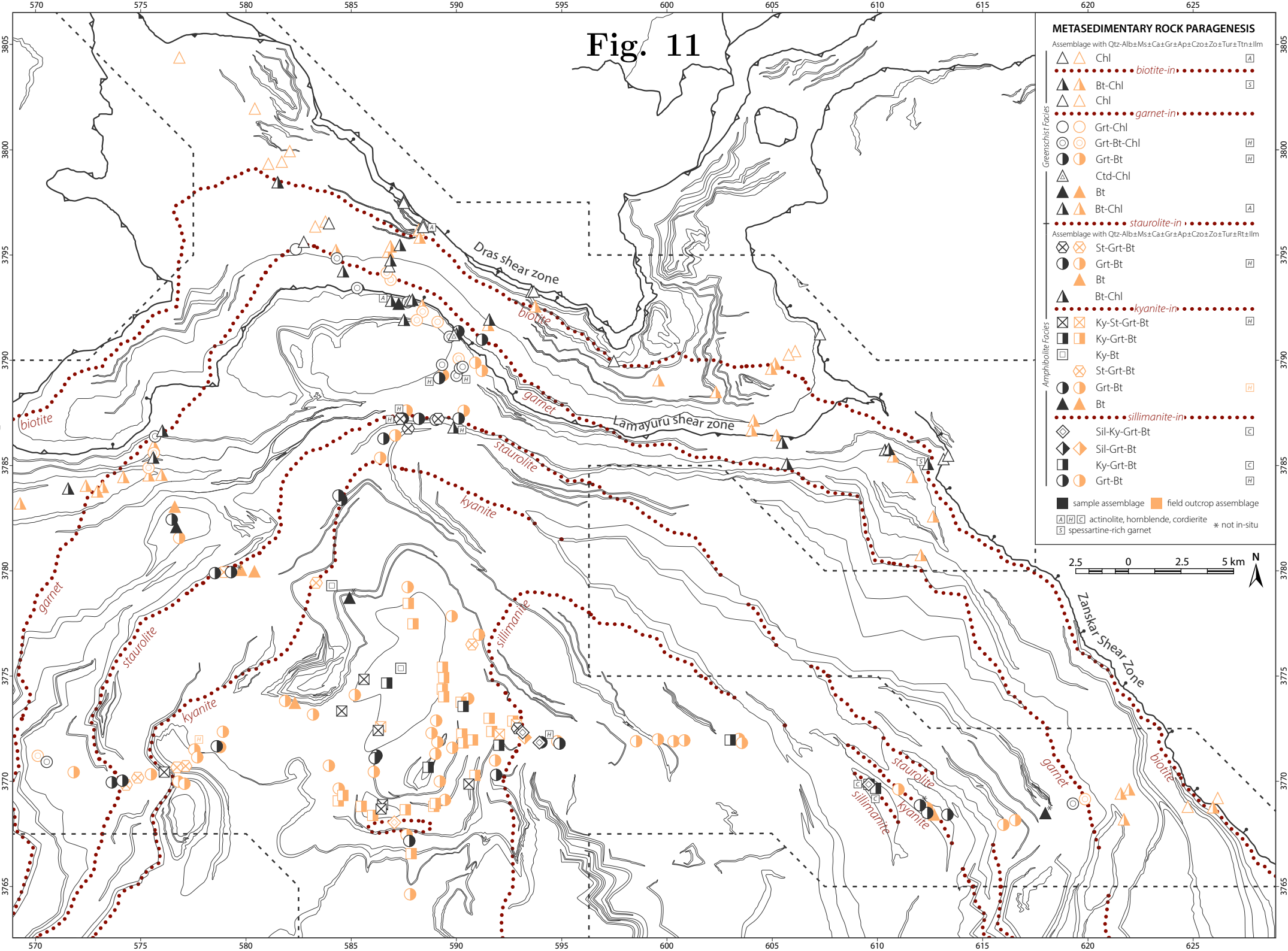
METASEDIMENTARY ROCK PARAGENESIS
Assemblage with Qtz-Alb±Ms±Ca±Gr±Ap±Czo±Zo±Tur±Ttn±Ilm
Chl
biotite-in
Bt-Chl
Chl
garnet-in
Grt-Chl
Grt-Bt-Chl
Grt-Bt
Ctd-Chl
Bt
Bt-Chl
staurolite-in
Assemblage with Qtz-Alb±Ms±Ca±Gr±Ap±Czo±Zo±Tur±Rt±Ilm
St-Grt-Bt
Grt-Bt
Bt
Bt-Chl
kyanite-in
Ky-St-Grt-Bt
Ky-Grt-Bt
Ky-Bt
St-Grt-Bt
Grt-Bt
Bt
sillimanite-in
Sil-Ky-Grt-Bt
Sil-Grt-Bt
Ky-Grt-Bt
Grt-Bt
Greenschist Facies
Amphibolite Facies
sample assemblage
field outcrop assemblage
A H C actinolite, hornblende, cordierite
S spessartine-rich garnet
* not in-situ
2.5 0 2.5 5 km
N
Dras shear zone
Lamayuru shear zone
Zanskar Shear Zone
biotite
garnet
staurolite
kyanite
sillimanite
570 575 580 585 590 595 600 605 610 615 620 625
3805 3800 3795 3790 3785 3780 3775 3770 3765

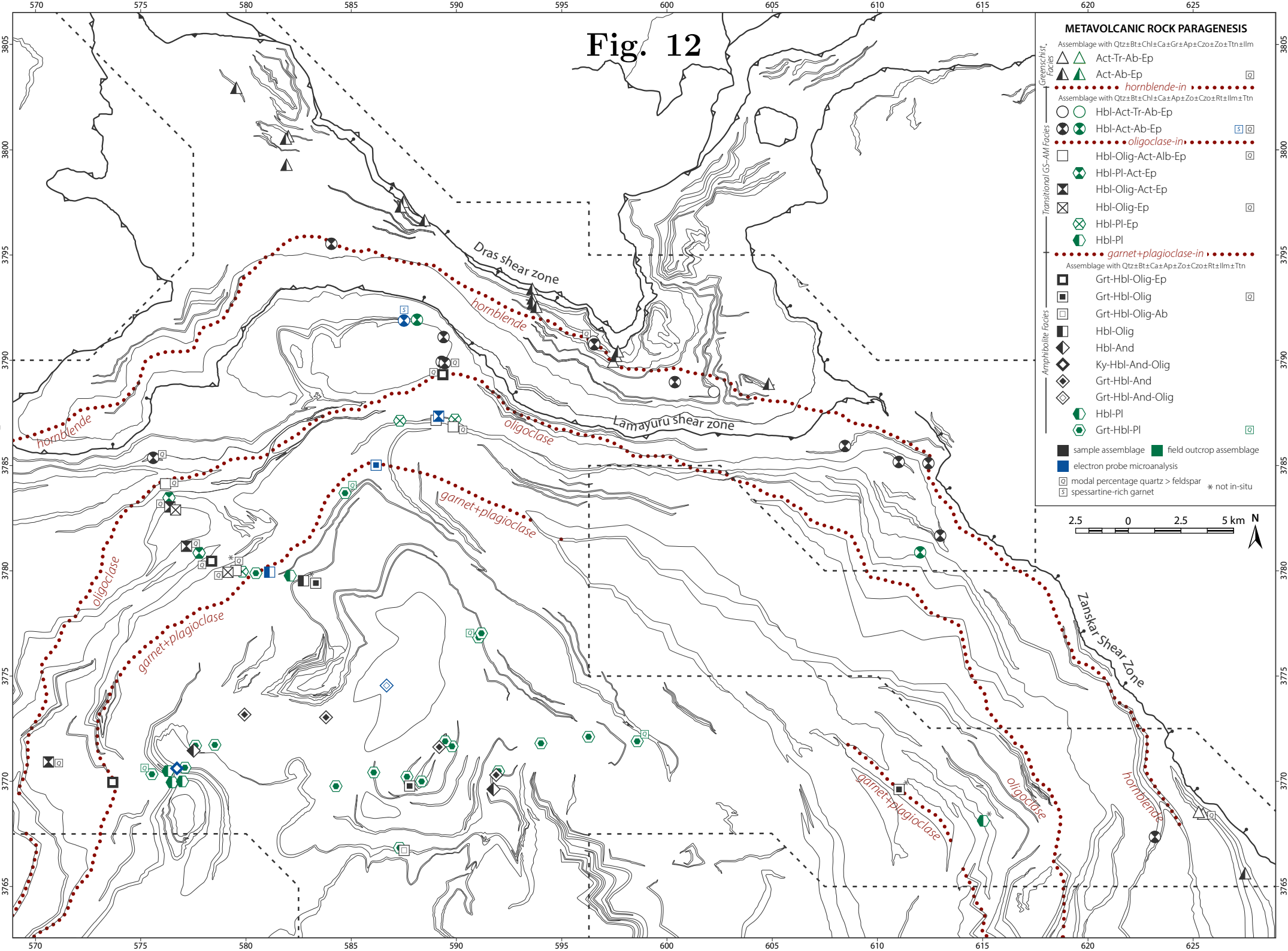
Fig. 12
METAVOLCANIC ROCK PARAGENESIS
Greenschist Facies
Assemblage with Qtz±Bt±Chl±Ca±Gr±Ap±Czo±Zo±Ttn±Ilm
Act-Tr-Ab-Ep
Act-Ab-Ep
hornblende-in
Transitional GS–AM Facies
Assemblage with Qtz±Bt±Chl±Ca±Ap±Zo±Czo±Rt±Ilm±Ttn
Hbl-Act-Tr-Ab-Ep
Hbl-Act-Ab-Ep
oligoclase-in
Hbl-Olig-Act-Alb-Ep
Hbl-Pl-Act-Ep
Hbl-Olig-Act-Ep
Hbl-Olig-Ep
Hbl-Pl-Ep
Hbl-Pl
garnet+plagioclase-in
Amphibolite Facies
Assemblage with Qtz±Bt±Ca±Ap±Zo±Czo±Rt±Ilm±Ttn
Grt-Hbl-Olig-Ep
Grt-Hbl-Olig
Grt-Hbl-Olig-Ab
Hbl-Olig
Hbl-And
Ky-Hbl-And-Olig
Grt-Hbl-And
Grt-Hbl-And-Olig
Hbl-Pl
Grt-Hbl-Pl
sample assemblage
field outcrop assemblage
electron probe microanalysis
Q modal percentage quartz > feldspar
S spessartine-rich garnet
* not in-situ
2.5 0 2.5 5 km
N
Dras shear zone
Lamayuru shear zone
Zanskar Shear Zone
hornblende
oligoclase
garnet+plagioclase
570 575 580 585 590 595 600 605 610 615 620 625
3805 3800 3795 3790 3785 3780 3775 3770 3765

Fig. 13

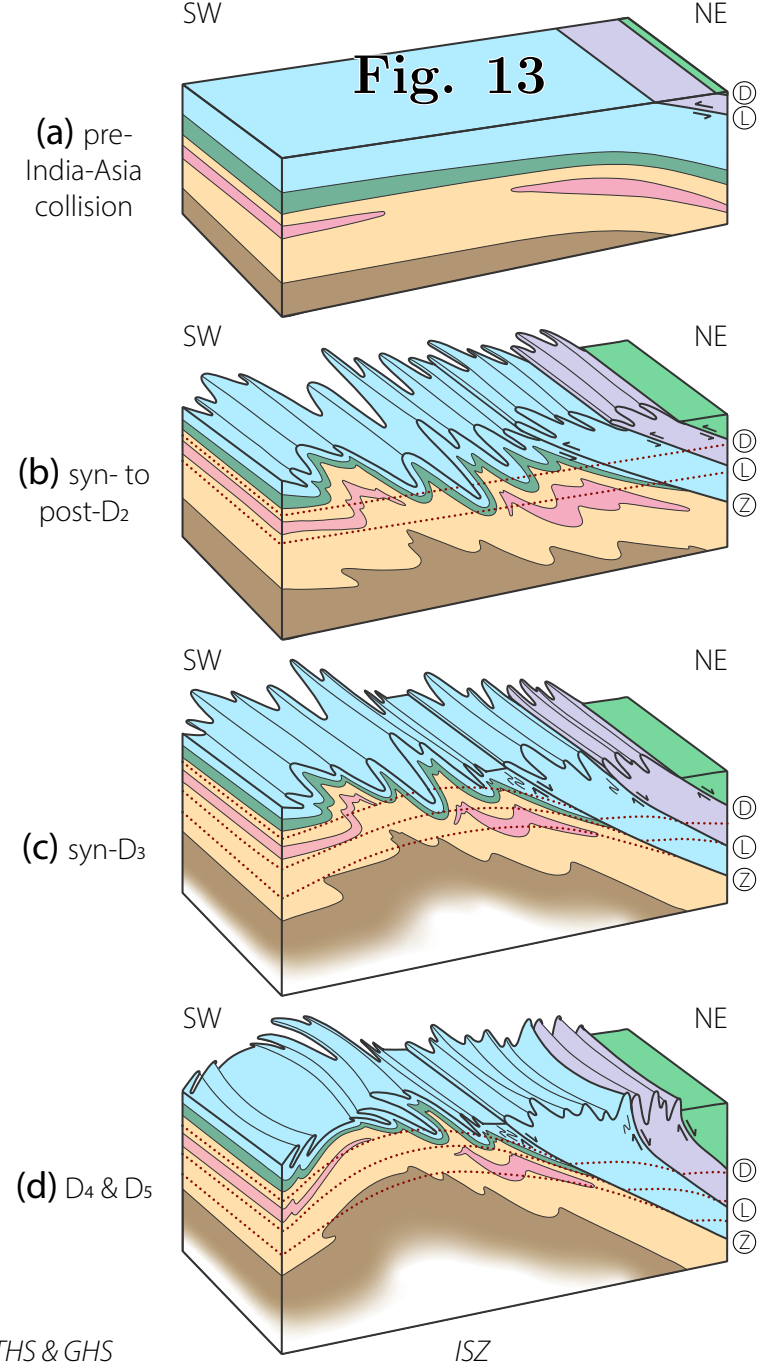
SW
NE
(a) pre-India-Asia collision
D
L
SW
NE
(b) syn- to post-D2
D
L
Z
SW
NE
(c) syn-D3
D
L
Z
SW
NE
(d) D4 & D5
D
L
Z
THS & GHS
metagranite
group A metavolcanic rock (Panjal Traps)
mixed semipelite, metacarbonate, and pelite
mixed psammite, pelite, and semipelite
pelite
ISZ
Dras Volcanics
Lamayuru Complex
D Dras shear zone
L Lamayuru shear zone
Z Zanskar Shear Zone
fault
mineral isograd

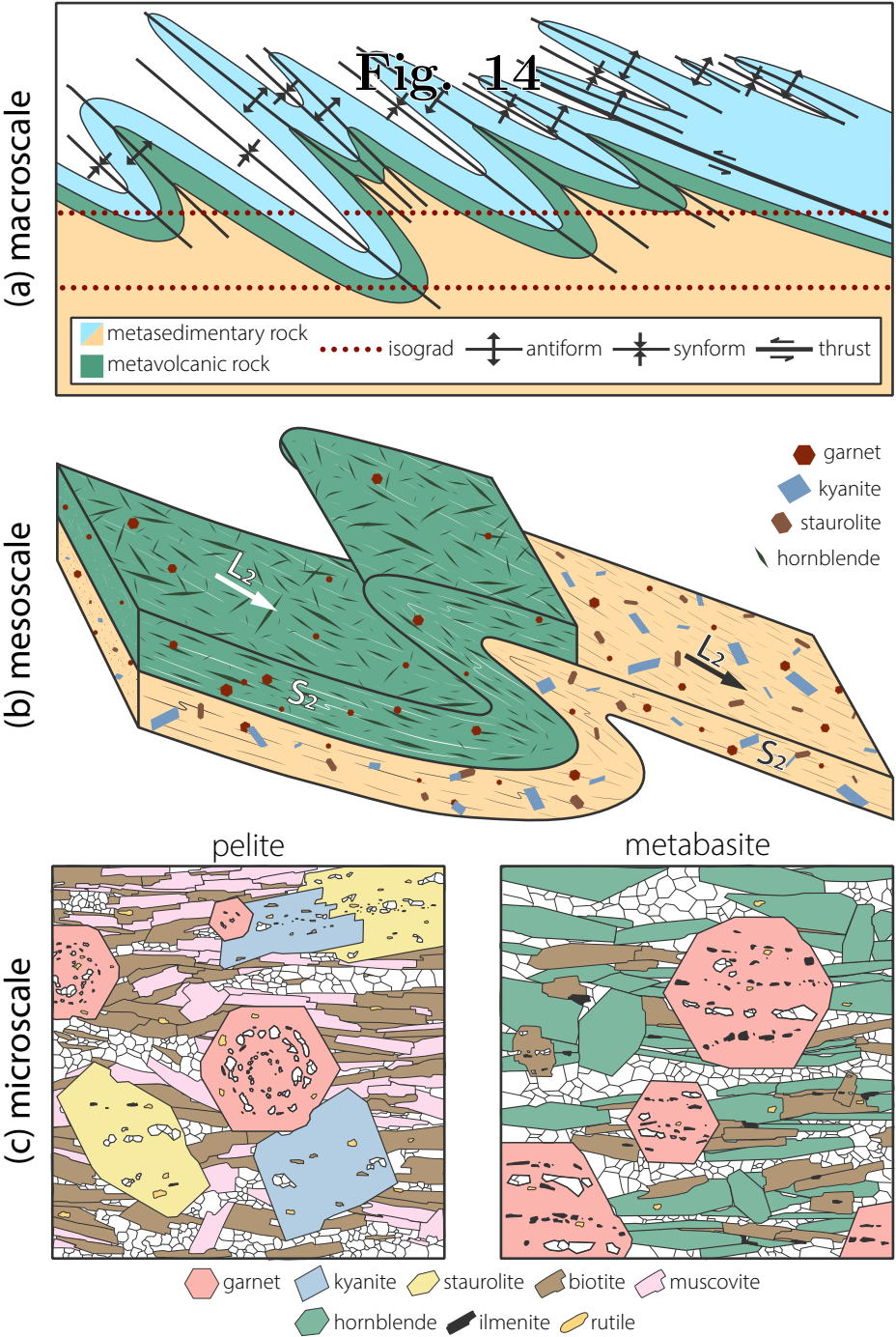
Fig. 14
(a) macroscale
metasedimentary rock
metavolcanic rock
isograd
antiform
synform
thrust
(b) mesoscale
garnet
kyanite
staurolite
hornblende
L2
S2
L2
S2
(c) microscale
pelite
metabasite
garnet
kyanite
staurolite
biotite
muscovite
hornblende
ilmenite
rutile

Table 1: Main deformation fabrics observed in Suru Valley area, Zanskar Himalaya. *N.b.,* F_3 measurements include both mesoscale F_3 and microscale crenulation measurements, i.e., $L_3(c)$

Planar and linear structural features	**Expression**	**Data**
S_1/L_1	S_1: NE- dipping schistosity parallel or sub-parallel to S_0. L_1: W- to E- plunging mineral stretching lineation (NE-directed where least reworked).	L_1: 19 → 090
$S_2/L_2/F_2$	S_2: NW- to NE-dipping fabric displaying crenulation cleavage, schistosity and C-S structures. L_2: SW- to NE-plunging mineral stretching lineation associated with thrust sense shearing. F_2: Folding of S_1 fabric. S_2 is axial planar to F_2.	L_2: 16 → 079 F_2: 17 → 082
$S_3/L_3/F_3$	S_3: NE-dipping composite fabric comprising mylonitic C-S-C' planar elements, schistosity, and a crenulation cleavage. Coaxial with S_2. L_3: NE-plunging mineral stretching lineation associated with normal sense shearing. Coaxial with L_2. F_3: Folding of S_2 (and locally S_1) fabric. S_3 is axial planar to F_3.	L_3: 38 → 071 F_3: 10 → 092
F_4	Open km-scale cross-folds with NE- and SW-plunging fold axes and SE- or NW-dipping axial surfaces. No penetrative fabric developed.	F_4: 07 → 056
F_5	Open km-scale folds with NW- and SE-plunging fold axes and sub-vertical axial surface. No penetrative fabric developed.	

Table 2: Microscale, mesoscale, and macroscale relationship between deformation and metamorphism in pelitic and metabasic rocks of the Suru Valley region.

Indicator mineral	**Macroscale**	**Mesoscale**	**Microscale**
		Pelitic sequence	
Biotite	Biotite isograd sub-parallel to D_2 and early–mid D_3 structures, weakly folded by mid–late D_3 backfolds.	Defines S_2 and aligned to L_2.	Low grade: Syn-D_2 and re-oriented by D_3. Mod–high grade: Syn- to post-D_2 and re-oriented by D_3. Recrystallisation and retrograde growth continues post-D_2 and syn-D_3.
Garnet	Garnet isograd sub-parallel to crosscutting D_2 structures and sub-parallel to early–mid D_3 structures, weakly folded by mid–late D_3 backfolds.	Garnet shows spiral inclusion trails or overgrow S_2 fabric, where wrapped by S_3 internal S_2 is disjunctive.	Low grade: Syn- to post D_2 growth. Mod–high grade: Syn-D_2 core with post-D_2 rim.
Staurolite	Staurolite isograd sub-parallel to D_2 structures.	Staurolite overgrows S_2 and is not aligned with L_2.	Dominantly post-D_2 with S_2 concordant inclusion trails, wrapped by S_3 where present.
Kyanite-grade	Kyanite isograd sub-parallel to crosscutting D_2 structures.	Kyanite overgrows S_2 and is not aligned with L_2.	Dominantly post-D_2 and wrapped by S_3 where present. Late growth (garnet breakdown) syn-D_3.
Sillimanite-grade	Sillimanite isograd sub-parallel to crosscutting D_2 structures.	Sillimanite overgrows S_2 and is oriented with (mimetic?) or crosscutting L_2.	Post-D_2.
Sillimanite+ K-feldspar-grade	No macro-scale observations.	Leucosome sub-parallel to crosscuting S_2. Sillimanite aligned to crosscutting L_2.	Sillimanite post-D_2. Garnet growth with sillimanite inclusions encloses previous garnet phases, and garnet growth in leucosome form during dehydration melting.
		Metabasic sequence	

Table 2 - continued

Indicator mineral	**Macroscale**	**Mesoscale**	**Microscale**
Actinolite	N/A	Greenschist facies: mats define a weak S_1 and S_2, grains aligned to L_1, and weakly aligned or crosscut L_2. Greenschist–amphibolite facies: strongly aligned to L_2 and defines S_2. All: reoriented by S_3 and L_3.	Syn-D_1 and syn-D_2 growth. Where present, reoriented by D_3.
Hornblende	Hornblende isograd subparallel to crosscutting D_2 structures. Subparallel to early–mid D_3 structures and weakly folded by mid–late D_3 backfolds.	Weakly aligned to misoriented to L_2 and S_2. Folded and reoriented by F_3 and S_3.	Syn- to post-D_2. Wrapped by S_3 where present.
Oligoclase	Oligoclase isograd subparallel to crosscutting D_2 structures.	N/A	N/A
Garnet+ plagioclase	Garnet+plagioclase isograd subparallel to crosscutting D_2 structures.	Overgrows and/or wrapped by hornblende defined S_2, wrapped by S_3.	Syn- to post-D_2. Locally kyanite occurs and is post-D_2.